Structures and Properties of Metastable Thin Films Made by Evaporation

Toshimasa YOSHIIE

Synopsis

The structures and properties of metastable vapour quenched thin films of Au-Si, iron and Au-Fe are studied by means of electrical resistivity measurement and electron microscope and diffraction observation. Au-65at.%Si films vacuum-deposited at room temperature show the amorphous structure, which transforms to a metastable structure on heating up to about 100°C and then to the stable eutectic mixture at about 200°C. The activation energies of these processes are obtained as 27 kcal/mol and 30 kcal/mol, respectively. With these values and estimated diffusion distances, processes and mechanisms of the transitions are well understood. Au-30at.%Si alloy evaporated films are crystalline from the beginning and it is observed that the migration of silicon atoms toward the surface takes place preferably in the oxidizing atmosphere, which forms the silicon oxide layer on the surface. 18 kcal/mol is obtained for the migration energy of silicon in the films. Au-Si bi-layer films show an interesting behaviour, i.e., amorphous-like Au-Si mixed phase appears by annealing. A calculation indicates that the strain energy stored in gold film can be the main driving force for the appearance of amorphous like mixture phase.

Electrical resistivity minimum is observed below 50 K with amorphous and defective crystalline films of pure iron and Au-Fe alloys (2~80at.%Fe), and a clear quantitative dependence of the resistivity minimum of the amount of lattice defects is obtained. The result strongly suggests that there is no essential difference between the defect structures of amorphous and crystalline materials and that the Kondo-like effect is closely related with the defect structure.

Contents

Chapter 1. Introduction

After solving so successfully many fundamental problems in thermal-equilibrium systems, solid state physics tried in recent years to attack problems associated with nonequilibrium systems. It is generally recognized that in many important fields of research a state of true thermodynamic equilibrium is not always attained in usual conditions. Obviously then, many of the phenomena in biology, meteorology, astrophysics and other subjects are of nonequilibrium systems or irreversible processes which take place outside the equilibrium state. These few examples may serve to illustrate the urgent need for an extension of the methods of thermodynamics so as to include irreversible processes. Such a generation is all the more important because the general microscopic theory of irreversible processes still in its initial stage of development.

It is, however, not our problem here to examine the general properties of nonequilibrium systems, and we shall limit our interest to the systems which have metallurgical metastable phases and defect structures. These systems would approach to the thermal-equilibrium states with the atomic movements by aging. If the systems are close to equilibrium, thermodynamic methods are still usefull and it is possible to describe the process approaching to equilibrium.

Although the metastable phases and defect structures might have been expected to exhibit properties of both fundamental and practical interest, any systematic study of the properties has begun only quite recently. The development of the suitable techniques, for example, vapour deposition, sputtering, splat cooling and so on, make it possible to produce remarkable

constitutional or structural deviations from equilibrium behaviour by rapid cooling from the gas or liquid to the solid state.

Three different approaches to these property studies emerge from the published work. One seeks the extent to which known near-equilibrium characteristics of particular alloys are retained or modified in their metastable forms. Examples for alloy phases formed by splat cooling are the semiconduction of crystalline tellurium retained in amorphous solid Te-25at.%Au-5 at.%Cu[1] and the ferromagnetism of crystalline iron retained in amorphous solid Fe-12.5at.%P-7.5at.%C[2]. The second approach is to introduce quite new characteristics. An example is the partial substitution of magnetic elements such as iron and cobalt for palladium, to introduce weak ferromagnetism into amorphous solid Pd-Si alloys made by splat cooling[3]. Thirdly, metastable phases with quite unexpected properties have been produced, such as the superconducting metastable phases formed by vapour-quenching of bismuth[4] and by splat cooling of certain alloys of silver or gold with tellurium or germanium[5], where none of these elements are normally superconducting in the pure state. Another example is that existing theories do not explain the resistivity minimum (Kondo effect) at 10-50 K observed on strongly ferromagnetic amorphous solid Fe-13at.%P-7 at.%C[6]. Previous theories and observations of Kondo effect had been limited to crystalline alloys containing only dilute additions of a magnetic element giving a resistivity minimum near 10 K.

Although the main research effort up to date in rapid quenching experiments has been concentrated in elucidating the structures and properties of as-deposited metastable phases, the

changes taking place on subsequent aging and heat treatment are now receiving more attention. New techniques such as splat cooling and vapour quenching offer the prospect of considerably extensive knowledge of solid state transformations by increasing the metastability attainable for the starting condition of annealing. The annealing behaviour of metastable crystalline phases offers the practical prospect of developing new age-hardening alloys, while that of amorphous metallic solid phases is of special interest in relation to both solidification and solid state transformations.

Another interesting nonequilibrium state is associated with thin films which have in essence topologically unstable shapes. It is commonly assumed that a thermodynamically stable film exhibits a structure to minimize the surface and interfacial energies. If a thin film is deposited on a substrate at a sufficiently low temperature where the adatom mobility is negligible, it is very unstable because of the presence of a sharp discontinuity of material at the surface and the interface between the film and substrate, and subsequent annealing yields the migration of atoms both laterally and vertically to minimize the energies.

Solid metal-semiconductor interfaces are usually envisaged as a quite abrupt transition from pure metal into intact semiconductor crystal. Indeed, this description is what is usually implied by the phrase, " Schottky diode ". According to this idealized model, a profile across the interface would show no intermediate values of chemical composition or lattice spacing. However, in practice most metal-semiconductor interfaces produced in device fabrication differ significantly from the idealized model, though they are always kept

at temperatures well below those at which any chemical compound, solid solution, or liquid is expected to be formed.

An example of non-ideal contact behaviour is afforded by gold contact on silicon. This contact often ages at room temperature accompanied the change in electronic parameters, like the barrier height, drifting noticeably over time periods as short as weeks or even days. Such electronic changes in gold contacts have been known for many years, but direct evidence for atom movements at the Au-Si interface has been given only rather recently[7 ~ 9].

The purpose of this study is to clarify the structure, stability, properties and annealing behaviour of nonequilibrium Au-Si alloys, iron and Au-Fe alloys which are obtained by the vapour quenching. The vapour quenching is attained by thermal evaporation of source material onto a suitable substrate maintained at sufficiently low temperature. This condition produces a high cooling rate (10^6 °C/sec), by which unstable shapes, very defective structures, metastable crystalline phases, and/or even amorphous phase could result in.

The system, Au-Si, has received considerable attention because of its importance in semiconductor device technology. Gold and silicon are almost totally inmiscible in the solid state and form a eutectic at about 363°C, as shown in Fig. 1 whereas many metastable phases have been obtained by rapid-cooling, [10 ~ 15] , and a surprisingly high diffusion rate of silicon in gold and the formation of a surface layer containing silicon, at temperature well below the eutectic[7], are of particular interest. According to the rapid diffusion and surface layer formation of silicon, the fast drifting of electronic characteristics of the Au-Si contact mentioned above could be well explained.

On the other hand, iron and Au-Fe system are of quite interest, since they form metastable magnetic phases by vapour quenching. These metastable phases are expected to have such new properties as mentioned before. Au-Fe can be the Kondo alloy, when the magnetic impurity, iron, is low enough in concentration. For instance, the resistivity minimum is observed with the concentration less than 0.2%[16]. However, as previously stated, among strongly ferromagnetic amorphous solids with high concentrations of ferromagnetic components, the resistivity minimum has been frequently observed, and this interesting behaviour is also expected with the Au-Fe system. The change of the Kondo-like minimum with the increasing iron content or with the degree of ordering in atomic arrangements in this alloy system are also worthy of investigation.

In order to realize the purposes of the present study, the electron microscopy, electron diffraction, and electrical resistivity measurement are carried out in various conditions, and the results are carefully analyzed to find the structures, electric characteristics and their changes by thermal treatments. Especially the emphasis is laid on the atomic movements and property changes of the metastable phases with approaching to the equilibrium state.

Chapter 2. Study of Au-Si Films

§1. Introduction

In this chapter, we describe the study carried out on the structures and their changes of the evaporated thin films of Au-Si.

The importance of the Au-Si system in the technology of solid state electronics has made it necessary to investigate precisely the phase diagram of the system. In 1920, di Capua[17] deduced from cooling curve studies that the Au-Si system contains a eutectic and obtained values of 370°C and 31at.%Si for the eutectic temperature and composition, respectively. In 1933, Jette and Gebert[18] concluded from lattice parameter measurements that there is no mutual solubility in the system. Since all of these studies were done when pure components were not available, they must be taken into account with some reserve.

Work up to 1965 has been summarized by Elliott[19]. Heath[20] used a gravity segregation technique to determine the eutectic composition and obtained a value of 18.60±0.3at.%Si and showed that the eutectic temperature is somewhere between 310°C and 380°C. Three independent sets of results summarized by Elliott have confirmed that the solubility of gold in silicon is very low. The largest solubility reported was 2×10^{-4}at.% at 1280°C where it is at a maximum.

A paper by Gerlach and Goel[21] describes work, apparently using gold containing 0.5at.%Sb. This work have values of 370°C and 17.04at.%Si respectively. These results must, however, be regarded as of limited value because of the presence of antimony in gold. Anderson, Bestel, Johnson and Post[12] obtained a value of 17.9at.%Si for the eutectic composition

using the gravity segregation technique. More recently, a precise measurement of this system has been reported by Anantatmula, Johnson, Gupta and Harylev[22] using high purity components, which gives a value of 363±2°C for the eutectic temperature and 19.0±0.5at.%Si for the eutectic composition. These conflicting results are rather disappointing. It is worth considering why the published values of the eutectic composition show such a large spread of values. We will give a possible explanation from the present work in connection with the easy silicon migration toward the surface in Au-Si alloys and formation of silicon oxide layer on the surface during the heat treatment. If this mechanism takes place, silicon content will change considerably.

A large number of metastable intermediate phases have been produced in Au-Si alloy system through the application of the comparatively new rapid cooling technique. On quenching Au-Si alloy from a melt around 25at.%Si onto a copper substrate, an amorphous phase is produced[14]. This phase was not stable at room temperature and transformed into a crystalline metastable form (not yet identified) after about 24 hr. A detailed X-ray diffraction investigation of an amorphous Au-Si alloy containing 30at.%Si has been reported by Dixmier and Guinier[15]. Various nonequilibrium crystalline phases have been observed by many investigators. For example, β-Mn-type[10] with the lattice parameter a=6.750A, β-fcc[11] with a=7.844A, γ-brass-bcc[12] with a=9.60A, δ-Au_3Si[13] with a=7.82, b=5.55A and c=11.16, and so forth. We obtained in this study new metastable phases, fcc with a=3.7A and simple cubic a=6.3A by vapour quenching.

These results show that the phases resulting from rapid quenching greatly depend on the average rate of cooling which

is difficult to control and cannot be measured accurately enough to be meaningful. Several different phases could, therefore, be obtained at a given composition, depending on the rate at which the liquid or vapour to solid transformations takes place. The well known empirical relations due to Hume-Rothery[23] that explain the occurrence of electron compounds in noble metal systems fail in the case of Au-Si alloys. None of the expected electron compounds has so far been produced in this system, even by rapid quenching.

Silicon has been found to dissolve and diffuse rapidly into thin gold films at temperatures considerablly below the eutectic temperature of the Au-Si binary system. Hiraki et al.[7] showed that rapid transport of silicon through thin (1000 A) gold films vacuum deposited on silicon single crystal substrates and, at the same time, growth of a SiO_2 layer on the gold surface occurred when the specimens were annealed in an oxidizing environmental atmosphere at temperatures as low as 150°C. Although, nonuniformity of the SiO_2 layer was inferred from the helium ion backscattering analysis. The importance of the interface was pointed out by the same investigators[9]. A spectrum of Auger electron spectroscopy taken from a thin gold film below 150 A in thickness during its deposition on clean surface of silicon substrate at 50°C was composed of both silicon which was different from that of pure silicon and gold, and they concluded that a fresh Au-Si interface was diffuse over the thickness of gold as thick as about 50 A and electronic (or chemical) nature of silicon in diffuse interface is metallic to interact with s and d-electrons of gold. The existance of Au-Si transient layer at the interface is as certain. However, taking account of the fact that the gold

film deposited on silicon at this temperature inevitably forms an island structure with irregular nonuniform thickness and that the observable depth of Auger electrons is of the order of 10 A, their conclusion that the thickness of the interface reaches as much as 50 A seems to be quite uncertain.

One of the purposes of this paper is to examine the formation of the transient layer and its structural changes at the interface of Au-Si two layer films which are made by vapour quenching and raised to various temperatures to allow fast diffusion of silicon in the gold layer.

§2. Experimental Procedures

(1) Sample Preparation

The materials used in the present experiment are gold, silicon, both of 99.999% purity, and alloys of them. Au-Si alloys are prepared by arc melting in argon atmosphere. The compositions of four kinds of alloys, Au-30at.%Si, Au-50at.%Si, Au-65at.%Si and Au-80at.%Si are obtained by about 5 grams each. The vacuum chamber used in this experiment is shown in Fig. 2: It consists of a quartz crystal film thickness monitor, two evaporaters with tungsten filament and electron gun, an evaporation shutter, copper base block, and cryo pump or liquid nitrogen trap. The base block is equipped with electric terminals and lead wires for the resistivity measurement, holders for substrate crystals, thermal shield cap, heater, and thermometer. Cleaved mica and NaCl substrate crystals are employed for the resistivity measurement and electron microscopy observation, respectively. The vacuum chamber is evacuated by an ultra-high vacuum system, and various vacuum conditions including vacuum better than 5×10^{-10} Torr are obtained.

The sample is evaporated from the tungsten conical filament or the electron gun and deposited onto freshly cleaved mica and NaCl pieces, which are kept at various temperatures. For the sake of outgassing, before evaporation, the sample and filament are pre-heated with the shutter closed. The liquid nitrogen trap is always filled before the evaporation even when a rather low vacuum evaporation is intended, in order to obtain a good vacuum immediately after the evaporation and during the resistivity measurement and a better control of the substrate temperature. By the evaporation, 100~2000 A thick films are deposited at the rates of 2~10 A/sec which are monitored by the quartz thickness meter. The source-to-substrate distance is 7 cm for the electron gun and 5 cm for the tungsten filament. The film thickness is measured with a quartz crystal monitor during the deposition or interferometrically after the experiment.

(2) Electrical Resistivity Measurement

The electrical resistance of the films deposited on the cleaved mica crystal is measured by the standard potentiometric technique. The resistance of Au-Si alloys immediately after the evaporation ranges from 10Ω to 100Ω. In order to investigate the structural changes, the electrical resistivity changes during both heating up to 300°C by a constant heating rate and isothermal annealing at various temperatures below 300°C are measured.

The substrate temperature is measured with a thermo-couple of 0.2 mm thick copper-constantan wire attached to a dummy mica plate held on the copper base block. In the annealing experiment, the substrate temperature is controlled by the heating current through a nichrome wire heater in the

block. The temperature flactuation in isothermal annealing is within 0.1 degree and in constant rate heating within 1 degree.

(3) Electron Microscopic Observation

The films deposited on cleaved NaCl substrates simultanously with those on mica substrates, which are used for the electrical resistivity measurement, are stripped from the substrates and observed under the electron microscope. The thickness of films ranges from 150 to 500 A, which is ideal for electron micrograph and diffraction. The films are floated off from the NaCl substrates in distilled water and collected on standard electron microscope grids for examination in Hitachi HU-11A. Three methods are employed for the electron microscopy, i.e., bright-field image, dark-field image and diffraction observations. For the study of microstructures and defect structures in films, the transmission electron micrographs of bright-field and dark-field images provide a great amount of information. On the other hand, two diffraction techniques, i.e., transmission electron diffraction and reflection electron diffraction the latter of which takes place in a thin surface layer of the specimens, are carried out to determine the structures and d-spacings of films.

(4) Ultra-High Vacuum System

Figure 3 shows the block diagram of the ultra-high vacuum system ULVAC FBD-40B used for the present experiment. It consists of the chamber, cryo pump (trap), sputter ion pump, titanium getter pump, adsorption pump and rotary oil pump.

The rotary oil pump is used to reduce the pressure from 1 atom to 10^{-2} Torr, and then it is valved off from the system. The adsorption trap pump (made by placing artificial zeolite in a stainless steel can) is then cooled to liquid

nitrogen temperature reducing the pressure to 10^{-5} Torr, before the system bake to outgas is started. After bake-out at 250°C for several hours, the system is allowed to cool to room temperature and then the ion pump and getter pump on the high vacuum side of system are started. After two hours the pressure is typically $5x10^{-10}$ Torr. The liquid nitrogen trap directly in the evaporation chamber reduces the pressure to the low 10^{-10} Torr region.

The adsorption pump is provided between the vacuum chamber and the rotary oil pump, and plays the role of a filter to eliminate the problems associated with the pump fluid, which makes it possible to get clean oil-free ultra-high vacuum.

§3. Results

(1) Structures of Au-Si Films

The effect of silicon concentration on the structure of films deposited at room temperature is studied by electron microscope and diffraction observation.

For comparison, pure gold and silicon films, are first investigated. Figures 4 and 5 show the microstructures and diffraction patterns of pure gold and silicon respectively. Gold film has fcc and polycrystalline structure with the average grain size of about 300 A, while, silicon film is structureless as far as the 20 A resolution of the electron microscope is used and, correspondingly, completely amorphous electron diffraction halos are obtained.

The electron micrographs and diffraction patterns of Au-Si alloys, Au 30at.%Si, Au-50at.%Si, Au-65at.%Si, and Au-80at.%Si are shown in Figs. 6,7,8 and 9 respectively. The diffraction patterns change with increasing silicon concentration. Unlike pure gold which shows the sharp diffraciton rings, the alloy with

30at.%Si concentration exhibits broad fcc rings. The observed peak positions correspond fairly well to those of the gold structure. In the 50at.%Si alloy, the diffraction still indicates the fcc structure, but (111) and (200) peaks no longer split into two. The electron micrographs show that the microstructures of these two alloys are polycrystalline with the average grain size of about 50 A, and no phase separation or precipitation is observed.

On the other hand, amorphous phases are obtained for two concentrations of Si, 65at.% and 80at.%. 65at.%Si alloy shows a typical amorphous pattern very similar to that of the amorphous Au-30at.%Si alloy made by splat cooling, which has been reported by Dixmier et al. [15], while in the case of 80at.%Si alloy an additional halo peak corresponding to the first halo ring of amorphous pure silicon appears. The electron micrographs of the latter two alloys are structureless as well as that of amorphous pure silicon.

(2) Silicon Migration and Precipitation in Au-30at.%Si Films

Since the resistivity is strongly dependent on the structure of the material, it can be considered as a good sensor for the metastable-stable transition. The electrical resistivity changes of Au-30at.%Si films deposited on the room temperature substrate are studied in various conditions of deposition and heat treatment. An unexpected resistance decrease is observed when films are exposed to air. Figure 10 shows a typical isothermal experimental curve of the resistance decay of a 300 A thick film with the time elapsed in air. The resistance decrease amounts to more than 60% of the initial value after the aging time of the order of 1000 minutes. The rate of the resistance drop varies from specimen to specimen,

depending on the film thickness and the vacuum deposition rate. When the samples exposed to air are put into vacuum again, the rate of decay becomes very small. Approximately a linear relation exists between the rate of resistance decrease and the vacuum degree where the samples are put. The decrease of resistance is observed in the atmosphere of pure oxygen as well, but no appreciable change appears in pure argon or nitrogen. This shows that oxygen plays a dominant role in the observed drop of the resistance. When the samples vacuum-deposited at room temperature are annealed at 150°C for 10 minutes in air, their resistance drops to 10~20% of their initial value. The amount of decay of resistance does not depend on the vacuum degree during the deposition when it is better than 5×10^{-5} Torr.

The microstructures and diffraction patterns observed at room temperature and after the annealing for 10 minutes at 150°C in air are shown in Figs. 6 and 11. After the annealing at 150°C in air the diffraction peaks become sharper.

In order to examine the structural changes of the film surfaces, the reflection electron technique is used with the accelerating voltage of 100 kV. Results are shown in Fig. 12. Immediately after deposition, only the diffraction lines of Au are observed as in Fig. 12(a). After the annealing for 10 minutes at 150°C in air, the diffraction rings become almost invisible except the halos corresponding to silicon oxide, as in Fig. 12(b). After taking the diffraction pattern, the specimen film is immersed in the CP-4 etching solution for 15 seconds. By this treatment the diffraction pattern of gold polycrystals is completely recovered as Fig. 12(c) shows.

Another remarkable phenomenon appears when the deposited films are annealed above 200°C in vacuum. An electron micrograph

of the sample deposited at room temperature and successively annealed at 300°C in vacuum for 10 minutes is shown in Fig. 13, where two large crystalline areas of some microns in diameter are seen. The selected area diffraction technique reveales that the large crystals are of pure silicon and the region other than them consists of pure gold crystallites. The changes of the lattice constant of the films is not detected after annealing in air or in vacuum.

The surface structural change induced by the exposure to air and the phase separation mentioned above can be distinguished from each other by the electrical resistance measurements during heating up to 300°C in vacuum and in air, as are shown in Fig. 14. The large resistivity decay between 25°C and 200°C in curve 2, which is taken during the heating in air, undoubtedly corresponds to the process of silicon migration toward the surface, which is associated with the formation of silicon oxide layer on the surface. A small steep decay at 25°C is caused by the introduction of air into the specimen chamber at that temperature, and, therefore, corresponds to the early stage of the isothermal resistivity change shown in Fig. 10. On the other hand, when the films are heated up in vacuum, as shown in curve 1, there appear two distinct stages at around 60°C and 200°C. Before and after the former stage, no changes but a slight grain growth of crystallites are found by the electron microscopy. While, after the latter stage, patched precipitation of silicon is observed as in Fig. 13. This clearly shows that the decay of the latter stage arises from the phase separation into pure silicon and pure gold. The former stage at around 60°C seems to be the same process as in curve 10.

The activation energies of these two processes are

estimated by slope change method in the isothermal experiments. Figure 15 shows the results of a series of isothermal annealings. From the slope changes between two successive isothermals, the activation energies E's are calculated by using the equation,

$$\ln \frac{R_1}{R_2} = -\frac{E}{k}\left(\frac{1}{T_1} - \frac{1}{T_2}\right),$$

where R is the solpe of an isothermal, and T the temperature of the isothermal. The activation energies of the migration toward the surface associated with the formation of the oxide layer on the surface and the phase separation into pure silicon and pure gold are estimated to be about 18 kcal/mol and 30 kcal/mol, respectively.

(3) Crystal Growth and Precipitation in Amorphous Au-Si Alloy

Amorphous-to-crystalline transition in Au-65at.%Si alloy films are investigated using electron microscopic and diffraction observation and electrical resistivity measurement.

In the as-deposited state at 25°C, the resistivity values are found to be quite large, for example 200~300 μΩcm with 300~500 A thick films. Figure 16 shows typical behaviour of the electrical resistance of the alloy film after deposition and upon subsequent in situ annealing in vacuo. The heating is carried up to 300°C at a constant rate of 5°C/min. The resistance remains nearly unchanged up to 100°C and decreases continuously in the temperature range, 100°C-150°C. A little bump of the resistance curve occurs at about 155°C, above which the resistance stays constant again. At about 200°C, a well-defined large drop, which looks like the amorphous-to-crystalline transition appears. The amount of this drop corresponds to about

70% of the initial value. Above this sharp drop reversible temperature dependence of the resistivity is observed. The electrical resistivity change during heating in air is shown in Fig. 17. Unlike the case of Au-30at.%Si films, the resistivity change in air is almost the same as in vacuum. But, when the amorphous films are aged in air for about ten months at room temperature, only the gold diffraction rings are observed as shown in Fig. 18. This indicates that silicon migration toward the film surface induced by air also occurs in amorphous Au-Si films.

In order to clarify the above stages, the amorphous films are examined in the hot stage of an electron microscope where heating rate is kept almost the same as that used in the electrical resistivity measurements.

Amorphous phase remains nearly unchanged for temperatures up to 100°C, and transformed homogeneously on heating at 100°C or above to a metastable unknown structure, and finally to the stable eutectic mixture of gold and silicon at above 200°C. Typical transmission electron micrographs and corresponding diffraction patterns, Figs. 19, 20, 21 and 22, are made at temperatures 100°C, 150°C, 200°C and 220°C, respectively. These results enable us to draw a fairly coherent picture of the successive steps in the crystallization process. They are illustrated in sequence in Fig. 23. In the " incipient crystalline stage" , there is splitting of the diffraction lines while some granularity in the electron microscope picture is observed as shown in Fig. 19. We note an increaes in the granularity on heating up to 150°C, and no changes are observed up to 200°C. Then silicon nucleates and grows as shown in Fig. 21, which corresponds to the abrupt decrease of the resistance at the

same temperature. No evidence of resistivity increase of 155°C is detected by the observation of electron microscopy and diffraction.

The activation energies of the reversion of the amorphous phase to metastable phase over the temperature range of 100~150°C and metastable phase to stable eutectic mixture phase are estimated by the slope change in the isothermal experiments as shown in Fig. 24, and about 27 kcal/mol and 30 kcal/mol are obtained respectively.

Another kind of phase change, from solid to liquid, is observed on heating the films to the temperatures above 400°C. Figure 25 shows the typical feature of melting. Selected area diffraction technique indicates that the most part in the view of the electron micrograph of Fig (a) is already in liquid state, as the pattern (b) shows, while small bright patches of crystalline pure silicon on the right hand side of Fig. (a) still remain, as sharp spotty diffraction lines in the pattern (c) shows, and their areas are diminishing because of dissolving of silicon from their peripheries into the melt. The dark patches in the electron micrograph are traces of silicon crystals, which are already melted and diffused away. The photometric traces of the diffraction patterns of amorphous and liquid Au-Si and gold are shown in Fig. 26. The difference between amorphous and liquid is not pronounced and the observed peak positions of amorphous and liquid state correspond approximately to those of gold.

The decrease of silicon content in liquid phase by oxidation is observed. When the sample melts completely at 450°C, it is cooled down to 400°C. After the annealing of several minutes at that temperature, the precipitation of gold begins. Heating up

to 420°C is necessary to melt gold precipitates again. The result shows that during the heat treatment, gold concentration changes remarkably because of relatively fast oxidation of silicon. When solidification starts at 400°C, slicon concentration in liquid would be about 18.5at.% which is in the hypoeutectic region, but after five minutes at 420°C the composition decreases by about 0.2at.% reaching to 18.3at.%.

Cutting off the current through the heater in electron microscope hot stage enable us to produce a cooling rate of 10 °C/sec. In this condition, new metastable Au-Si phases are obtained. The structure analysis of these new forms is carried out by trial and error method by comparing and measuring many diffraction patterns. Fortunately, from the pattern given in Fig. 27, one type of structure is readily identified to be fcc with the lattice parameter, a=3.7 A. In addition to this fcc structure, there still remain five sorts of diffraction patterns which cannot be accounted for by that as are shown in Fig. 28. By the trial analysis it can be concluded that they arise from a simple cubic structure with a=6.3 A. The compositions and atomic arrangements in the two new structures are not clear yet.

(4) Interfacial Reaction in Au-Si bi-layer Films

Silicon and gold bi-layer are prepared by successive vacuum evaporations. The study is carried to clarify the structures and their changes of the silicon and gold layers and/or their interface. A 200 A thick silicon film is deposited with electron gun onto a cleaved NaCl crystal kept at room temperature and, then, it is covered with gold in the second evaporation by using a conical tungsten filament. The electron micrograph and diffraction patern are shown in Fig. 29

(a) and (b), respectively. In the diffraction pattern, the amorphous silicon halos and fcc gold rings are clearly seen. The transmission micrograph shows a polycrystalline structure with the grain size of about 300 A.

The structural changes during heating up to 350°C are shown in Figs. 30, 31, 32 and 33. The heating rate is of 2°C/min. The micrographs and diffraction patterns remain nearly unchanged up to 130°C. At a temperature between 130°C and 150°C, the gold diffraction rings begin to become weak gradually. At around 180°C, silicon crystallizes to produce sharp diffraction rings, while the gold rings disappear. In parallel with these changes, a set of new halo rings identified as belonging to amorphous Au-Si arises. Figure 34 shows that halos of the pattern of the annealed film mentioned above and that of the amorphous Au-65at.%Si film made by evaporation of the alloy colsely resemble each other. After the annealing at 350°C gold rings appear again as Fig. 33 shows.

In order to investigate if amorphous structure of silicon has any influence on the appearance of amorphous Au-Si during the annealing, a polycrystalline Si-Au layer film is used. Silicon is made by first evaporating onto a NaCl maintained at 400°C, then evaporating gold at room temperature. Gold and silicon layer are 150 A and 300 A, respectively. Diffraction patterns of this film as-deposited and after annealing at 250°C are given in Fig. 35 (a) and (b), respectively. It is observed that gold rings change into halos.

We also study the effect of the structure of gold layer on this transition. Gold film which has large grain of about 3000 A is made by first evaporating onto a NaCl crystal kept at 300°C, and silicon is deposited on the gold film at room

temperature. The thickness of the gold film is 200 A and that of silicon is 200 A. This bi-layer film is examined in the normal manner. Appearance of amorphous like Au-Si is, however, not observed at the annealing up to 250°C as Fig. 36 shows. These results show that some property of gold film plays a dominant role in the reaction of the interface.

The structure of bi-layer films are studied to find the effect of substrate temperatures during the evaporation. The electron micrographs and diffraction patterns of Au-Si bi-layer films deposited on the substrates at 100°C, 130°C, 150°C and 180°C are shown in Figs. 37, 38, 39 and 40, respectively. The diffraction patterns of the films deposited below 100°C are almost the same as that of films deposited at room temperature, but, the films deposited at 130°C and 150°C show a complex structure as are shown in Figs. 38 and 39. The decomposition product of this structure is detected at 180°C as shown in Fig. 41. And it is quite similar to Au-Si bi-layer film deposited at 180°C which is shown in Fig. 40. Their diffraction patterns show sharp lines belonging to silicon and weak rings of gold. These might indicate that some reactions between gold and silicon occur during depositions at above 130°C.

§4. Discussion

(1) Structures of Au-Si Films

The electron micrographs and diffraction patterns of Au-Si films of all compositions employed in the present experiment show that no precipitates of silicon or its compound appear immediately after deposition at room temperature. From 30at.% and 50at.%Si films, broad diffraction rings of fcc structure with the lattice constant almost the same as that of pure gold

lattice are obtained. This suggests either that in the super-saturated or forced solid solution of Au-Si alloy distribution of silicon atoms is so inhomogenenous that the lattice keeps the lattice constant of pure gold and, instead, is heavily distorted and possibly subjected to fine fragmentation or that the silicon atoms are distributed homogeneously in the solid solution which is in the form of micro-crystallite aggregates. The fact that the lattice constant of super-saturated solid solution of this alloy system remains relatively constant with the increase of silicon content seems to support the former concept.

It is somewhat interesting that the vapour-deposition in the present experiment always gives the micro-crystalline state when the silicon concentration is below 50at.%, and more than 65at.%Si is necessary to obtain the amorphous state. It has been reported that the amorphous phase of Au-30at.%Si alloy was obtained by splat cooling of the melt to room temperature[14,15]. Since the cooling rates in the two methods are probably not quite different, many amorphous films could be obtained by vapour deposition when the substrate is kept at very low temperature where the surface migration of arriving atoms is extensively suppressed.

(2) Silicon migration and Precipitation in Au-30at.%Si Films

The annealing of the deposited film allows silicon atoms to diffuse and agglomerate. In an oxidizing atmosphere, silicon atoms migrate and accumulate on its front surface, where they can meet oxygen and form the silicon oxide layer. As a result of such diffusion, the silicon content of the inside will decrease and gold will be the only constituent of the film. It is natural to expect that the electrical resistance of the film

approaches that of pure gold and grain growth of crystallites occurs. The fact that the diffraction lines in reflection technique become scarcely visible by the annealing at 150°C in air, that they appear again by the surface etching treatment, as Fig. 12 (a), (b) and (c) show, and that the transmission patterns show only the lines corresponding to the gold lattice, as Figs. 6 (b) and 11 (b) show, do not only support the above conjectures but also strongly suggest that the silicon oxide layer on the film surface has the amorphous structure.

Another interesting result that, when the deposited film is annealed in vacuum, most of the silicon atoms diffuse and accumulate in the interior of the film and finally form the crystalline silicon precipitates could be interpreted in such a way that the film surface without oxygen does not attract silicon atoms and, therefore does not act as the sink of diffusion silicon atoms.

Anderson et al.[13] reported that, when the metastable δ-Au-Si phase which was obtained by rapid cooling from the melt was converted to the equilibrium alloy structure by heating, only the X-ray diffraction lines corresponding to pure gold were observed. As mentioned above, presumably the fast silicon migration toward the surface took place in the oxidizing atmosphere in their specimen and resulted in the growth of the amorphous silicon oxide layer on the surface which could not be observed by X-ray diffraction.

Phlofsky et al.[24] observed that the rate of transformation from the metastable phase to the equilibrium phase of Au-Si alloy was affected by the annealing atmosphere; less time was required for the transformation in air than in pure nitrogen gas below 150°C. Their result is in good agreement with the

present result that the recovery of the deposited films is much faster in air than in vacuum, as Fig. 14 shows. It is most likely that the strong affinity between silicon and oxygen atoms makes the chemical potential of silicon extremely low at the surface where silicon atoms can react with oxygen so that the diffusion of silicon toward the surface preferably takes place in the oxidizing atmosphere and any reactions in which the motion of silicon atoms is involved is accelerated.

It must also be pointed out that the migration of silicon atoms at low temperature in the deposited films is much faster than that in the ordinary silicon lattice. According to Hiraki et al.[8], in the gold rich Au-Si metastable phase each silicon atom may have metallic bonding with surrounding gold atoms. Silicon atoms in such a state in the alloy phase must be more mobile than in the ordinary silicon lattice in which all the silicon atoms have covalent Si-Si bonds.

The activation energy of self diffusion of semiconductor silicon is 98 kcal/mol[25]. Our result yeilding the activation energy of 18 kcal/mol for the silicon movement in Au-Si film is much lower than the above value and well agrees with the observation and explanation by Hiraki et al. The value of the activation energy for the phase separation into pure silicon and pure gold, 30 kcal/mol, is also far smaller than that of self diffusion of semiconductor silicon, but, on the other hand, yet larger than the migration energy of silicon in Au-Si film. This activation energy is explained as follows: At low temperatures below 200°C, although the silicon atoms migrate very fast, the mobility of gold may still be negligible. Since for the growth of silicon crystallites replacement of a large amount of gold atoms by silicon atoms is required,

the process will be suppressed unless the mobility of gold reaches to a certain extent. For the replacement both of jumping out of gold atoms and jumping of silicon atoms into the vacant site are necessary, but the latter process needs presumably very small energy. For this reason it is concluded that the migration energy of gold in Au-Si film is 30 kcal/mol, which is a little lower than the activation energy, 40 kcal/mol[26], for self diffusion of gold.

(3) Amorphous-to-crystalline Transition

It is somewhat interesting to compare the stability of the Au-65at.%Si amorphous films made by evaporation with that of the amorphous Au-30at.%Si films obtained by splat cooling[14,15]. The former films tansform into the metastable phase at about 100°C and into the equilibrium mixture at 200°C, while the latter films are unstable even at room temperature and the equilibrium mixture phase is obtained below 150°C. This discrepancy is mainly due to the difference of silicon concentration; the increase of " glass forming element ", silicon, may make more stable amorphous phases.

It is also worthwhile to consider the resistivity decay curves in annealing of the amorphous films, such as in Fig. 16. A little bump of the resistance curve at 155°C is remarkable, but no changes corresponding to it are detected by electron micrographs and diffraction patterns. The resistivity increase just before the crystallization of amorphous Au-Ge-Si alloy has been reported by Chen and Turnbull[27]. They suggested the possibility that it is due to formation of very small crystallites. Nevertheless, it is not the case in the present study because the increase occurs after crystallization. It could be caused by nucleation of silicon crystallites which

act as additional scattering centers for conduction electron.

The kinetics of two annealing stages, the first one from 100°C to 150°C and the second from 200°C to 250°C, are studied in some more details with regard to phase transformations. Various methods of analysis of resistivity decays in thermal processes are based on the assumption that the change of the resistivity ρ obeys an equation of the form,

$$\frac{d\rho}{dt} = -\nu F(\rho) e^{-\frac{E}{kT}} ,$$

where E is the activation energy for the process, k is Boltzmann constant, ν is a frequency factor and $F(\rho)$ is a continuous function of ρ. This equation is derived from the assumption that the residual resistivity reflects, must likely linearly, some internal parameter, for example concentration of constituent atoms, in the material. Hence, the resistivity changes in the present experiment may be read as the internal change of the films due to atomic diffusion. Assuming the energy E to be the migration energy of atoms, the probability of jumps available for an atom during a particular period of oscillation is given by $e^{-\frac{E}{kT}}$, and if the oscillation frequency of atom is ν, the rate of jumping is $D = \frac{dn}{dt} = \nu e^{-\frac{E}{kT}}$. Using this equation with the usual value of atomic frequency factor 10^{13} sec^{-1}, and the activation energies, 27 kcal/mol and 30 kcal/mol, for the two stages respectively, D is estimated as $5x10^{-3}$ at 120°C for the first stage and 0.6 at 210°C for the second stage. At the first stage, atoms can jump for about 3 times in 10 minutes, during which the main part of the reaction can proceed and be finished. The mean diffusion distance is then equal to 3 or ~ 2 in units of the interatomic spacing. On

the other hand, atoms make about 360 jumps for 10 minutes which correspond to the diffusion distance of about 19 atomic distances or ~60 A at the second stage. If we use the frequency factor 10^{14} sec^{-1}, which includes both an entropy of activation and a numerical factor to represent the capture cross section for vacancy, atoms can migrate for about 200 A. This result is somewhat lower than, but reasonably consistent with the particle size of silicon, 1000~2000 A, observed in the electron microscope near the end of this annealing stage.

In the view of the fact that the D-values are consistent with observations, the values 27 kcal/mol and 30 kcal/mol may then be interpreted as the activation energy for the process of interdiffusion in the alloy. As mentioned in the previous section, the activation energy 30 kcal/mol represents the migration energy of gold in Au-30at.%Si alloy films. The two values in amorphous Au-Si films are almost the same as that value. For this reason, the activation energies of the first stage and the second stage would represent the migration of gold or diffusionless transformation is responsible for the transition of amorphous Au-Si to metastable phase, whereas long range migration of gold is necessary for the growth of silicon crystallites just the same as in Au-30at.%Si films.

It must be noticed that a remarkable decrease of silicon concentration in both liquid phase and solid phase of Au-Si films by oxidation is observed. This result enable us to consider the cause of the ambiguity in the determination of the eutectic composition of Au-Si system. If an experiment to determine the eutectic composition was under the influence of oxidizing atmosphere, some changes of composition would take place during the heat treatment. Even in a high vacuum of the

order of 10^{-6} Torr, the samples are not free from the influence of oxygen, as the study in the electron microscope hot stage clearly shows the decrease of silicon concentration in liquid phase by oxidation. Accordingly the effect of oxidation should be taken into account in addition to that of gravitational segregation on the determination of the eutectic point. Actually, recent values of the eutectic point determined by many investigators are not in agreement with each other, but scattering between 17.0at.%Si and 19.0at.% and between 363°C and 370°C[20~22].

(4) Au-Si bi-layer Films

During the heat treatment of Au-Si bi-layer films, a set of halo rings identified as amorphous Au-Si arises in parallel with the disappearance of gold rings. This clearly shows that silicon atoms dissolve into the gold film. The formation of Au-Si mixed phase seems to closely relate to the work by Hiraki et al.[7~9] As is mentioned in the introduction of the chapter, they have shown transport of considerable amount of silicon through gold films deposited on silicon substrate and formation of a SiO_2 layer on the film surface above 100°C. The mechanism of this process is, however, still unsolved. Since it is well known that gold and silicon are totally inmiscible in the solid state, the mixing process of Au-Si should be understood as rising from a certain origin and/or a special mechanism. We will first discuss it thermodynamically as follows.

The configurational entropy will inevitably change associated with the random mixing of gold and silicon. The molar entropy ΔS to form a random solid solution is given by the ideal entropy of mixing,

$$\Delta S = -R [C \ln C + (1-C) \ln (1-C)],$$

where R is the gass constant and C is the atomic fraction. Assuming the concentration of gold in Au-Si mixed phase to be C=0.3, the change in the molar Gibbs free energy ΔG by mixing at 180°C is then

$$\Delta G = -T\Delta S = -550 \text{ cal/mol}.$$

Comparing with an experimental value of the heat of crystallization of amorphous Au-Si alloy 760 cal/mol, which has been obtained by Chen and Turnbul[28], at least, free energy of 210 cal/mol is necessary to be contained in the bi-layer film including lattice strain and defect energy. The appearance of the halo rings from heat treated Au-Si film is almost parallel with crystallization of amorphous silicon, the heat of mixing of gold and silicon seems to compensate the heat of crystallization of silicon. The heat of crystallization of germanium has been measured also by Chen and Turnbull to be 2.75 kcal/mol[29]. Though that of silicon has not been reported, by using the ratio of their melting points, it is roughly estimated as about 3.7 kacl/mol. This energy could be transfered, when the silicon film crystallizes, into that to form the amorphous-like Au-Si film. But, since halo rings are observed even when polycrystalline silicon film is used as a component of bi-layer film as Fig. 35 shows, heat of crystallization of silicon cannot always be the principal part of the motive force for the formation of amorphous Au-Si films.

It has been reported that large stresses exist in thin films deposited at room temperature, and more than 1 percent strain is

caused by the stresses in many materials. The internal stress in gold films obtained at room temperature is tensile[30], and appreciable strain energy is stored. The strain energy in the molar is estimated by the formula, $\frac{1}{2} K \varepsilon^2 V$, where K is the bulk modulus, ε is the strain, V is the molar volume. Using $K=2\times10^{12}$ dyn/cm, $\varepsilon=0.03$ and $V=10$ cm^3 for gold, 214 cal/mol is obtained. If the stress relief happens in gold film by mixing of silicon atoms, the increase of internal energy by the formation of Au-Si amorphous phase can be compensated by 214 cal/mol.

Since this value is almost the same as 210 cal/mol, which must be contained in the bi-layer film in order to make the structural change from bi-layer to amorphous possible, it is concluded that the strain energy stored in gold film could almost be only the driving force for the appearance of amorphous-like mixture.

This mechanism is strongly supported by the fact that the halos are not observed when the gold films are deposited at high temperatures. At lower substrate temperatures, metal films exhibit tension which decreases with increasing temperature and finally goes to zero or even changes to compression. Figure 42 shows typical data of the substrate temperature dependence of the stress in copper, nickel iron and Permalloy summarized by Chopra[30]. Consequently, if the dissolving of silicon atoms into gold film is caused by the stress relief of the gold film during annealing, it is readily understood that the mixing of silicon is not detected in the gold film which is deposited at high temperature. The successive annealing after the stress relief of the films may cause the migration of silicon atoms toward the surface and formation of silicon oxide layer on the

surface, and then gold rings appear again as are shown in Fig. 33.

According to this mechanism, the thickness of the silicon oxide layer on the surface after annealing may depend on the amount of silicon atoms which are used for the stress relief of gold films. This model also explains the results which have been reported by Hiraki et al.[7 9]. Their experiment shows that the thickness of the deposited gold film has a strong effect on the growth of the oxide layer. The final oxide-layer thickness is nearly proportional to that of the original gold film, and after removal of a " saturated-growth " oxide layer by HF, no further oxide growth is observed following the heat treatment. It can be interpreted as follows. Silicon atoms will migrate into the gold films to relieve the stress of them. After the accomplishment of stress relief, if all silicon atoms migrate to the surface and form the SiO_2, the thickness is expected to be proportional to that of original gold films. After removal of the " saturated growth " oxide layer, it is natural to expect that no further oxide growth is observed after the treatments, since the gold films have stress no longer.

The complex structure is observed in the two layer films deposited on the substrate higher than 120°C. It can be interpreted that during deposition, the stress relief begins, and metastable phase is obtained.

Chapter 3. Study of Iron and Au-Fe Films

§1. Introduction

Binary alloys, consisting of a magetic and a nonmagnetic component have been extensively studied especially with regard to the properties of localized magnetic moments in various matrices and the related low temperature anomaly in the electrical resistivity. The investigations however are restricted by the limited solubility of the component with the localized magnetic moment in host metal. No example exists, that such an alloy can be produced as a stable solution throughout the whole concentration range. At room temperature, for example the solubility of iron in gold lies below 12at.%.

By the method of quench-condensation insoluble alloys can be forced into a solid solution over a limited temperature range. In this study Au-Fe films between 2 and 100at.%Fe are obtained in that way and investigated by the electrical resistivity measurement, resistivity minimum is observed at low temperatures throughout the whole concentration range of iron.

The phenomenon of resistivity minimum associated with small amounts of paramagnetic impurities in crystalline alloys is well understood as arising from the spin flip scattering of conduction electrons by the local magnetic monents, randomly distributed in the alloys. With increasing impurity concentration, the minimum is suppressed and finally washed out as magnetic ordering sets in, since magnetic ordering of the local spins destroys the freedom of the spin to flip, which is the basic mechanism needed to have a resistivity minimum within the accepted Kondo theory[31]. While this seems

to be true of all reported crystalline systems, a variety of amorphous ferromagnetic materials have been reported in the recent past where a resistivity minimum is found well below the magnetic ordering temperature[6,32]. The coexistence phenomena have been studied experimentally and theoretically, and they are said to be entirely attributed to amorphous nature of the alloy.

But, our results show that this anomaly does not necessarily follow only the nature of amorphous state but also follows the appreciable amount of lattice defects. Because, resistivity minimum is observed even in crystalline films. We will discuss this phenomenon in connection with the amount of lattice defects.

§2. Experimental Procedures

Experimental procedures for the preparation of thin films, resistivity measurement, electron microscopy and electron diffraction for the study of Au-Fe alloy and pure iron films are almost the same as those for Au-Si films. The cryostat used in this experiment is schematically shown in Fig. 43: It consists of an evaporator with a tungsten filament, a base block to hold the substrate, terminals and leads for the resistivity measurement, a heater for temperature control and thermometers. Sample materials are 99.999 purity gold, 99.99 purity iron, and alloys of them which are prepared by arc melting.

The sample is evaporated in vacua from a conical tungsten filament onto a freshly cleaved mica piece, which is kept at about 5 K by immersing the bottom of the cryostat in liquid helium. Before evaporation, the sample and filament are pre-heated with the shutter just below the filament closed. The liquid nitrogen baths are filled before the cryostat is immersed in liquid helium. This treatment prevents the residual gas

from condensing on the substrate. The liquid nitrogen inner bath, the shield caps around the filament and the substrate are so devised as to minimize the loss of helium and the temperature rise of the substrate during the evaporation. With this device the loss is as little as 30cc and the substrate temperature rise is below 1 degree during the evaporation.

At low temperatures the temperature is measured with a calibrated carbon resistor, and at temperatures higher than 50 K with a thermo-couple of copper-constantan. In the annealing experiment, the substrate temperature is controlled by heating the manganin wire wound on the base block, and by changing the height of the cryostat bottom above the liquid helium level. The temperature fluctuation in each annealing is within 0.1 degree in the range between 4 K and 30 K.

§3. Results

Au-Fe alloy films with the iron concentrations, 2, 5, 10, 20, 40, 60 and 80at.%, respectively are condensed in mica substrate at 5K in the vacuum of 5×10^{-8} Torr. Figures 44, 45, 46, 47, 48, 49 and 50 show their temperature dependence of the electrical resistivity after annealing successively up to the temperatures indicated in the figures. Below the annealing temperature the measurements of the resistivity are always reversible. The electrical resistivity minimun is observed throughout the whole concentration range of iron. By annealing at 300 K, the resistivity increase at low temperature becomes smaller or disapper. The films which contain iron more than 40at.% are found to be amorphous. It is evident from the abrupt decrease in resistivity during annealing that the crystallization occurs at a certain temperature mostly below room temperature.

Au-40at.%Fe film transforms to fcc at 200 K, Au-60at.%Fe to bcc at 270 K and Au-80at.%Fe to bcc at 90 K, respectively. On the other hand, below 20at.% of iron concentration, the films are fcc in the as-deposited state at 5 K. This is obvious from the fact that, in these films, the irreversible part of the resistivity as a function of temperature gives no indication of a phase change and only decreases monotonously, and the diffraction pattern after annealing up to 300 K shows fcc polycrystalline structure.

Similar study is performed for pure iron films. Figure 51 shows the temperature dependence of electrical resistivity of an amorphous iron film which is deposited on the helium temperature substrate in a vacuum of 2×10^{-5} Torr and warmed up to the temperatures indicated in the figure. Resistance minima and their change with the annealing temperature are clearly seen. This film shows a sharp drop of resistivity at around 60 K corresponding to the amorphous-crystalline transition. When the vacuum degree is as high as 10^{-9} Torr, the film is crystalline from the beginning, but the resistance minimum is still observed as shown in Fig. 52. The resistances in Fig. 51 decrease linearly with the logarithmic temperature increase at low temperatures, so that the following empirical equation can be obtained for all curves:

$$\rho(T) = \rho_o + \rho_1 (T) - A \ln T$$

where ρ_o is the residual resistivity, $\rho_1 (T)$ is the normal resistivity change caused by the temperature scattering, and $- A \ln T$ is the anomalous part which produces the minimum. Since A decreases with annealing temperature as well as ρ_o, a simple relation is to be expected between them. Actually, as in Fig. 53, through the whole temperature range above and below the amorphous-crystalline transition, a linear relation,

$$\rho_o = \rho_{oo} + \text{const. } A,$$

is obtained. ρ_o is considered to represent the amount of lattice defects contained in the film.

§4. Discussion

Lin[6] first showed the resistance minimum at low temperature of a ferromagnetic amorphous alloy of Fe-P-C made by rapid cooling from the melt. The resistance minimum was also found in a rapidly cooled deposited film of iron and other materials by Lazarev et al[32]. However, it is clarified in our study that this behaviour does not show an essential difference between the amorphous and crystalline states. Because, the resistivity minimum can be observed even in the defective crystalline state.

Explanation of the resistivity minimum in ferromagnetic amorphous and crystalline films is difficult. Difference from the case of the Kondo effect, which arises from the interaction between the flipping magnetic moments of dilute impurity atoms and conduction electrons, all atoms in the ferromagnetic film are considered to have fixed moments. Hasegawa et al[33] and Kaneyoshi et al[34] discussed the minimum in amorphous alloys as originated from electron magnon interaction. Recently another model based on a nonmagnetic nature of amorphous materials has been proposed by Cochran et al[35]. In such a manner the resistivity minimum in ferromagnetic materials is not conclusively clarified yet.

However, our result that the minimum is observed throughout the whole concentration range of iron, supports the coexistence of Kondo minimum and ferromagnetism, since it is difficult to assume that at lower iron concentration the minimum is caused by Kondo effect, while,at higher iron concentration, it is caused by

entirely another mechanism. If it is assumed that among the ferromagnetically aligned rigid moments there exist some unstable flippable moments associated with lattice defects, then an interaction of them with conduction electrons similar to that in the Kondo effect could be expected. As the number of such moments may be proportional to the total amount of lattice defects contained in the film. A decrease of the lattice defects reduces unstable moments. Consequently, it is natural to expect that linear relation exists between residual resistivity and pre-logarithmic factor A.

The fact that the character of the resistivity minimum can be described without discontinuity through the amorphous and crystalline states and, in addition, can be expressed, by the amount of lattice defects strongly suggests that there is no essential difference between the two states with respect to the lattice defect structure. As an extreme expression, one could state that the amorphous film can be regarded as very defective micro-crystalline aggregates.

Summary and Conclusions

The experimental results and conclusions in the present study are summarized as follows.

1) Au-Si films vacuum deposited on the room temperature substrate always appear as the micro-crystalline state when the silicon concentration is below 50at.%, and more than 65at.% is neccessary to obtain the amorphous state.

2) In Au-30at.%Si alloy films, migration of silicon atoms toward the surface takes place preferably in the oxidizing atmosphere, which forms the silicon oxide layer on the film surface.

3) The Au-65at.%Si amorphous film transforms to a metastable structure on heating up to about 100°C and then to stable eutectic mixture at about 200°C. The obtained activation energies of these processes, the direct observation by electron microscope, and the electrical resistivity changes during annealing are consistent with each other, and are well accounted for by a proposed model for the transformation of amorphous Au-Si alloys.

4) The strain energy stored in the gold film deposited on silicon film could be the driving force for the transformation of the Au-Si bi-layer film into a amorphous-like mixed phase.

5) The resistivity minimum appeared in ferromagnetic amorphous and crystalline films of Au-Fe alloys and pure iron is closely related with their defect structures, and it is strongly suggested that there is no essential difference in the atomic arrangement and electronic state between the defect structures of amorphous and crystalline materials.

Acknowledgements

The author would like to express his hearty thanks to Prof. F. E. Fujita for continuous guidance, valuable discussions and encouragements throughout the course of this study and also to Prof. M. Kiritani for his kind encouragements.

He wishes to express his appreciation to Dr. K. Yamakawa for valuable discussions and advices, and to Dr. R. Oshima and T. Sohmura for many helpful suggestions. Thanks are also due to Mr. T. Hamada, C. Fujita, S. Soematsu and S. Fujimura for their assistance in the experiments and to Miss T. Ohkubo for her great help in the preparation of the paper.

References

1) C. C. Tsuei: Phys. Rev., 170 (1968) 775.

2) P. Duwez and S.C.H. Lin: J. Appl. Phys., 38 (1967) 4096.

3) C. C. Tsuei and P. Duwez: J. Appl. Phys., 37 (1966) 435.

4) W. Buckel and R. Hilsch: Z. Phys., 138 (1954) 109.

5) H. L. Luo, M. F. Merriam and D. C. Hamilton: Science., 145 (1964) 581.

6) S. C. H. Lin: J. Appl. Phys. 40 (1969) 2173.

7) A. Hiraki, E. Luqujjo and J. W. Mayer: J. Appl. Phys. 43 (1972) 3643.

8) A. Hiraki, A. Shimizu, M. Iwami, T. Narusawa and S. Komiya: Appl. Phys. Lett. 26 (1975) 57.

9) A. Hiraki, M. Iwami: Proc. 2nd Internl. Conf. on Solid Surfaces, 1974 Japan J. Appl. Phys. Suppl. 2, Pt. 2, (1974) 749.

10) C. Suryanarayana and T. R. Anantharaman: Mater. Sci. Eng., 13 (1974) 73.

11) H. L. Luo, W. Klement, Jr., and T. R. Anantharaman: Trans. Indian Inst. Metals, 18 (1965) 214.

12) P. Predecki, B. C. Giessen and N. J. Grant: Trans. AIME, 233 (1965) 1438.

13) G. A. Anderson, J. L. Bestel, A. A. Johnson and B. Post: Mater. Sci. Eng., 7 (1971) 83.

14) W. Klement, Jr., R. H. Willens and P. Duwez: Nature, 187 (1960) 869.

15) J. Dixmier and A. Guinier: Rev. Metallurgie., 64 (1967) 53.

16) P. J. Ford, T. E. Whall and J. W. Loran: Phys. Rev. B, 2 (1970) 1547.

17) C. di Capua: Red. accad. nazl. Lincei, 29 (1920) 111.

18) E. R. Jette and E. B. Gebert: J. Chem. Phys., 1 (1933) 753.

19) R. P. Elliott: Constitution of Binary Alloys, First Supplement, McGraw-Hill (1965)

20) E. G. Heath: J. Electron Control, 11 (1961) 13.

21) W. Gerlach and B. Goel: Solid State Electronics, 10 (1967) 589.

22) R. P. Anantatmula, A. A. Johnson, S. P. Gupta and R. J. Horylev: J. Electron Mater, 4 (1975) 445.

23) N. F. Mott and H. Jones: The Theory of the Properties of Metals and Alloys, Dover Publications. Inc. 1958 Chap. 6.

24) E. Philofsk, K. V. Ravi, J. Brooks and E. Hall: J. Electochem. Soc., 119 (1972) 527.

25) C. A. Wert and R. M. Thomson: Physics of Solid, (McCraw-Hill, Inc. 1970) Chap. 4.

26) B. Okkerse. A. H. Rowe and A. D. Leclaire; Proc. Phys. Soc., B70 (1957), 545.

27) H. S. Chen and D. Turnbull: J. Chem. Phys., 48 (1968) 2560.

28) H. S. Chen and D. Turnbull: J. Chem. Phys., 38 (1967) 3646.

29) H. S. Chen and D. Turnbull: J. App. Phys., 40 (1969) 4214.

30) K. Chopra: Thin Film Phenomena (McGrow-Hill, Inc. 1969) Chap. 5.

31) J. Kondo: Progr. Theor. Phys. 32 (1964) 37.

32) B. G. Lazarev, V. M. Kuz'menko, A. I. Sudovtsov and V. I. Mel'nikov: Soviet Physics-JETP 17 (1973) 917.

33) R. Hasegawa and J. A. Demon: Phys. Letters 42A (1973) 407.

34) T. Kaneyoshi and R. Honmura: Phys. Letters 46A (1973) 1.

35) R. W. Cochrane, R. Harris, J. O. Ström-Olson and M. J. Zuckermann: Phys. Rev. Letters, 35 (1975) 676.

Figure Captions

Fig.1 The phase diagram of Au-Si system.

Fig.2 Schematic representation of cross section of the cryostat.

Fig.3 Schematic representation of the ultra-high vacuum system.

Fig.4 Transmission electron micrograph (a) and diffraction pattern (b) of gold film deposited at room temperature.

Fig.5 Transmission electron micrograph (a) and diffraction pattern (b) of silicon film deposited at room temperature.

Fig.6 Transmission electron micrograph (a) and diffraction pattern (b) of Au-30at.%Si film immediately after deposition at room temperature in a vacuum of 3×10^{-5} Torr.

Fig.7 Transmission electron micrograph (a) and diffraction pattern (b) of Au-50at.%Si film immediately after deposition at room temperature in a vacuum of 2×10^{-5} Torr.

Fig.8 Transmission electron micrograph (a) and diffraction pattern (b) of Au-65at.%Si film immediately after deposition at room temperature in a vacuum of 2×10^{-5} Torr.

Fig.9 Transmission electron micrograph (a) and diffraction pattern (b) of Au-80at.%Si film immediately after deposition at room temperature in a vacuum of 3×10^{-5} Torr.

Fig.10 The electrical resistance decay of vacuum deposited Au-30at.%Si film exposed to air at room temperature.

Fig.11 Transmission electron micrograph (a) and diffraction pattern (b) of Au-30at.%Si film deposited at room temperature and annealed at 150°C for 10 minutes in air.

Fig.12 Reflection electron diffraction patterns of Au-30at.%Si film; (a) immediately after deposition, (b) after annealing at 150°C for 10 minutes in air, and then (c) after etching with CP-4 for 15 seconds.

Fig.13 Transmission electron micrograph of Au-30at.%Si film deposited at room temperature and annealed up to 300°C in a vacuum of $3x10^{-5}$ Torr.

Fig.14 The electrical resistivity changes of Au-30at.%Si films during heating in vacuum (curve 1) and in air (curve 2). Heating rate is 5°C/min.

Fig.15 Isothermal resistivity decay curves for Au-30at.%Si film deposited at room temperature.

Fig.16 Electrical resistivity change of amorphous Au-65at.%Si film during heating in vacuum. Heating rate is 5°C/min.

Fig.17 Electrical resistivity change of amorphous Au-65at.%Si film during heating in air. Heating rate is 5°C/min.

Fig.18 Electron diffraction pattern of Au-65at.%Si film deposited at room temperature and aged for 10 months in air at that temperature.

Fig.19 Transmission electron micrograph (a) and diffraction pattern (b) of Au-65at.%Si film annealed up to 100°C on the hot stage of electron microscope.

Fig.20 Transmission electron micrograph (a) and diffraction pattern (b) of Au-65at.%Si film annealed up to 150°C on the hot stage of electron microscope.

Fig.21 Transmission electron micrograph (a) and diffraction pattern (b) of Au-65at.%Si film annealed up to 200°C on the hot stage of electron microscope.

Fig.22 Transmission electron micrograph (a) and diffraction pattern (b) of Au-65at.%Si film annealed up to 220°C on the hot stage of electron microscope.

Fig.23 Transformation sequence of amorphous Au-65at.%Si film deposited at room temperature.

Fig.24 Isothermal resistivity decay curves for Au-65at.%Si film deposited at room temperature.

Fig.25 Transmission electron micrographs (a) and selected area diffraction patterns (b) and (c) of Au-65at.%Si film annealed at 450°C. The diffraction patterns show co-existence of silicon crystallites and liquid Au-Si.

Fig.26 The photometrical traces of electron diffraction pattern of amorphous Au-Si, liquid Au-Si and gold films.

Fig.27 Transmission electron diffraction pattern of fcc structure of Au-Si films.

Fig.28 Transmission electron diffraction pattern of simple cubic structure of Au-Si film.

Fig.29 Transmission electron micrograph (a) and diffraction pattern (b) of Au-Si bi-layer film deposited at room temperature.

Fig.30 Transmission electron micrograph (a) and diffraction pattern (b) of Au-Si bi-layer film deposited at room temperature and annealed up to 130°C.

Fig.31 Transmission electron micrograph (a) and diffraction pattern (b) of Au-Si bi-layer film deposited at room temperature and annealed up to 180°C.

Fig.32 Transmission electron micrograph (a) and diffraction pattern (b) of Au-Si bi-layer film deposited at room temperature and annealed up to 220°C.

Fig.33 Transmission electron micrograph (a) and diffraction pattern (b) of Au-Si bi-layer film deposited at room temperature and annealed up to 350°C.

Fig.34 Transmission electron diffraction pattern of Au-Si bi-layer film annealed up to 220°C (a), amorphous Au-65at.%Si alloy (b).

Fig.35 Transmission electron diffraction patterns of Au-Si bi-layer film. Gold is deposited on polycrystalline silicon. (a) is as deposited and (b) is at 250°C.

Fig.36 Transmission electron diffraction pattern of Au-Si bi-layer film annealed at 250°C. The film is made by evaporating silicon at room temperature after deposition of gold at 300°C.

Fig.37 Transmission electron micrograph (a) and diffraction pattern (b) of Au-Si bi-layer film deposited at 100°C.

Fig.38 Transmission electron micrograph (a) and diffraction pattern (b) of Au-Si bi-layer film deposited at 130°C.

Fig.39 Transmission electron micrograph (a) and diffraction pattern (b) of Au-Si bi-layer film deposited at 150°C.

Fig.40 Transmission electron micrograph (a) and diffraction pattern (b) of Au-Si bi-layer film deposited at 180°C.

Fig.41 Transmission electron diffraction pattern of Au-Si bi-layer film deposited at 130°C and annealed at 180°C.

Fig.42 Temperature dependence of the average intrinsic stress in films of Permalloy, copper, iron and nickel (after K. Chopra[30]).

Fig.43 Sehematic representation of cross section of the cryostat for low temperature.

Fig.44 The temperature dependence of the electrical resistivity of Au-2at.%Fe film deposited at 5 K, and warmed up to the temperatures indicated in the figure.

Fig.45 The temperature dependence of the electrical resistivity of Au-5at.%Fe film deposited at 5 K, and warmed up to the temperatures indicated in the figure.

Fig.46 The temprature dependence of the electrical resistivity of Au-10at.%Fe film deposited at 5 K, and warmed up to the temperatures indicated in the figure.

Fig.47 The temperature dependence of the electrical resistivity of Au-20at.%Fe film deposited at 5 K, and warmed up to the temperatures indicated in the figure.

Fig.48 The temperature dependence of the electrical resistivity of Au-40at.%Fe film deposited at 5 K, and warmed up to the temperatures indicated in the figure.

Fig.49 The temperature dependence of the electrical resistivity of Au-60at.%Fe film deposited at 5 K, and warmed up to the temperatures indicated in the figure.

Fig.50 The temperature dependence of the electrical resistivity of Au-80at.%Fe film deposited at 5 K, and warmed up to the temperatures indicated in the figure.

Fig.51 The logarithmic temperature dependence of the resistivity of amorphous iron film deposited at 2×10^{-5} Torr and annealed to various temperatures. The arrows indicate the minimum points of the resistivity.

Fig.52 The logarithmic temperature dependence of the resistivity of crystalline iron film deposited at 10^{-9} Torr, and warmed up to the temperatures indicated in the Figure.

Fig.53 The relation of the residual resistivity, ρ_o, and the coefficient of logarithmic part, A, through the amorphous and crystalline state of iron film.

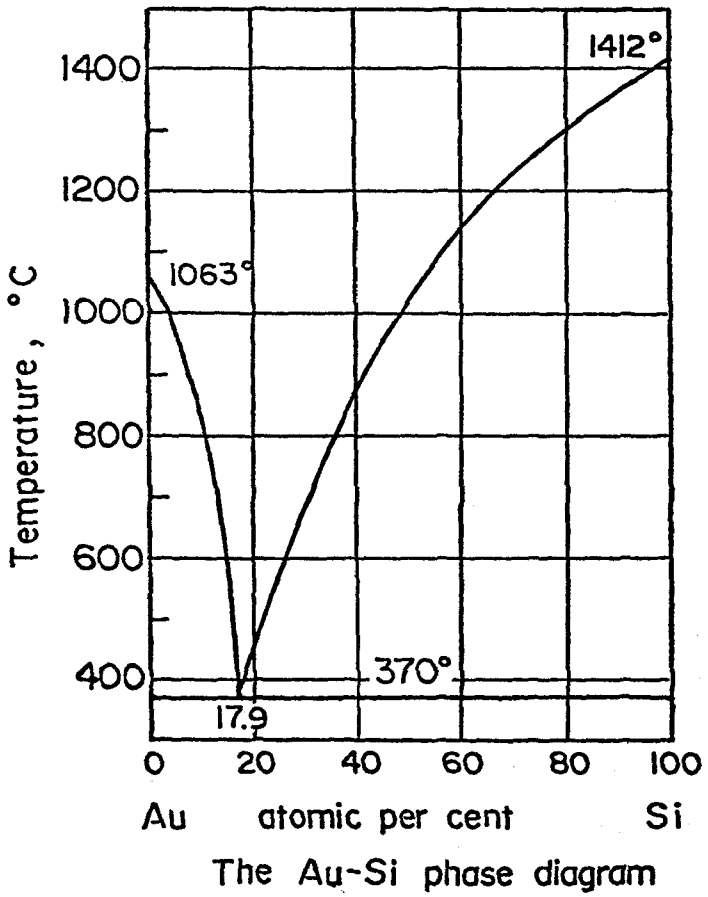

The Au-Si phase diagram

FIG. I

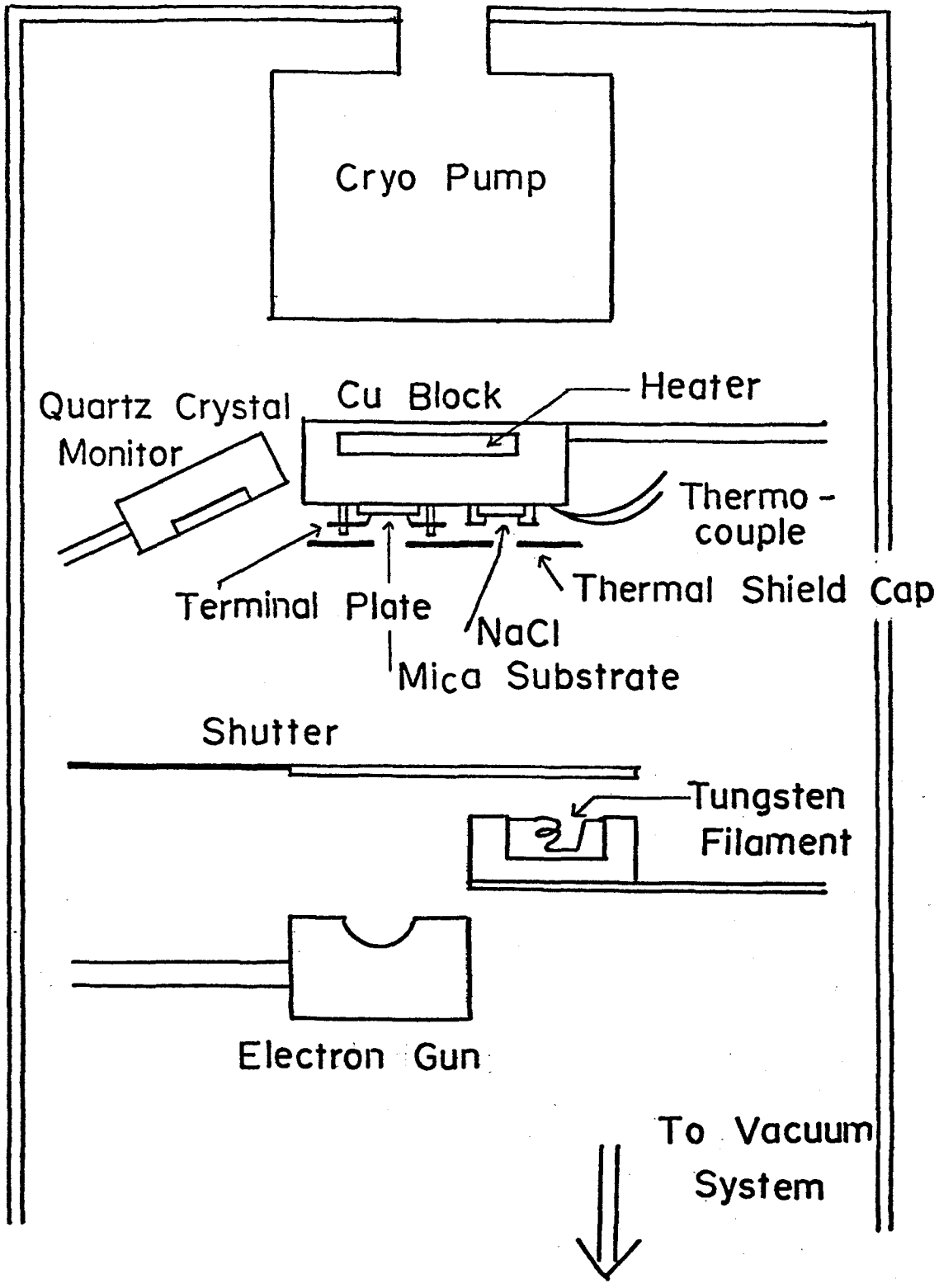
Cryo Pump
Quartz Crystal Monitor
Cu Block
Heater
Thermo - couple
Terminal Plate
NaCl
Mica Substrate
Thermal Shield Cap
Shutter
Tungsten Filament
Electron Gun
To Vacuum System

FIG. 2

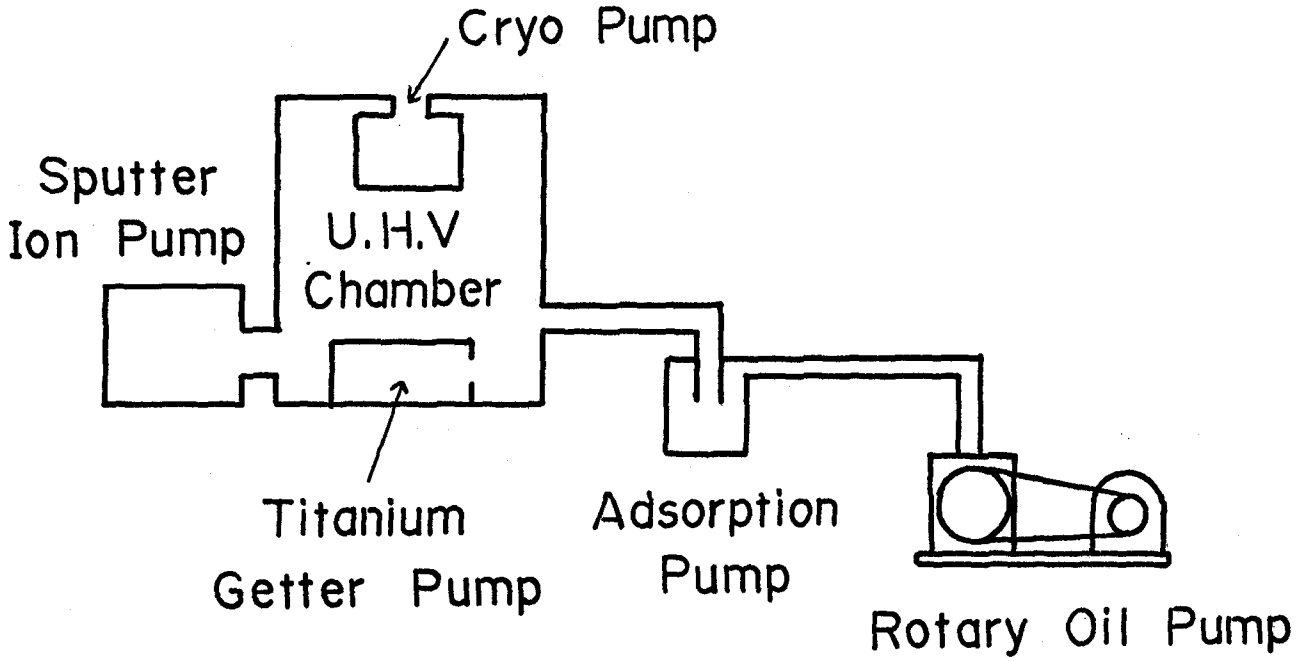
Cryo Pump
Sputter
Ion Pump
U.H.V
Chamber
Titanium
Getter Pump
Adsorption
Pump
Rotary Oil Pump

FIG. 3

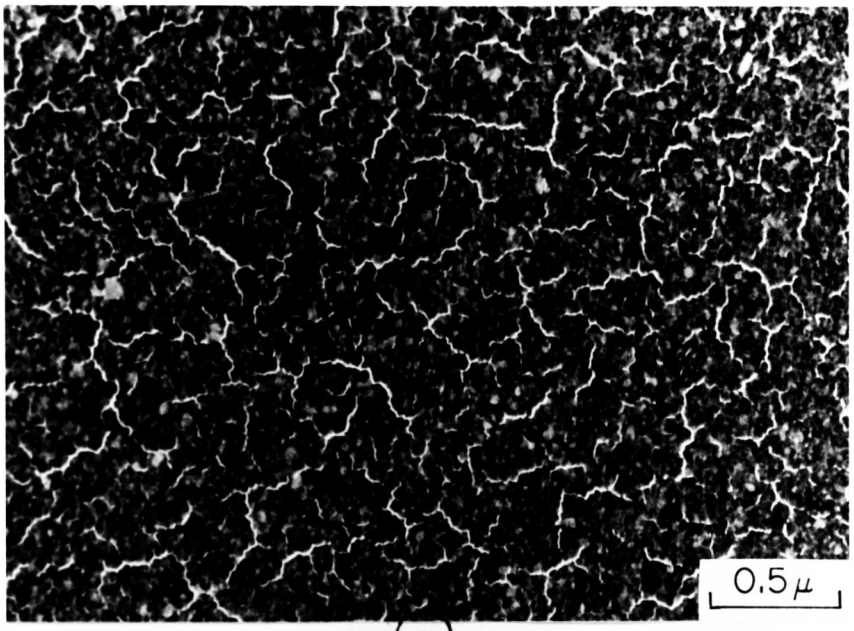

(a)

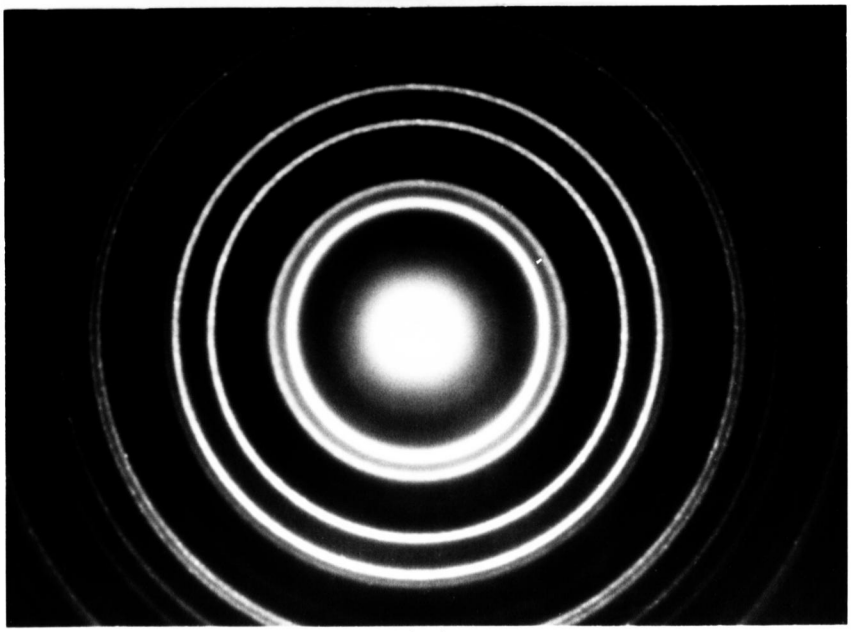

(b)

FIG. 4

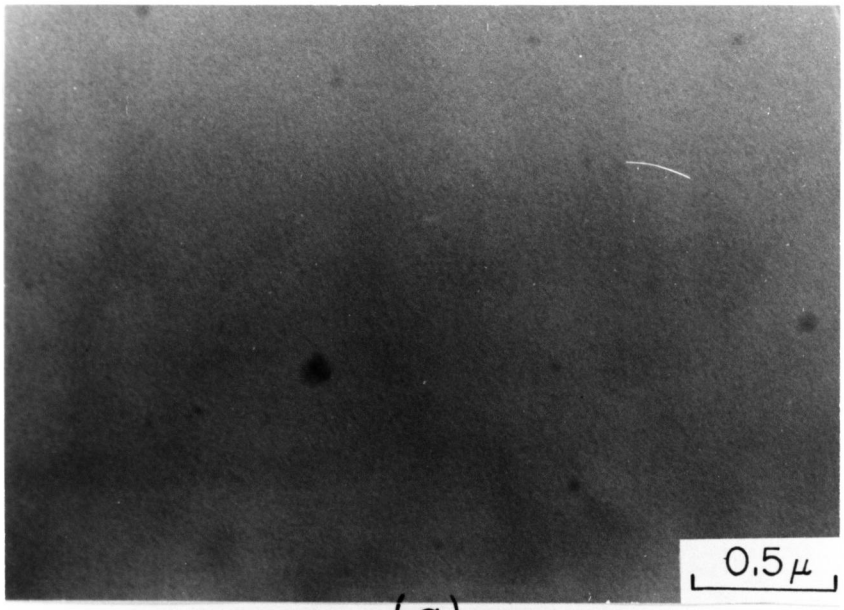

(a)

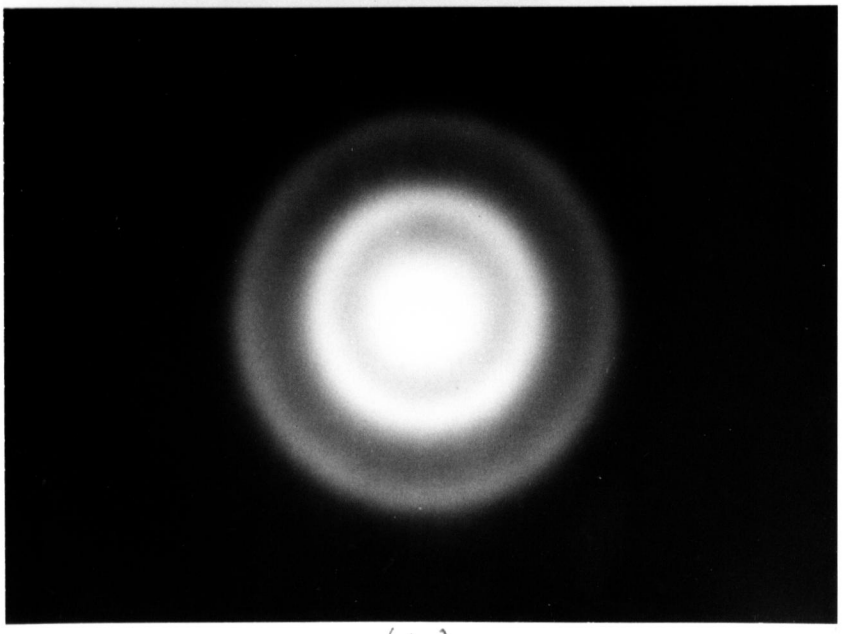

(b)

FIG. 5

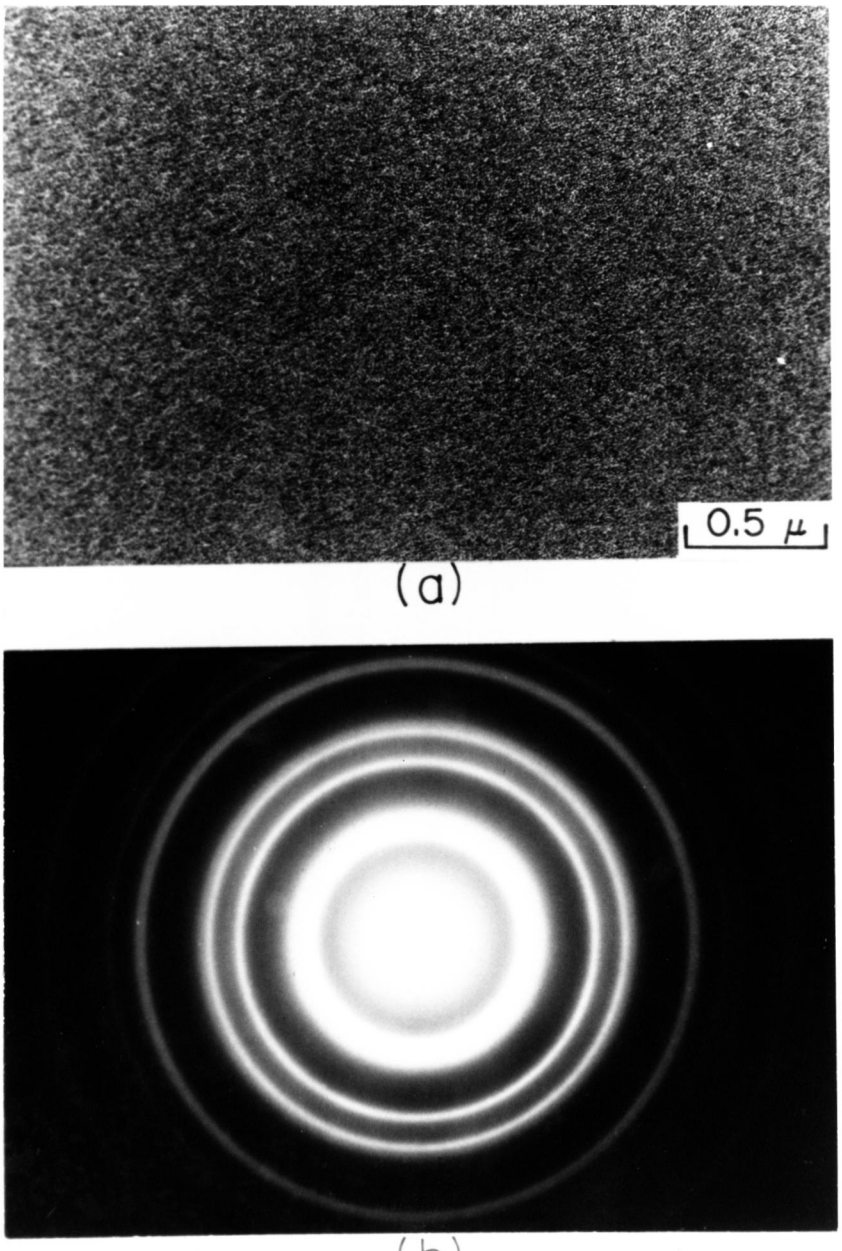

FIG. 6

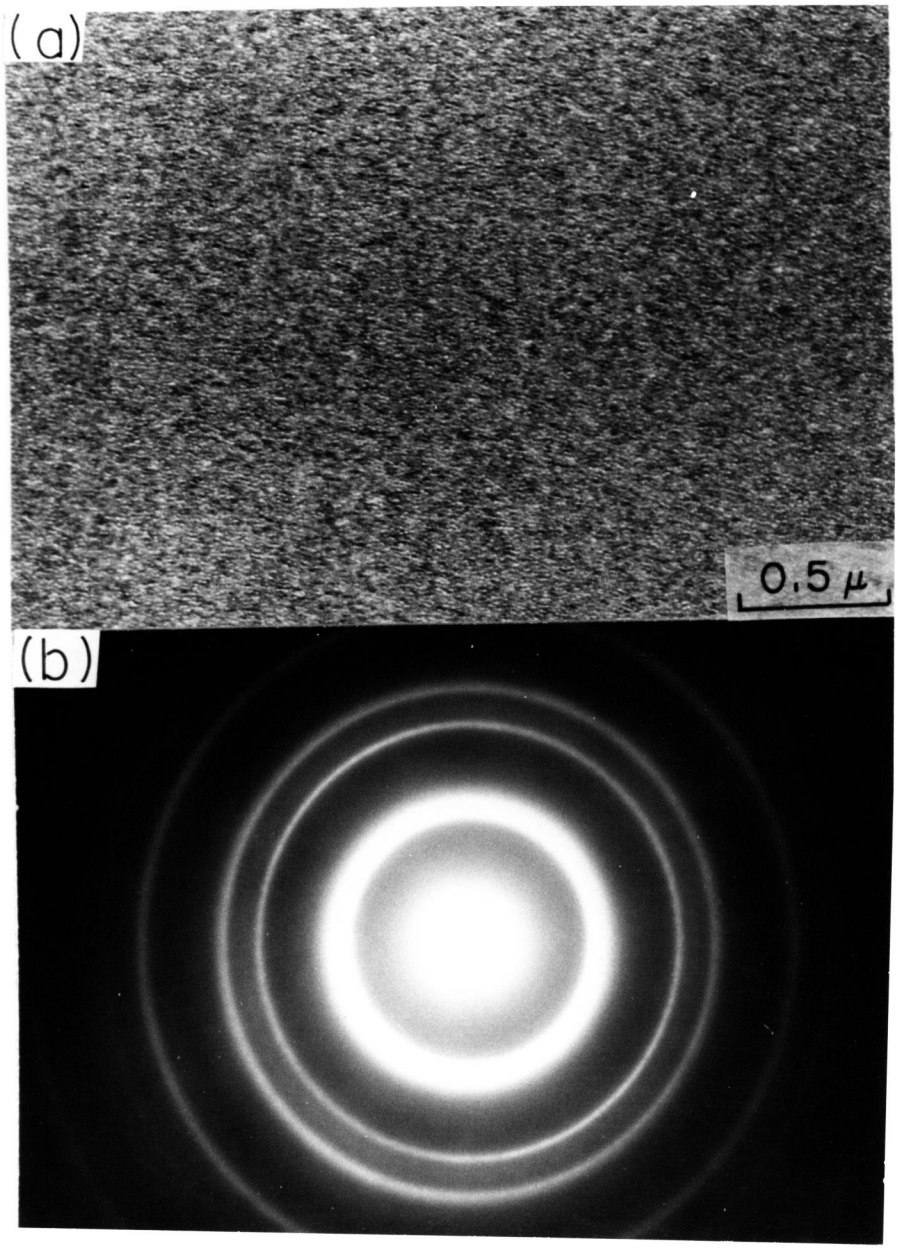

FIG. 7

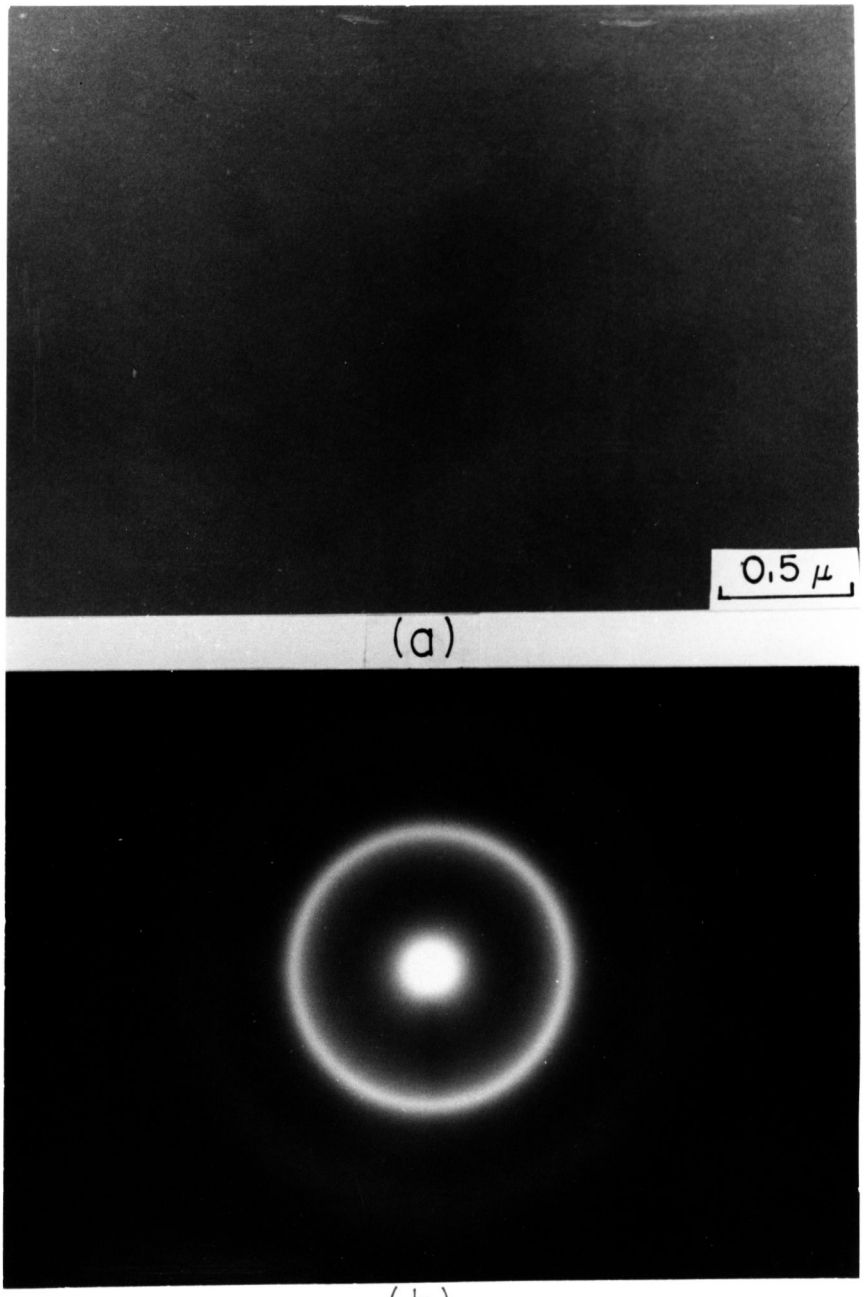

FIG. 8

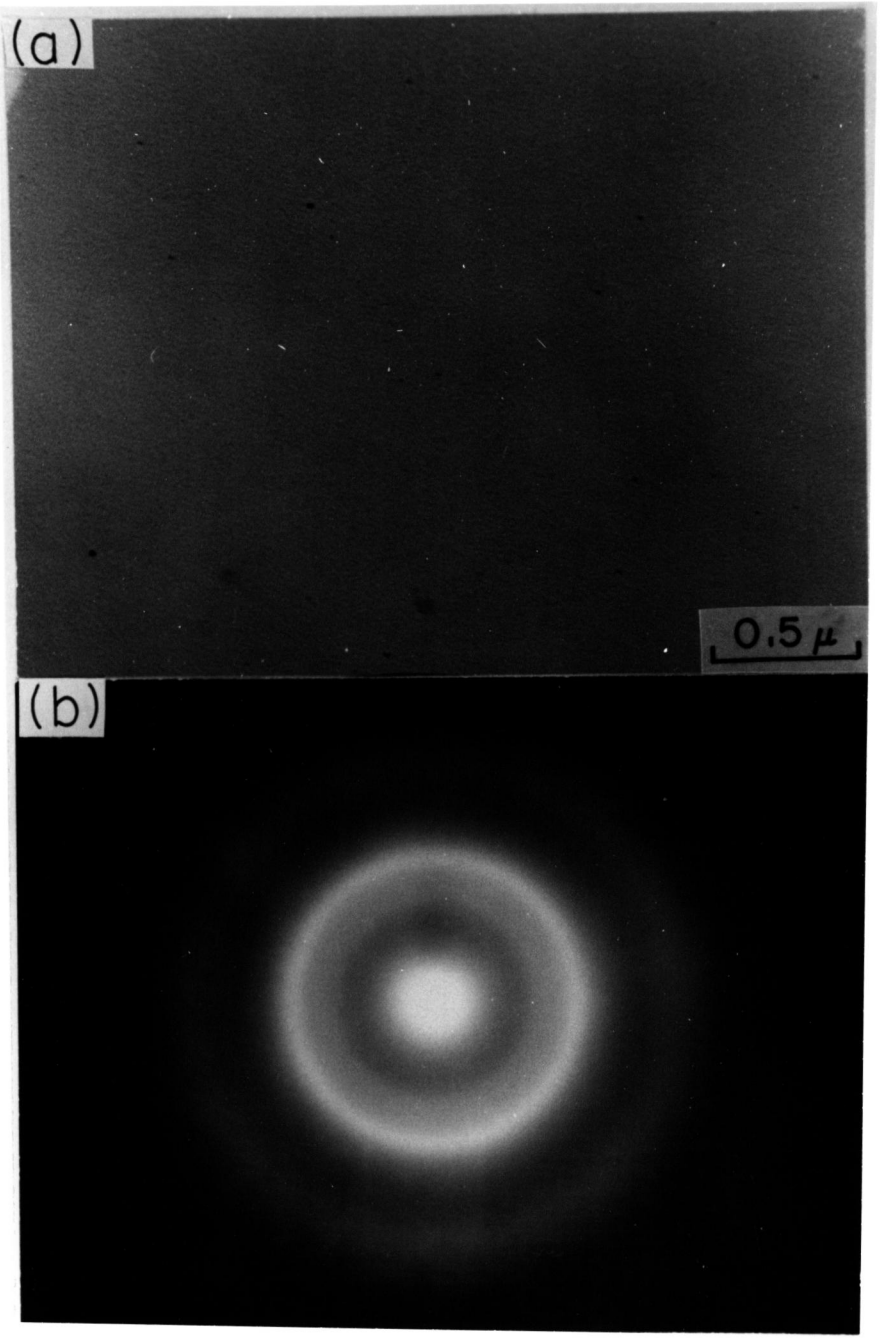

FIG. 9

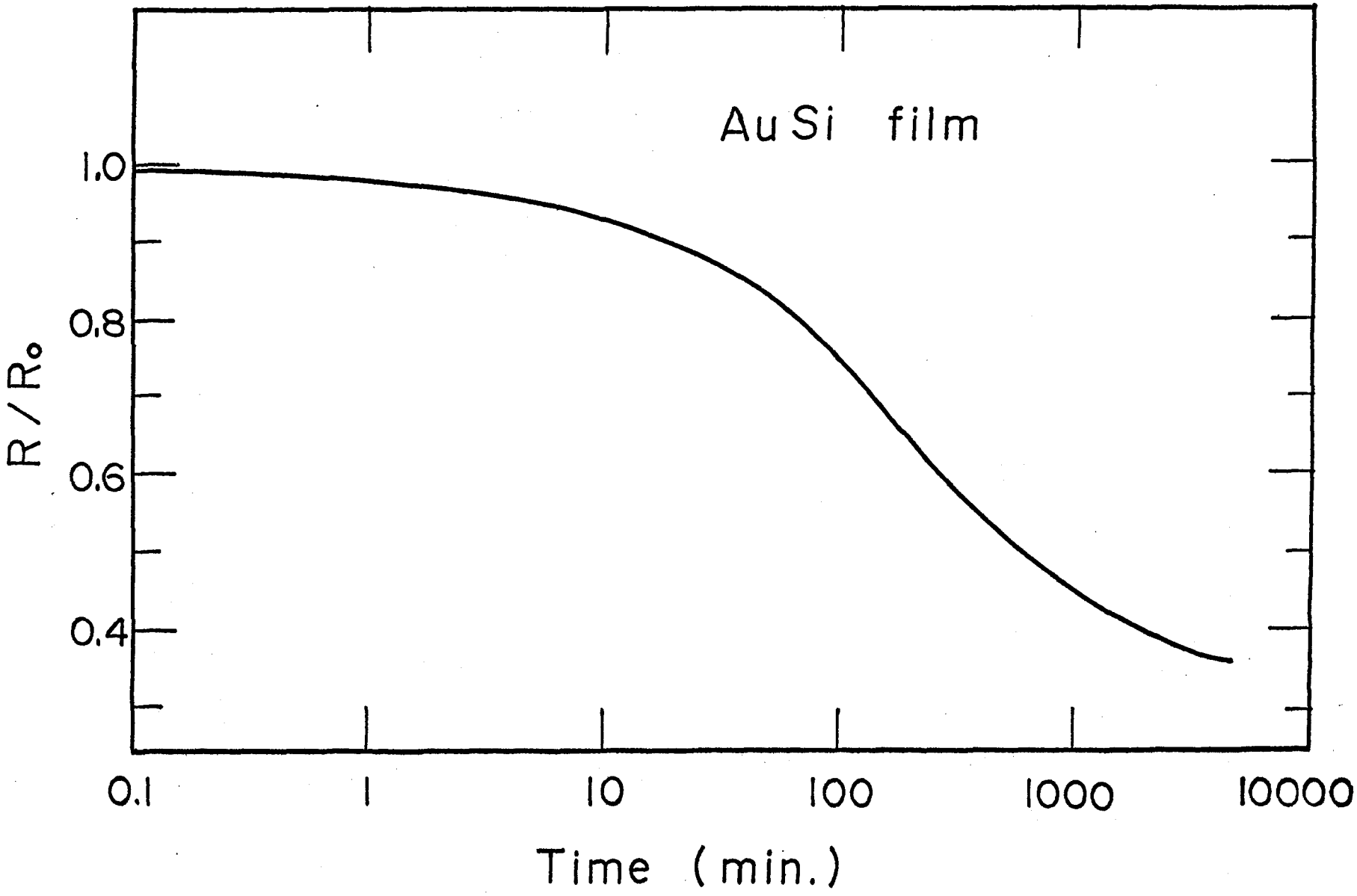

FIG. 10

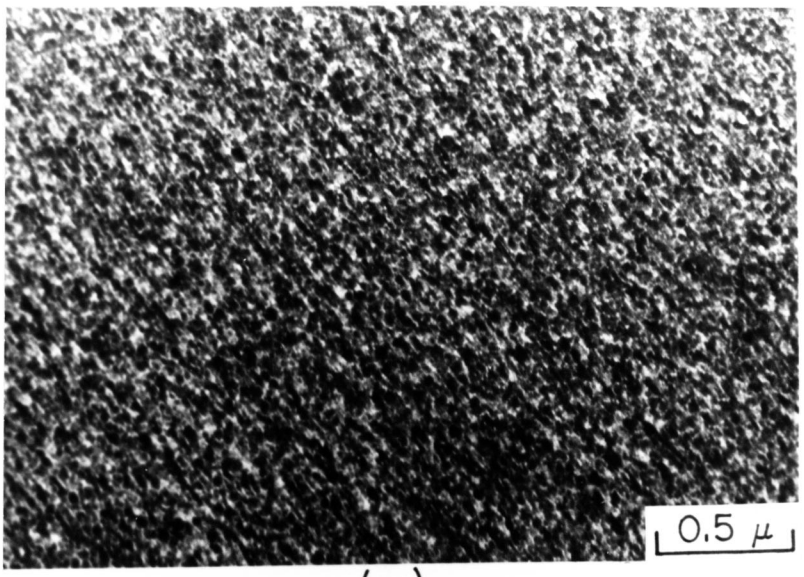

(a)

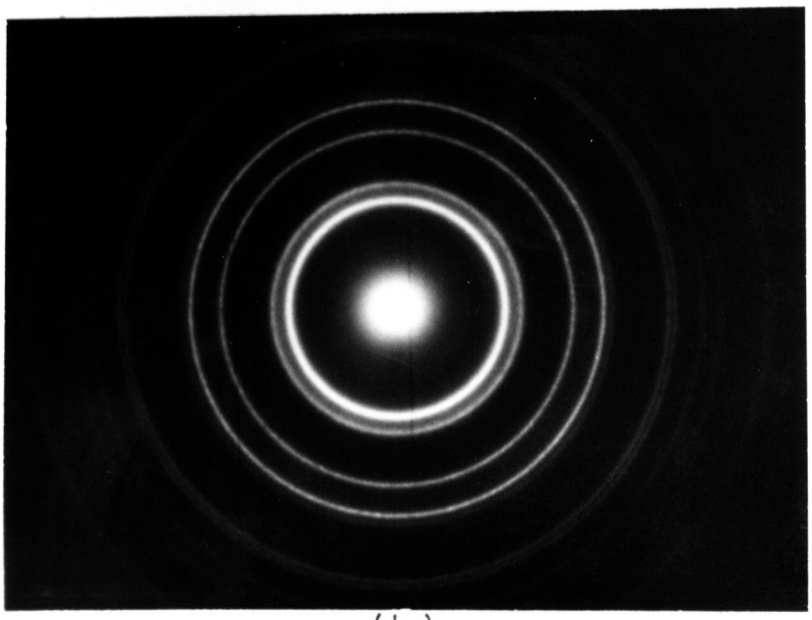

(b)

FIG. II

(a)

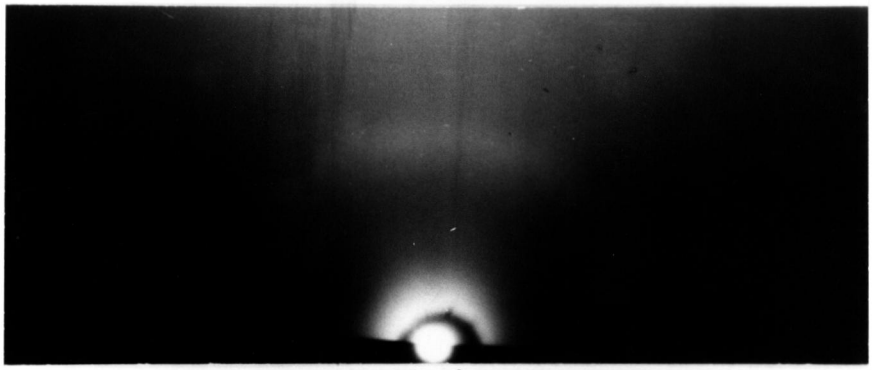

(b)

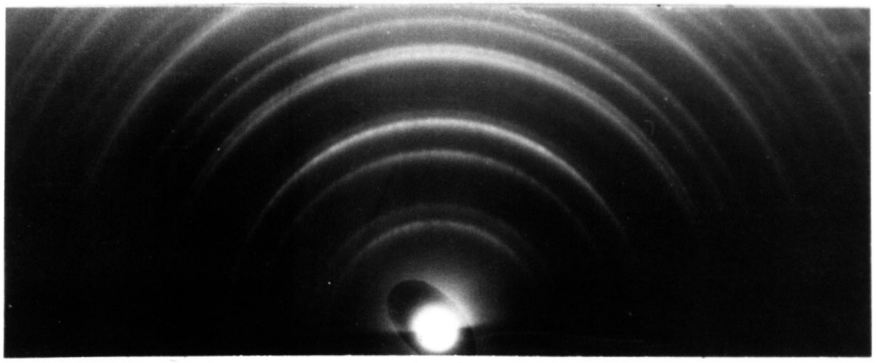

(c)

FIG. I2

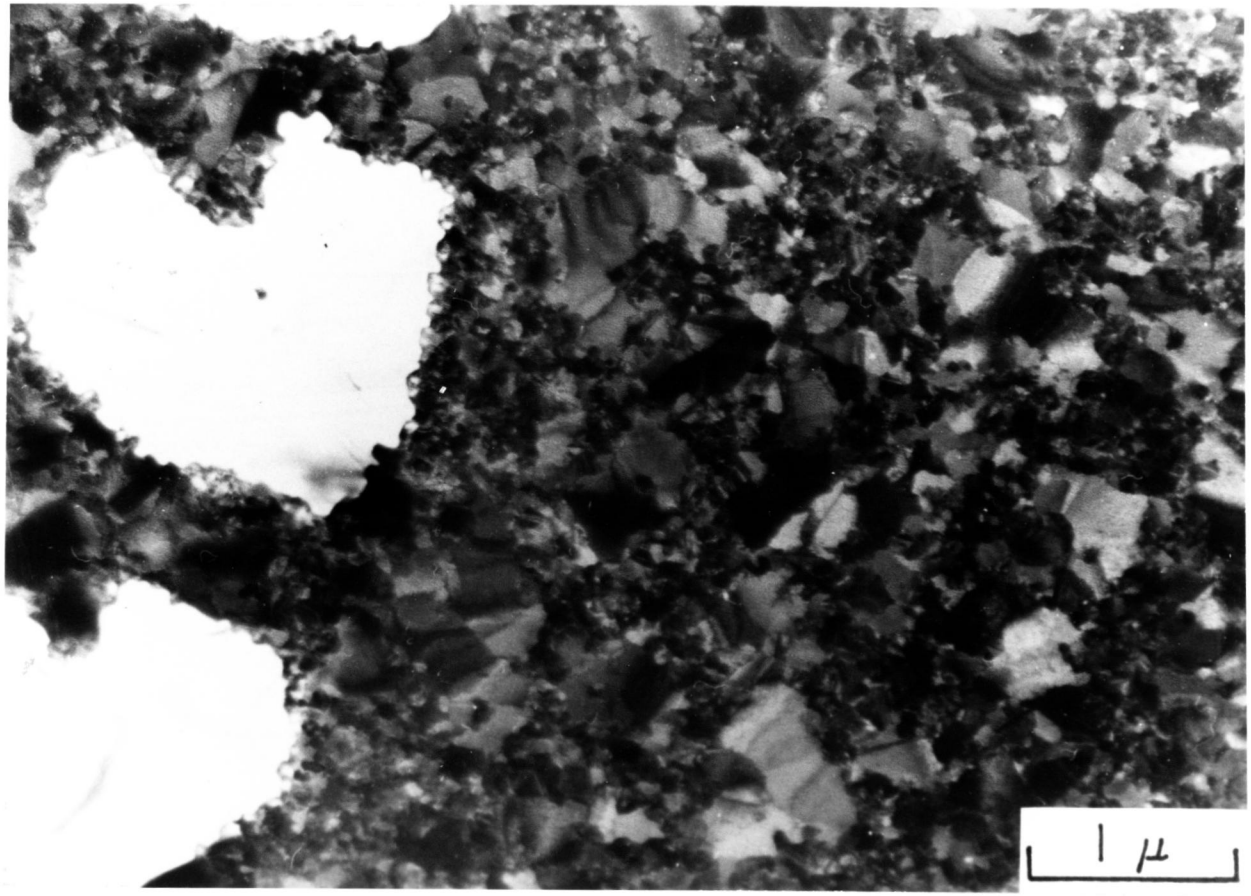

FIG. 13

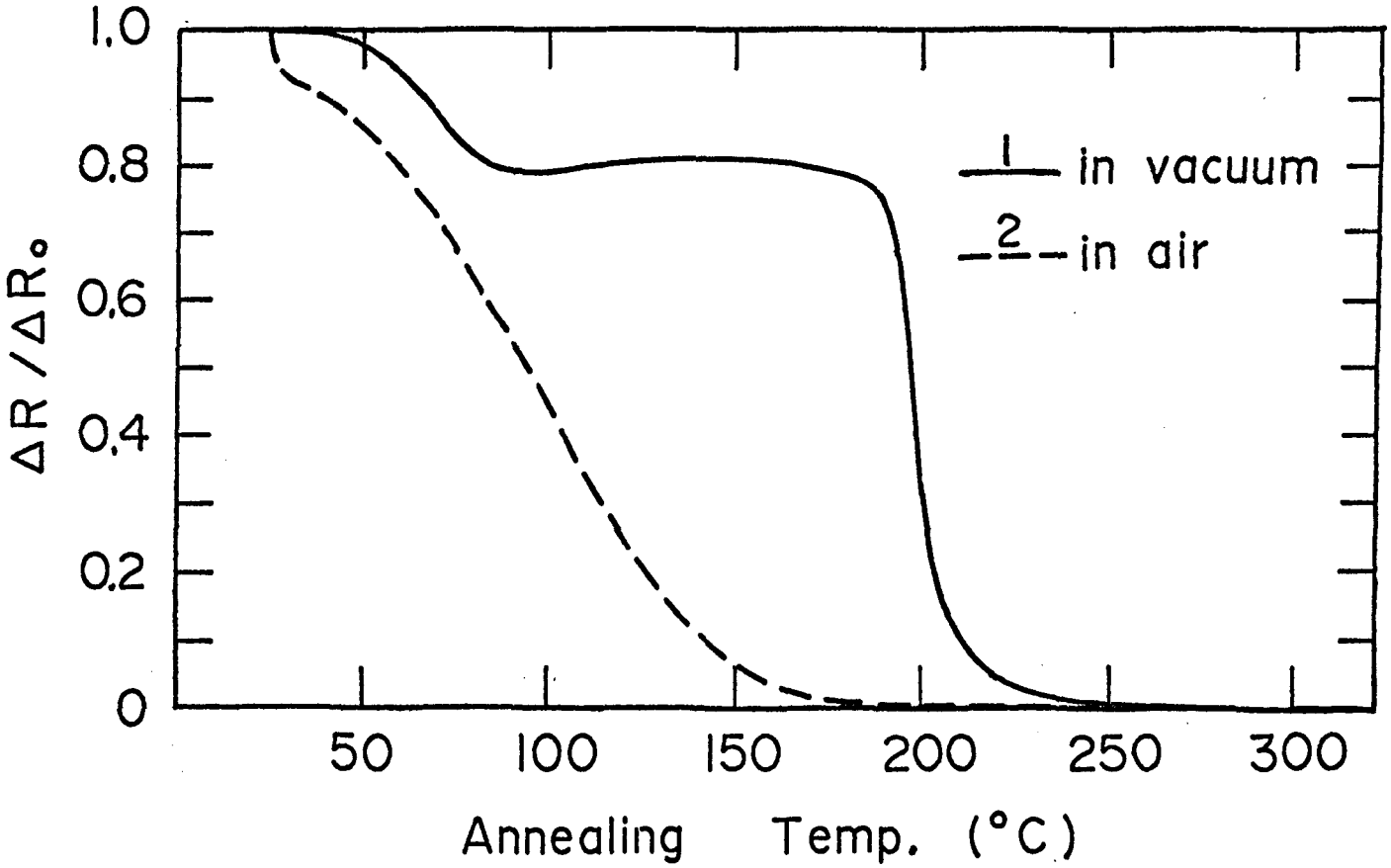
1.0
0.8
0.6
0.4
0.2
0
ΔR / ΔR₀
1 in vacuum
2 in air
50
100
150
200
250
300
Annealing Temp. (°C)

FIG. 14

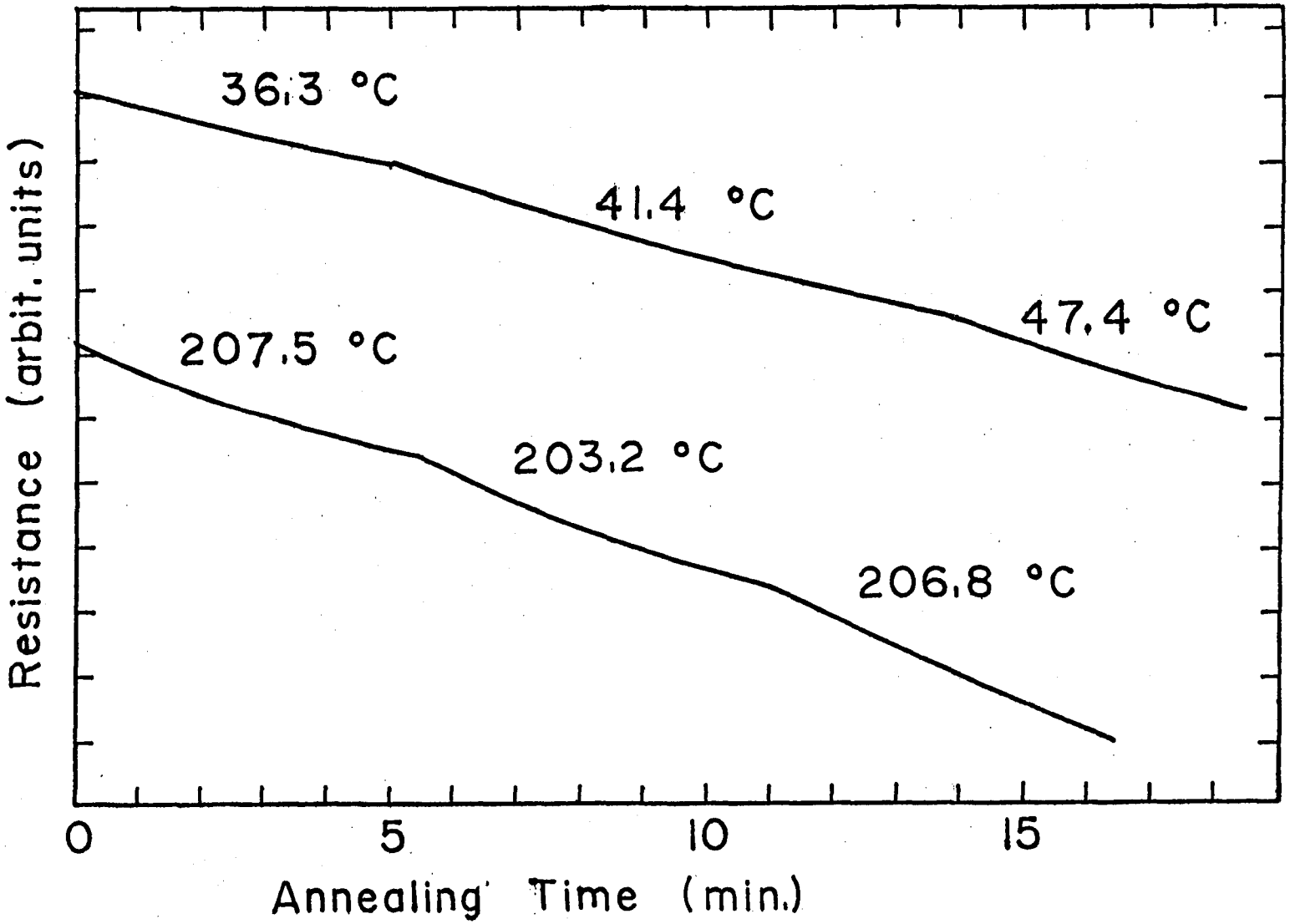
36.3 °C
41.4 °C
47.4 °C
207.5 °C
203.2 °C
206.8 °C
Resistance (arbit. units)
0
5
10
15
Annealing Time (min.)

FIG. 15

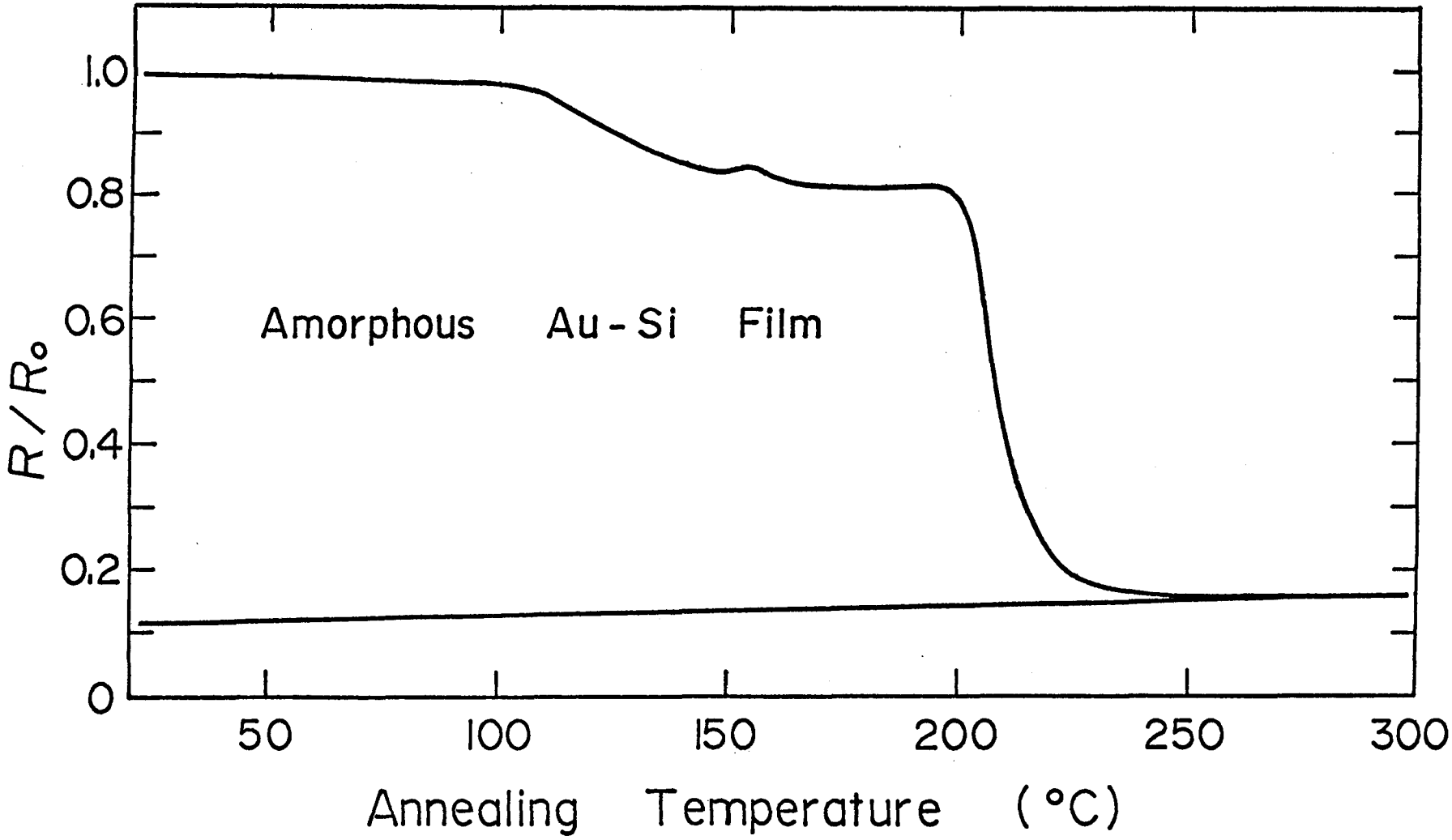
1.0
0.8
0.6
0.4
0.2
0
R/Ro
Amorphous Au-Si Film
50
100
150
200
250
300
Annealing Temperature (°C)

FIG. 16

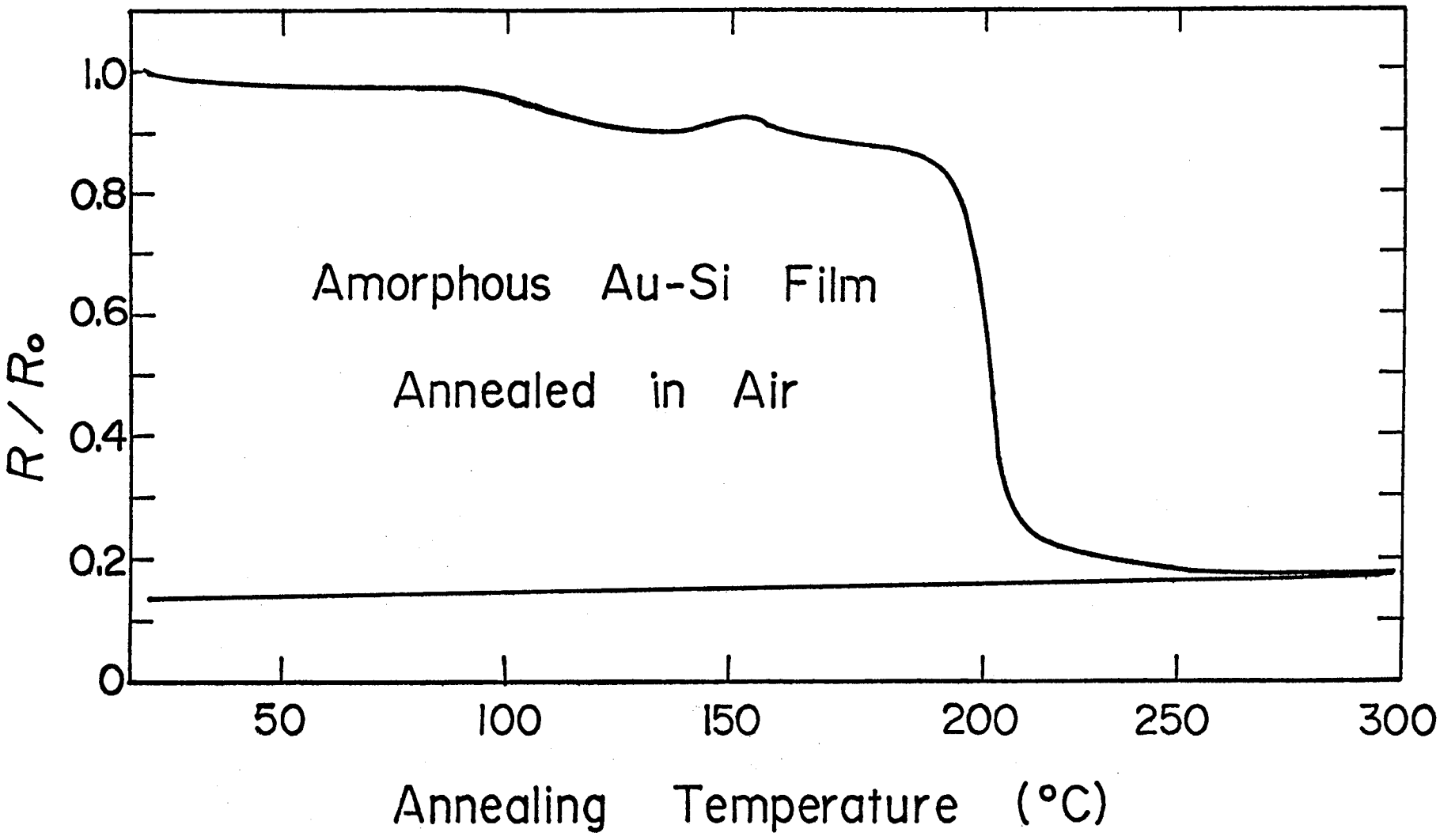
1.0
0.8
0.6
0.4
0.2
0
R / R₀
Amorphous Au-Si Film
Annealed in Air
50
100
150
200
250
300
Annealing Temperature (°C)

FIG. 17

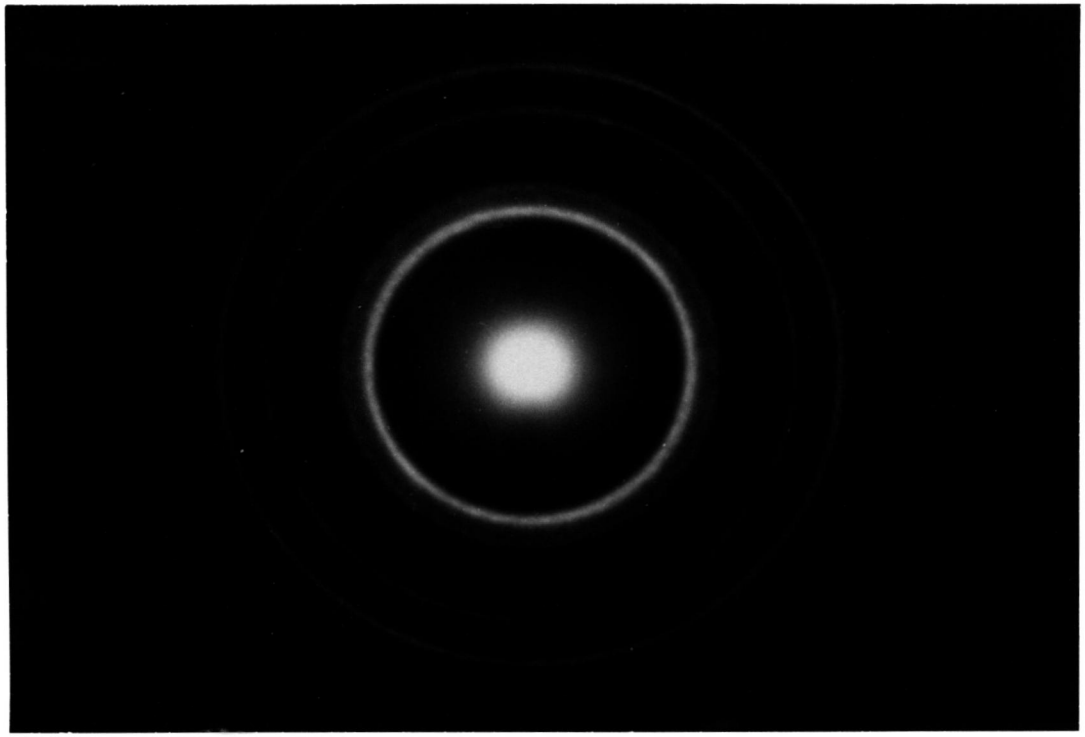

FIG. 18

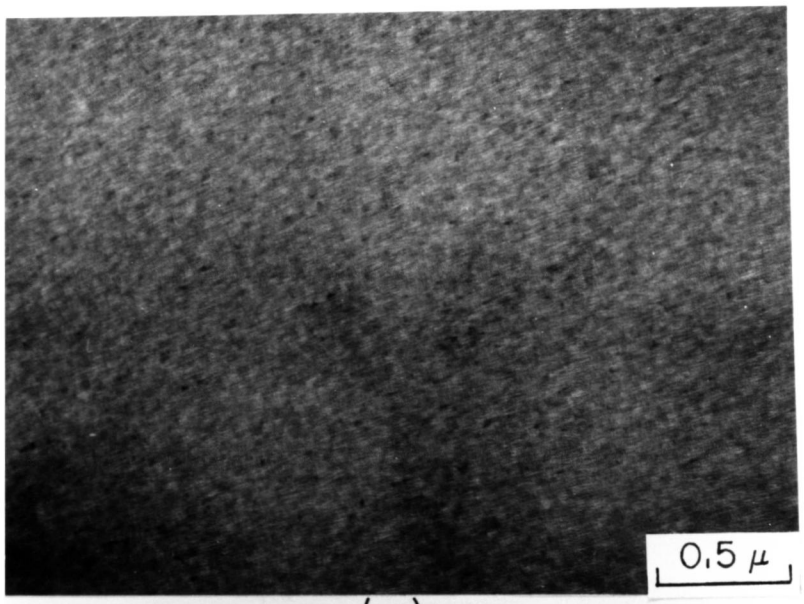

(a)

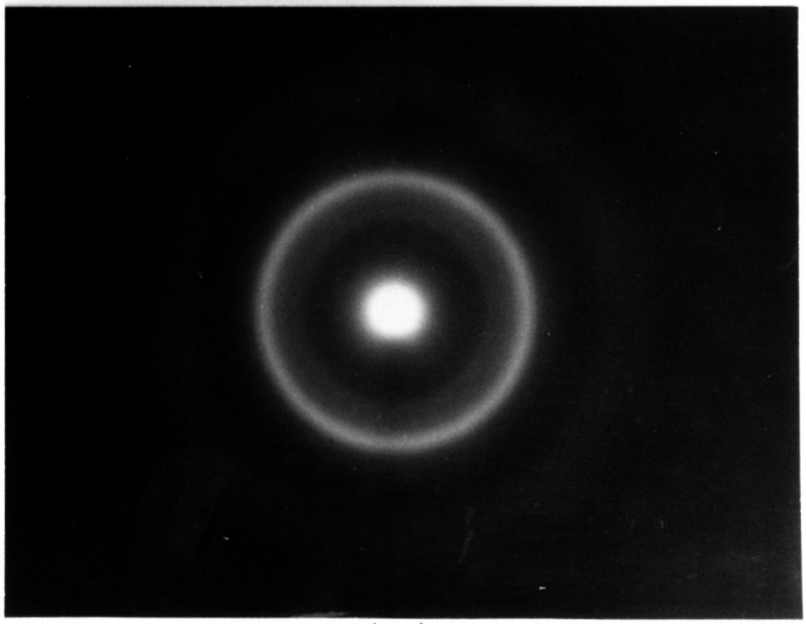

(b)

FIG. 19

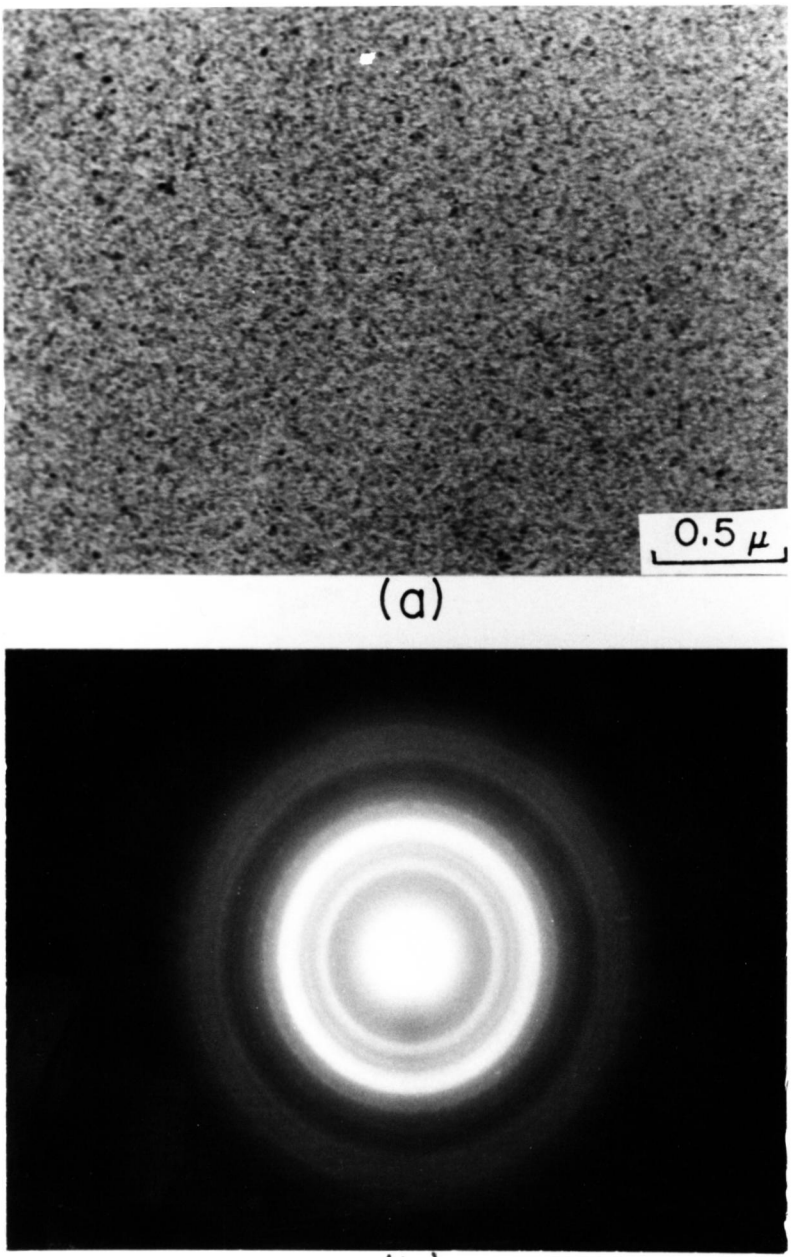

FIG. 20

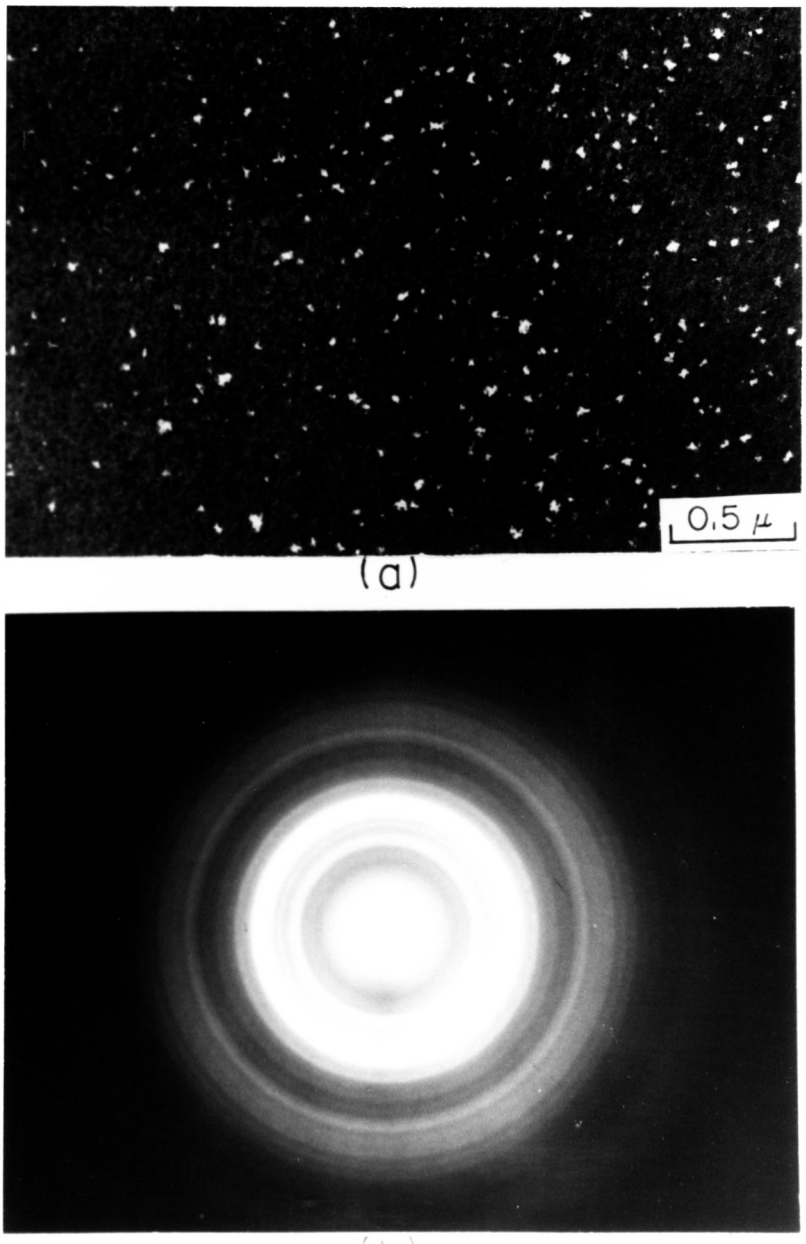

FIG. 2I

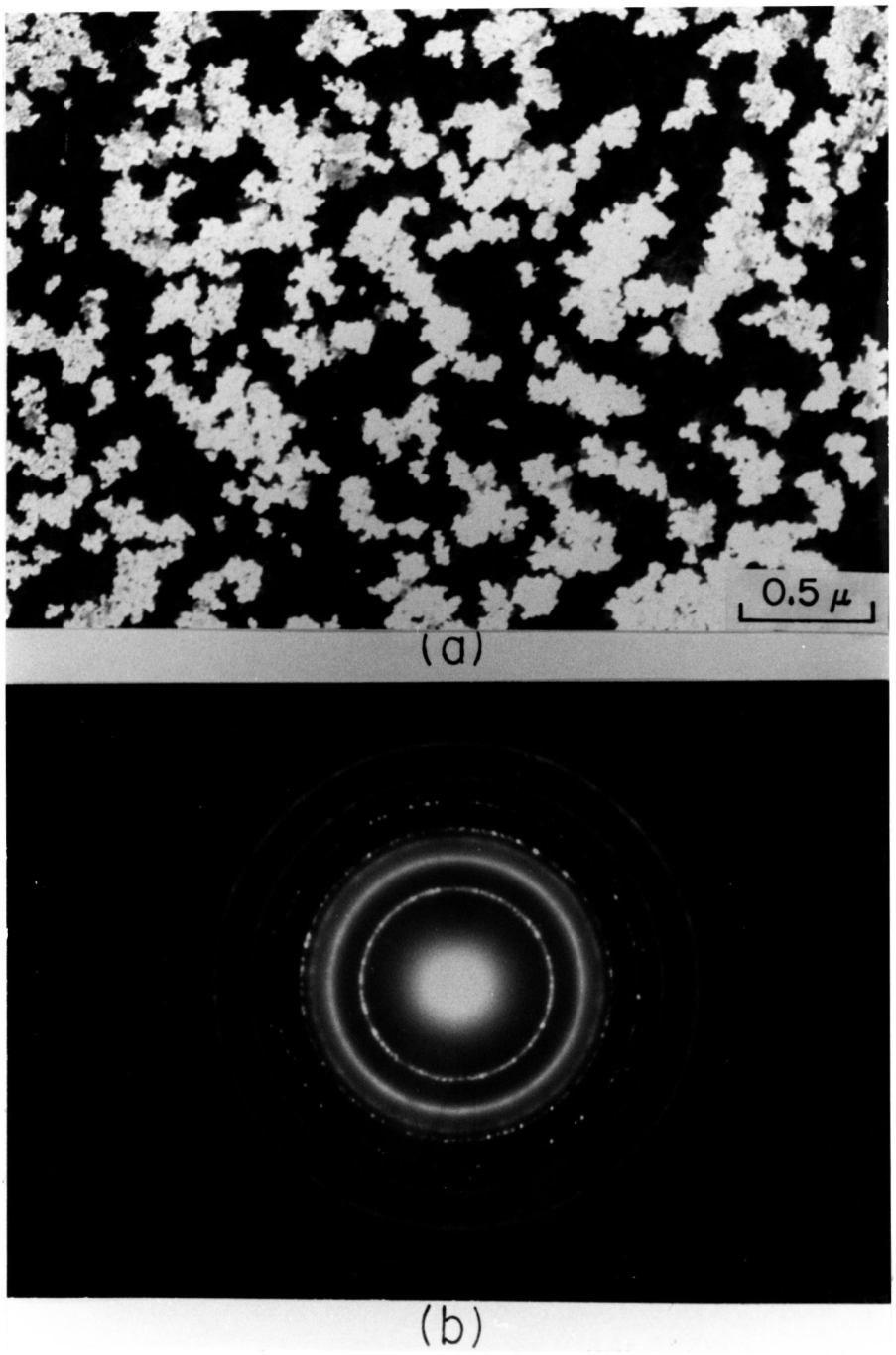

FIG. 22

Au - Si Amorphous Film

Amorphous structure	~ 100 °C
Incipient stage of crystallization	100 °C ~ 150 °C
Metastable phase (Complex structure)	150 °C ~ 200 °C
Stable eutectic mixture phase	200 °C ~

Fig. 23

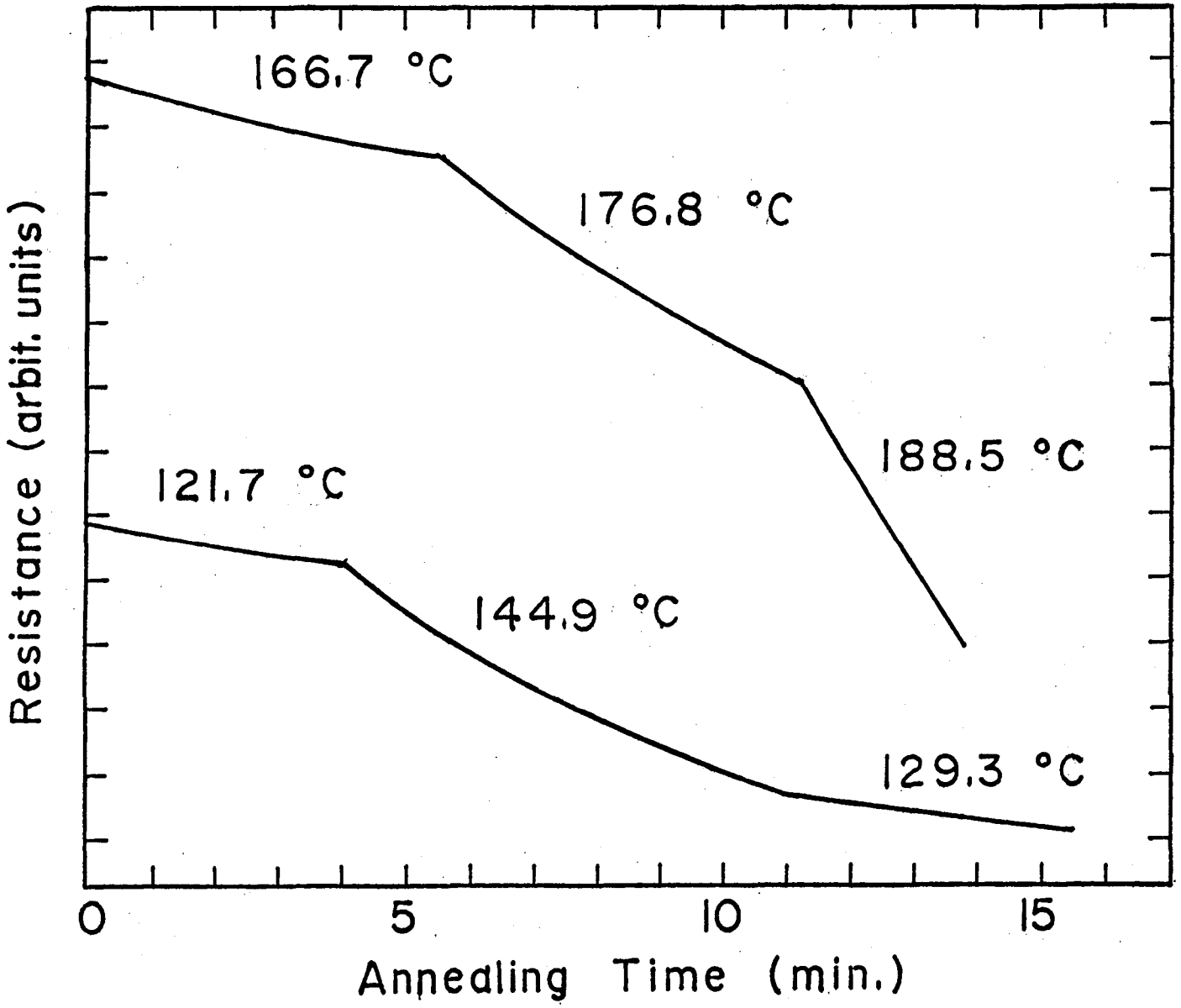
166.7 °C
176.8 °C
188.5 °C
121.7 °C
144.9 °C
129.3 °C
Resistance (arbit. units)
0
5
10
15
Annealing Time (min.)

FIG. 24

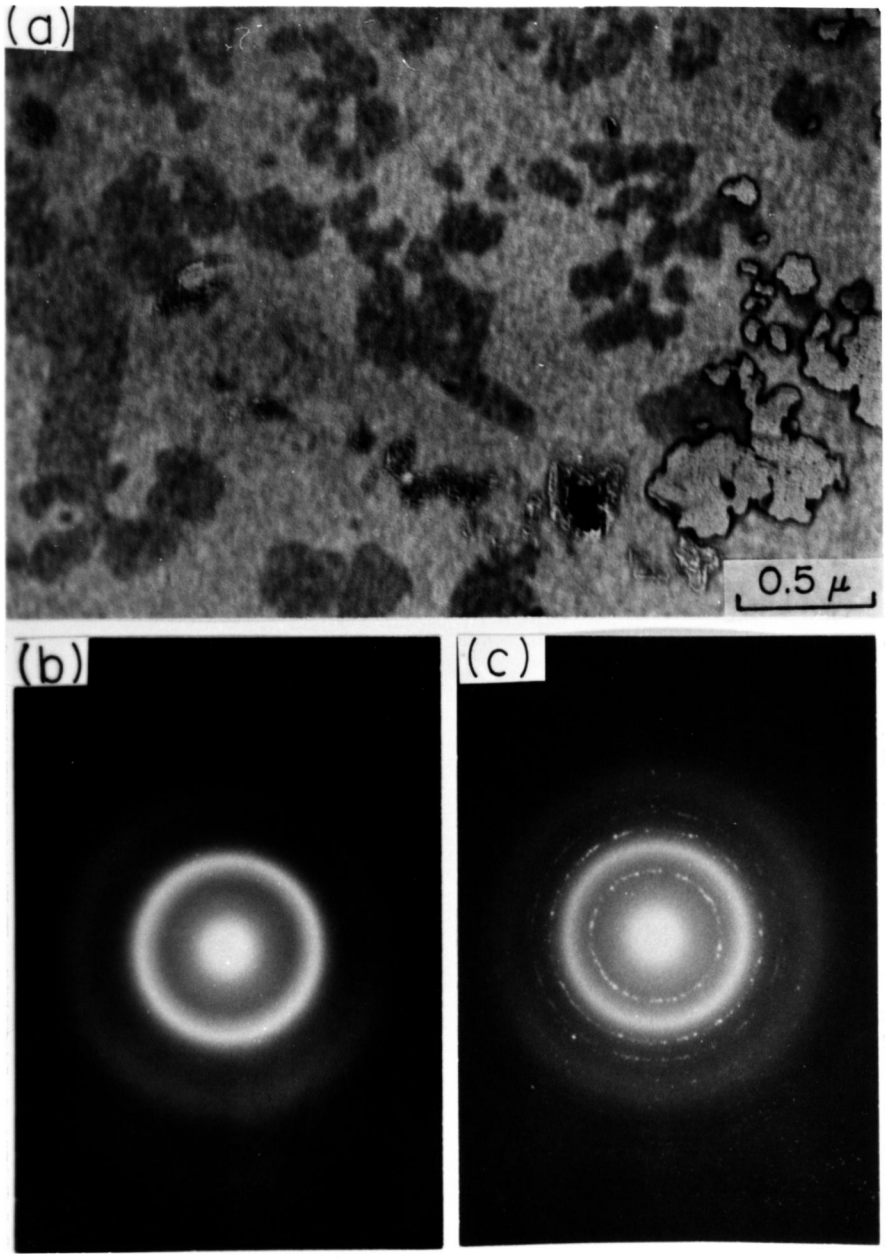

FIG. 25

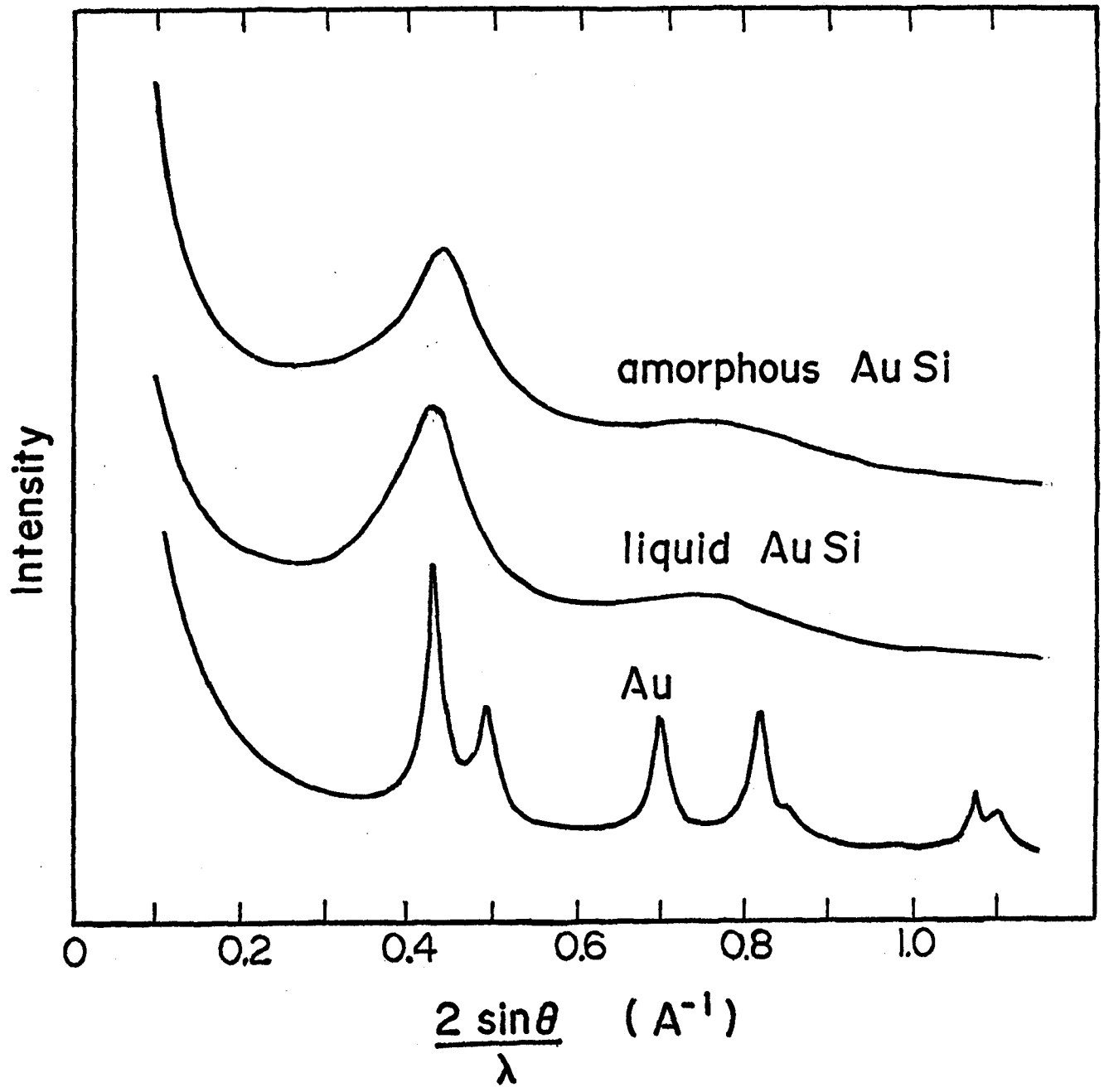
amorphous Au Si
liquid Au Si
Au
Intensity
0
0.2
0.4
0.6
0.8
1.0
2 sinθ / λ (A⁻¹)

FIG. 26

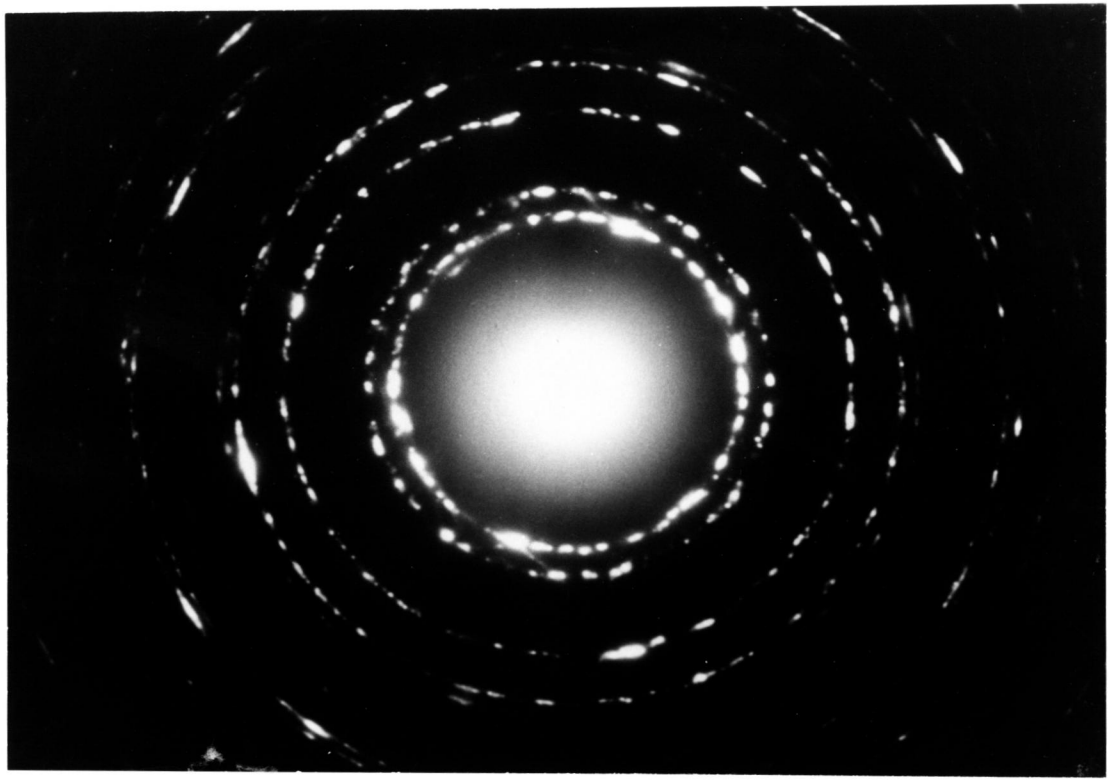

FIG. 27

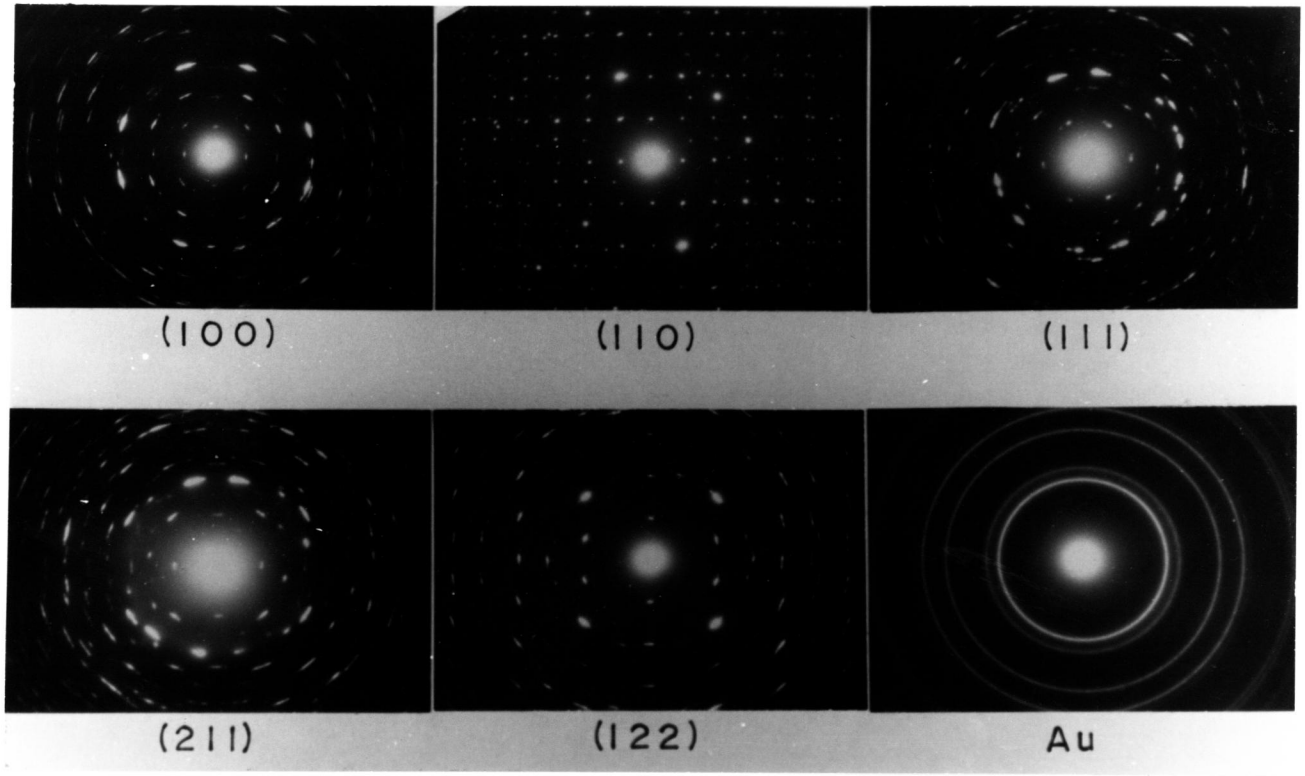

FIG. 28

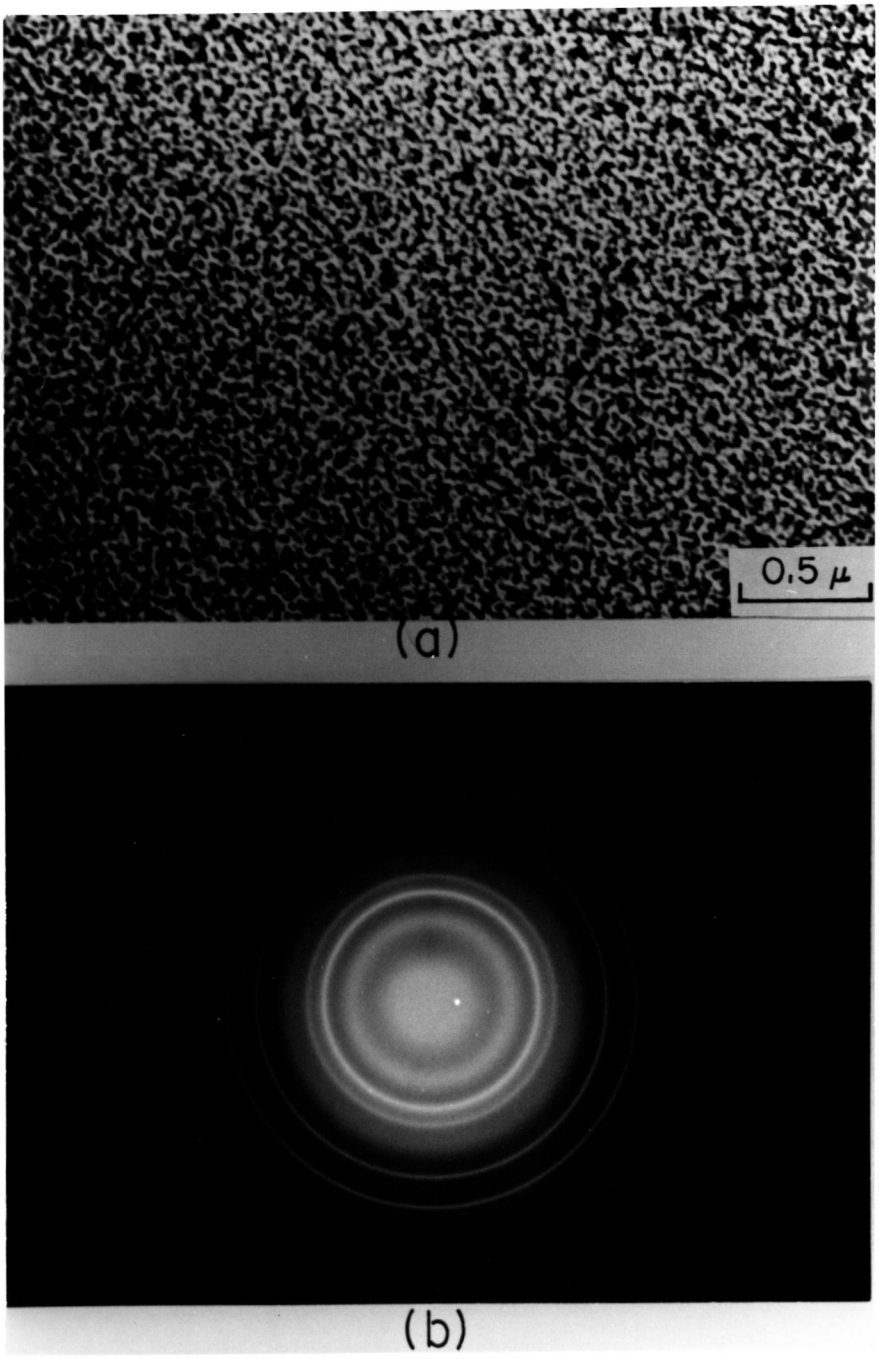

FIG. 29

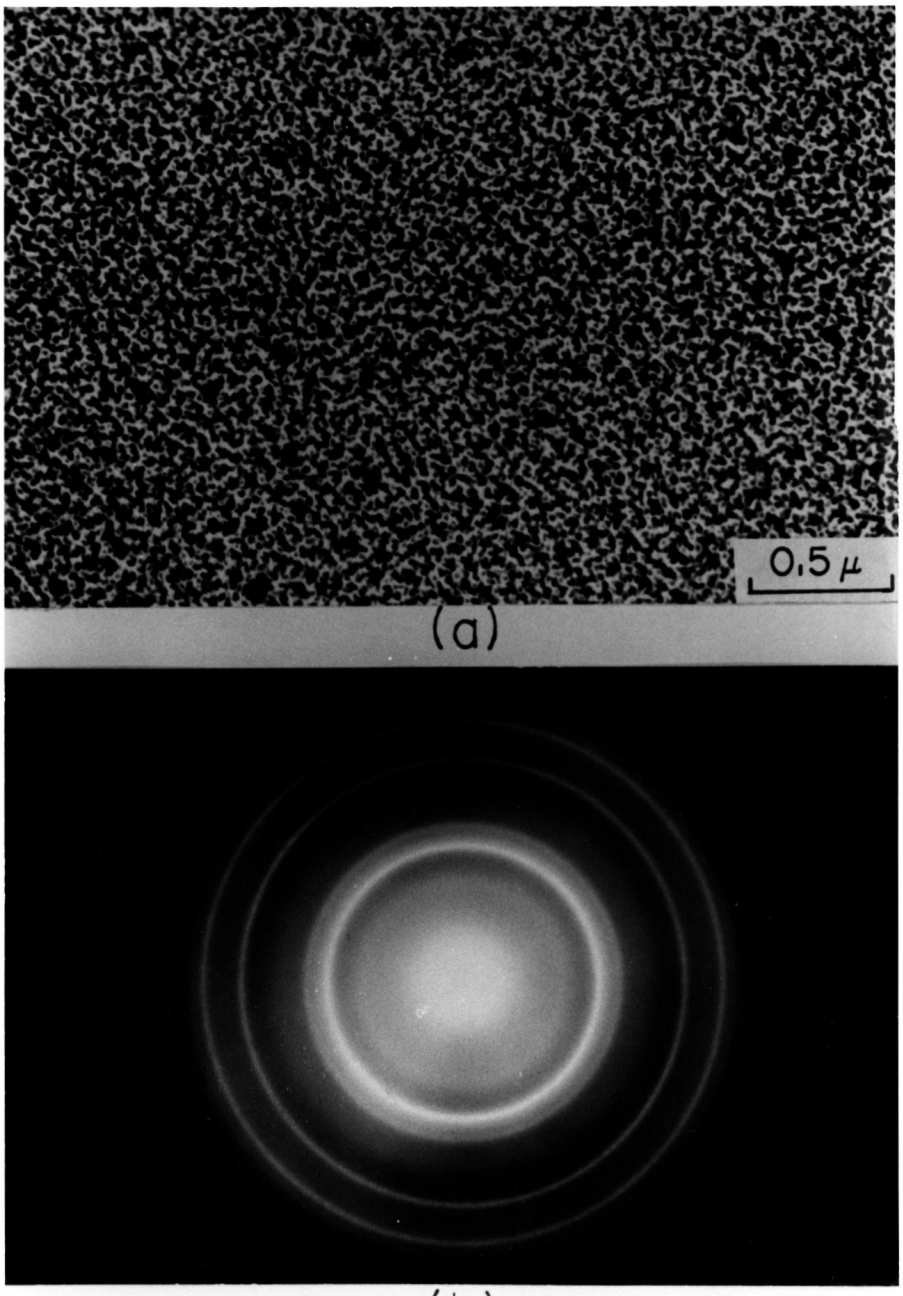

FIG. 30

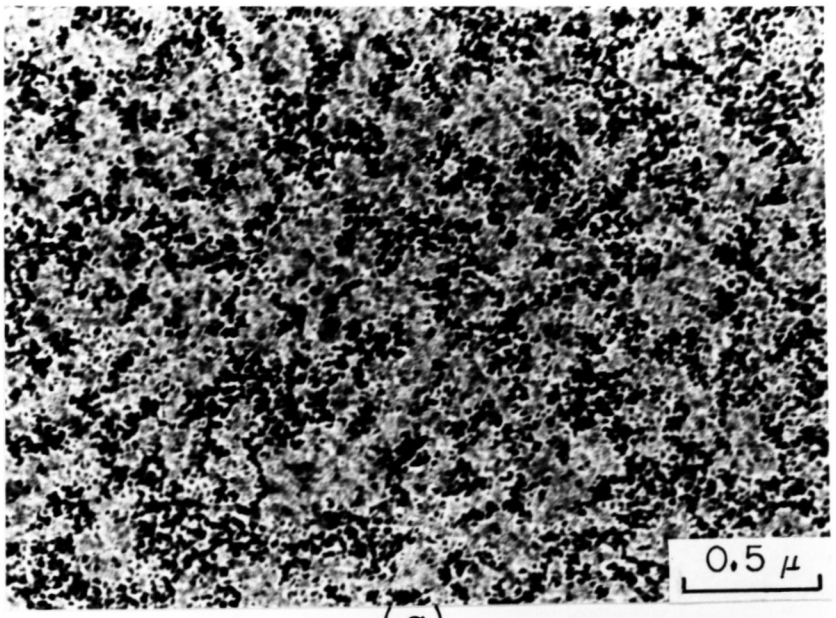

(a)

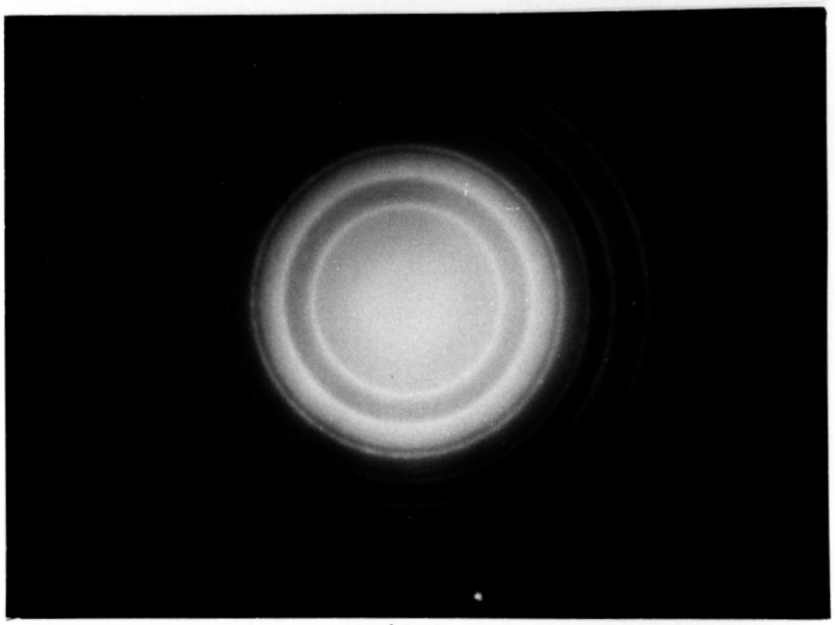

(b)

FIG. 3I

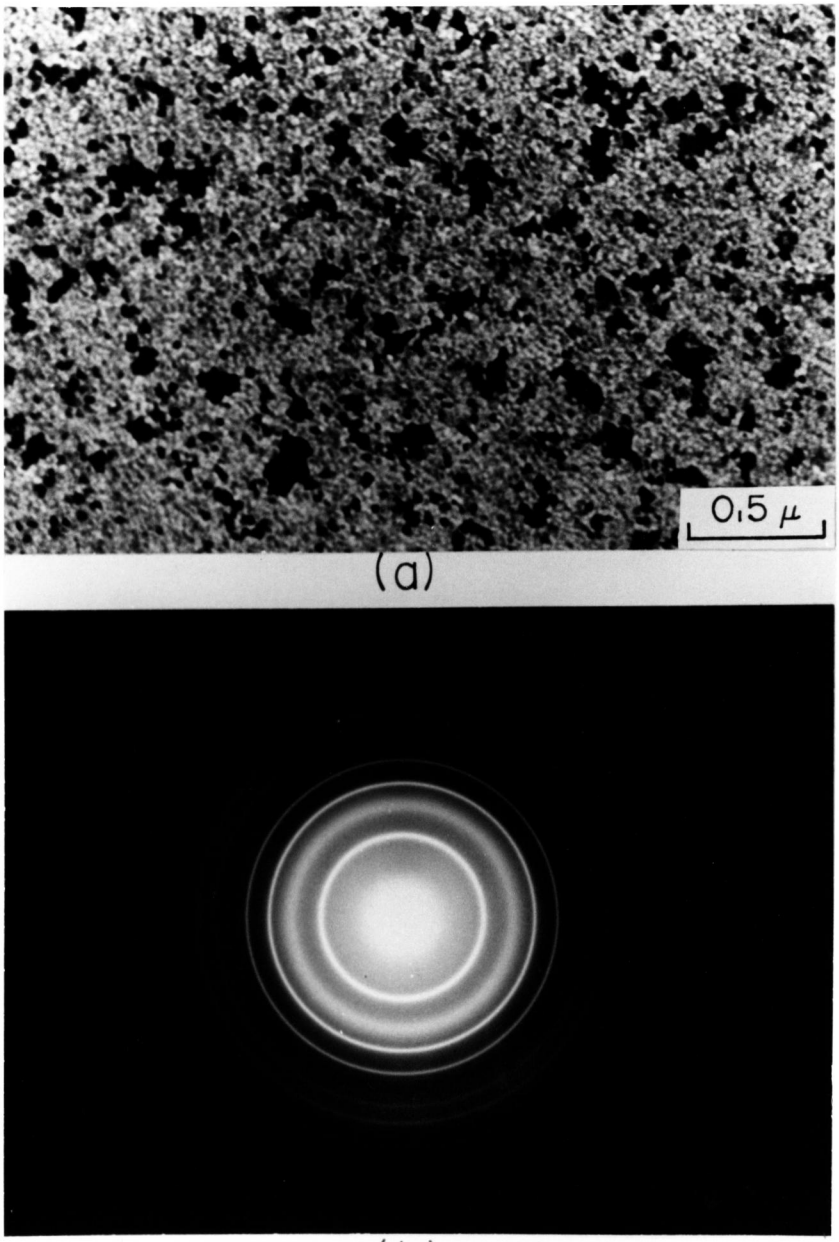

FIG. 32

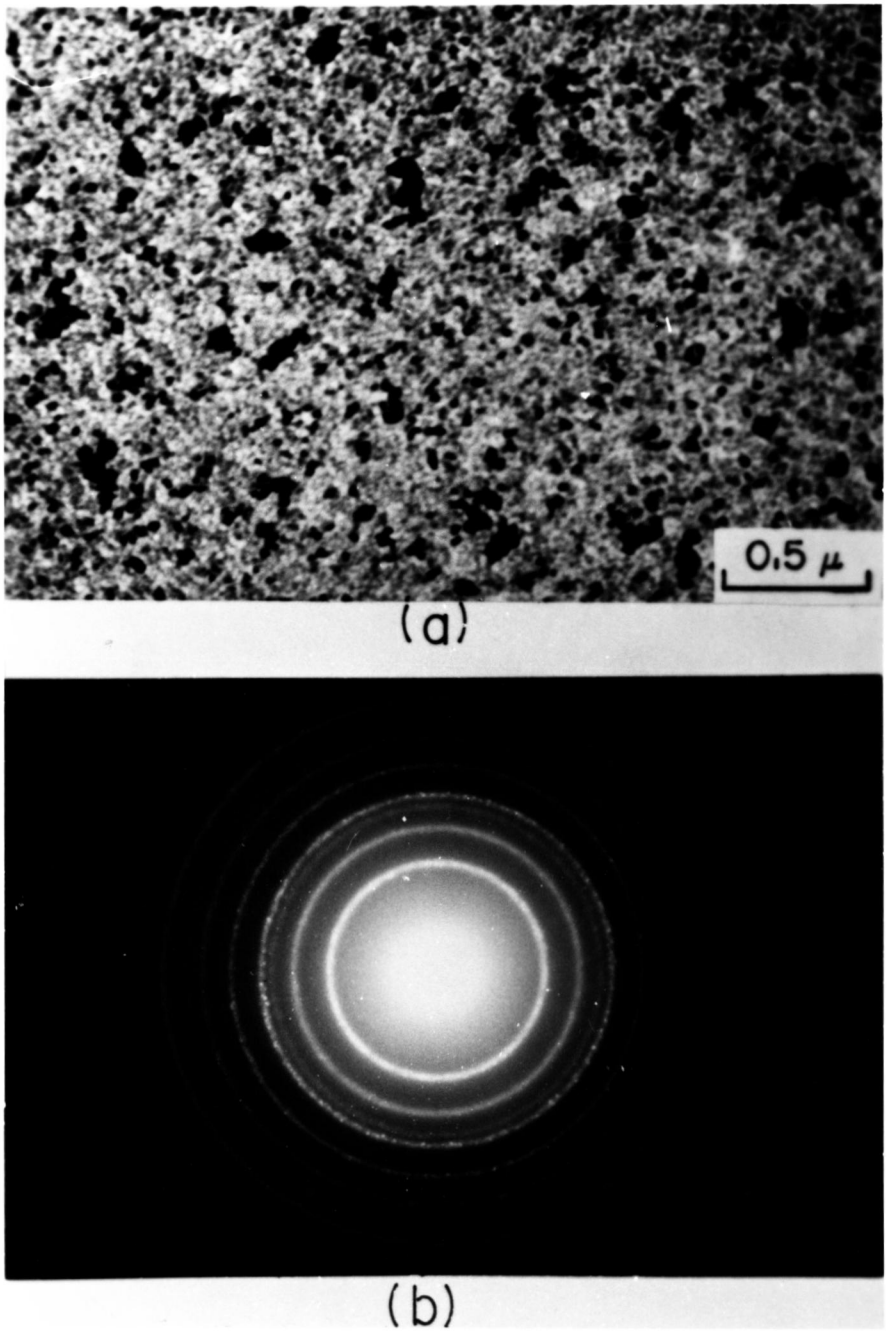

FIG. 33

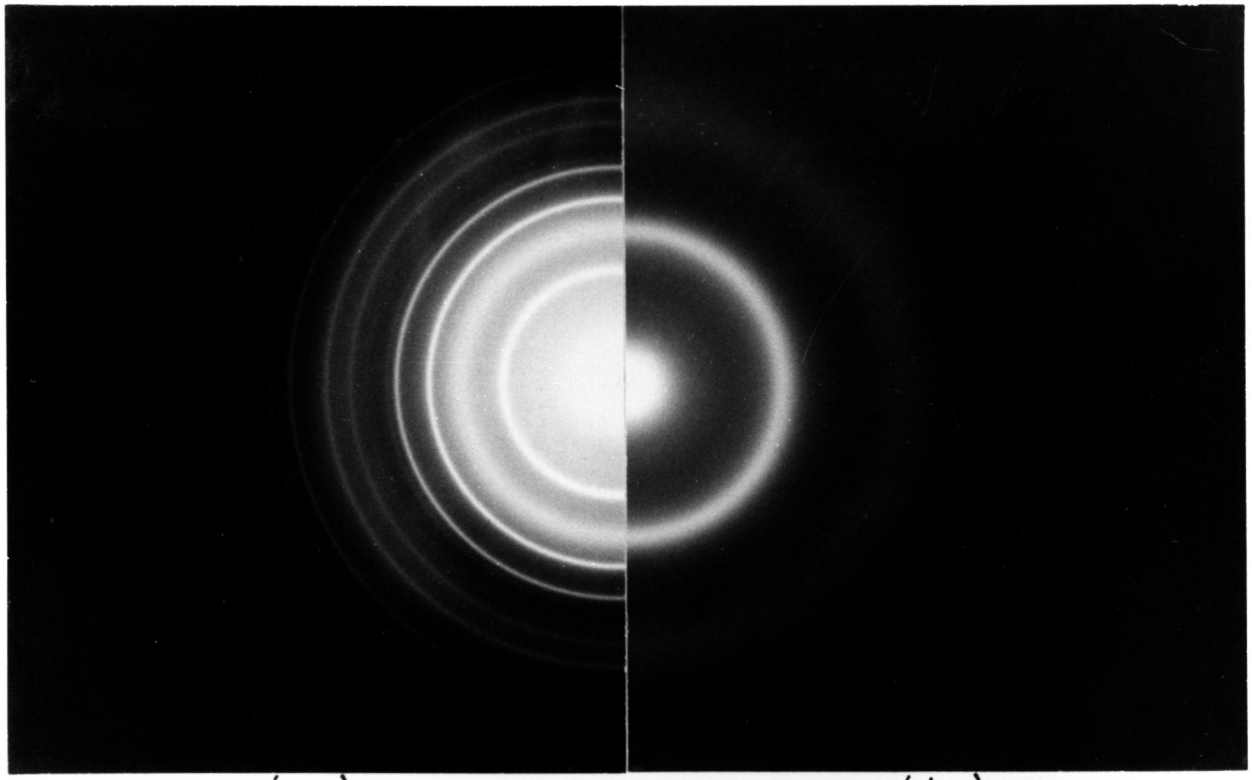

FIG. 34

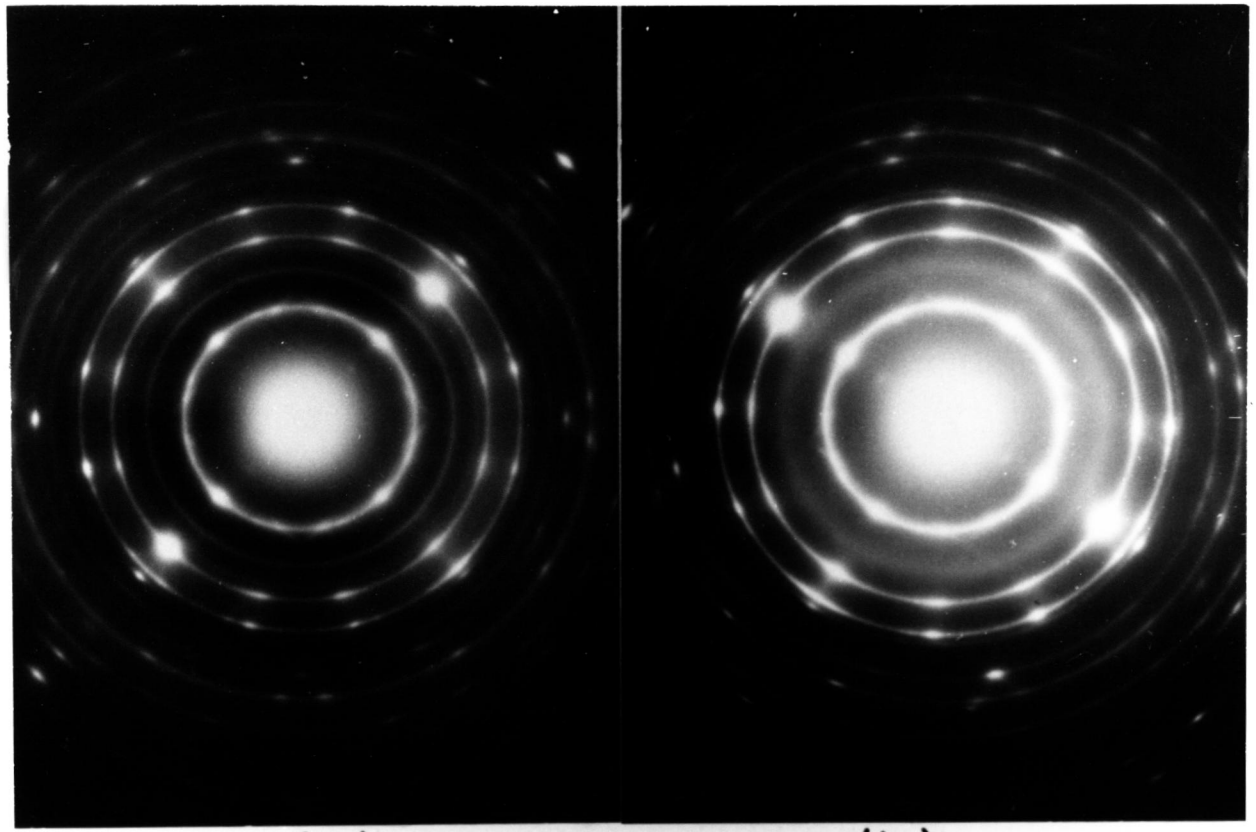

FIG. 35

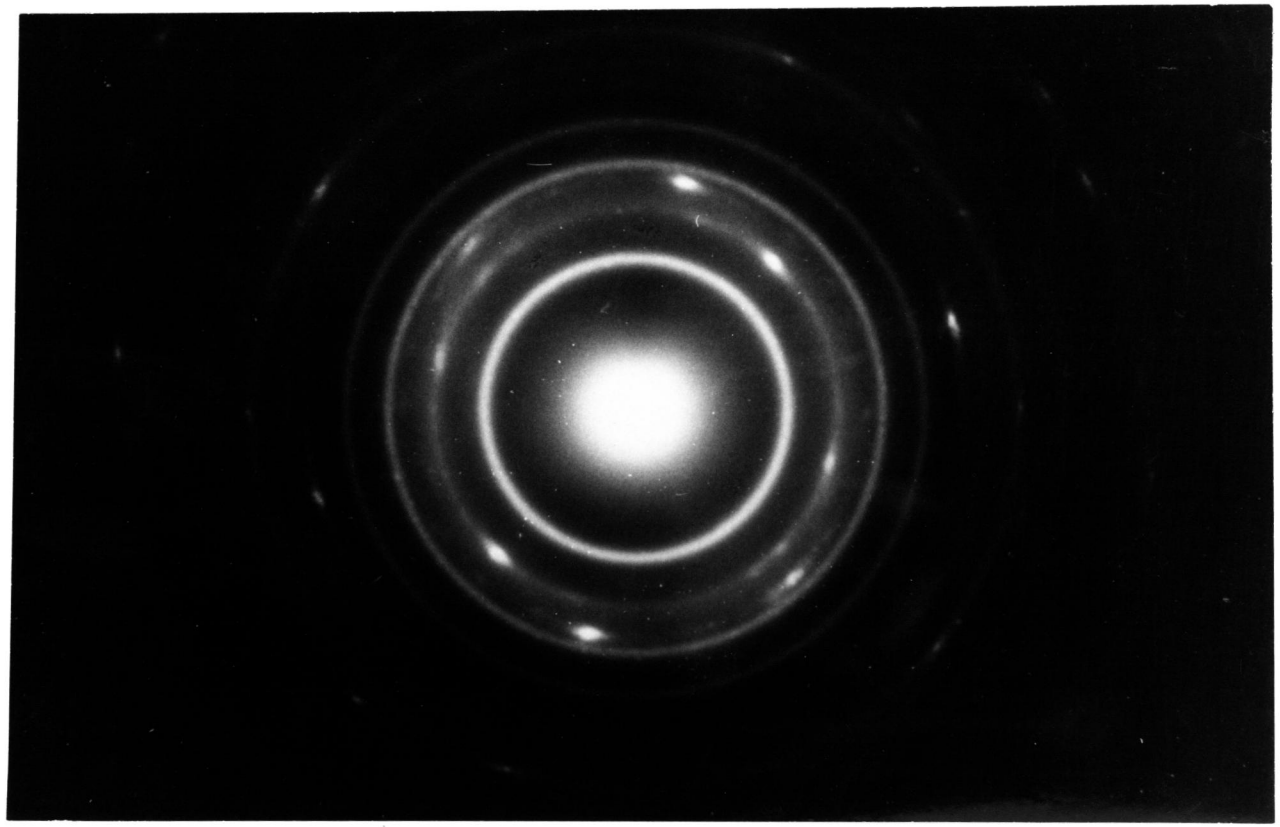

FIG. 36

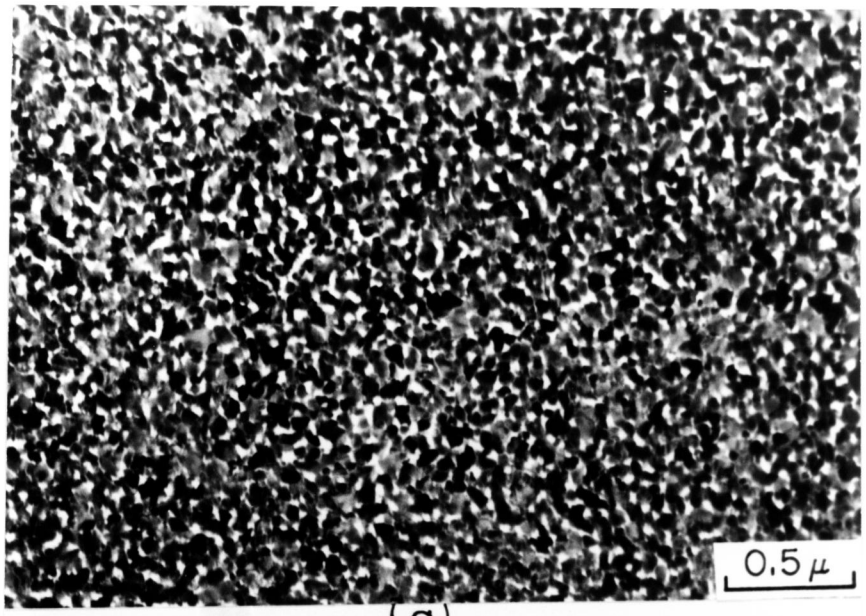

(a)

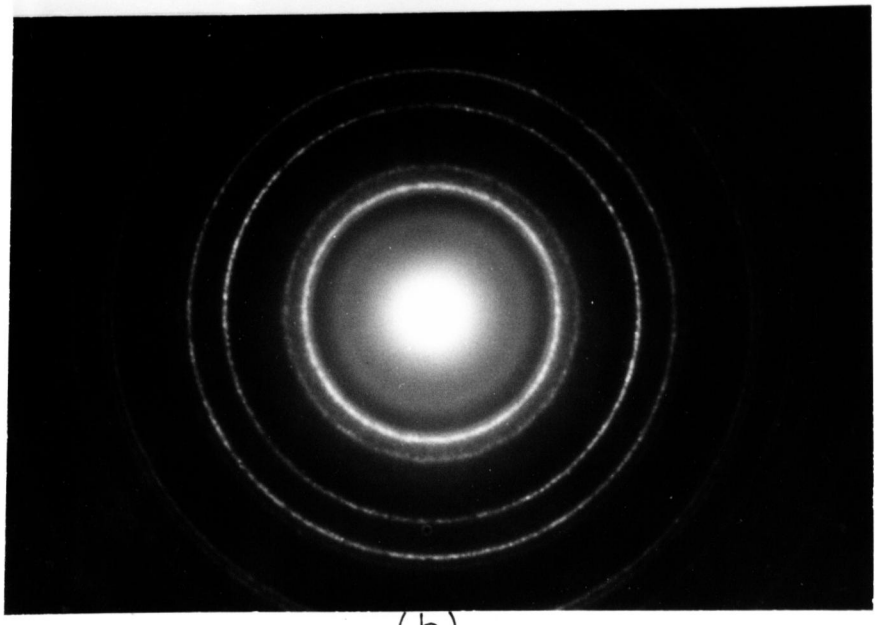

(b)

FIG. 37

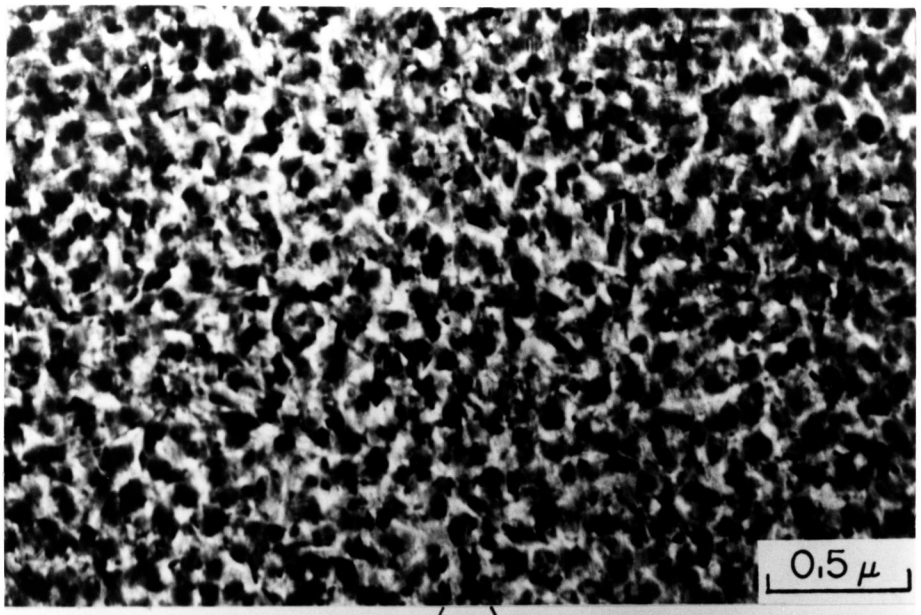

(a)

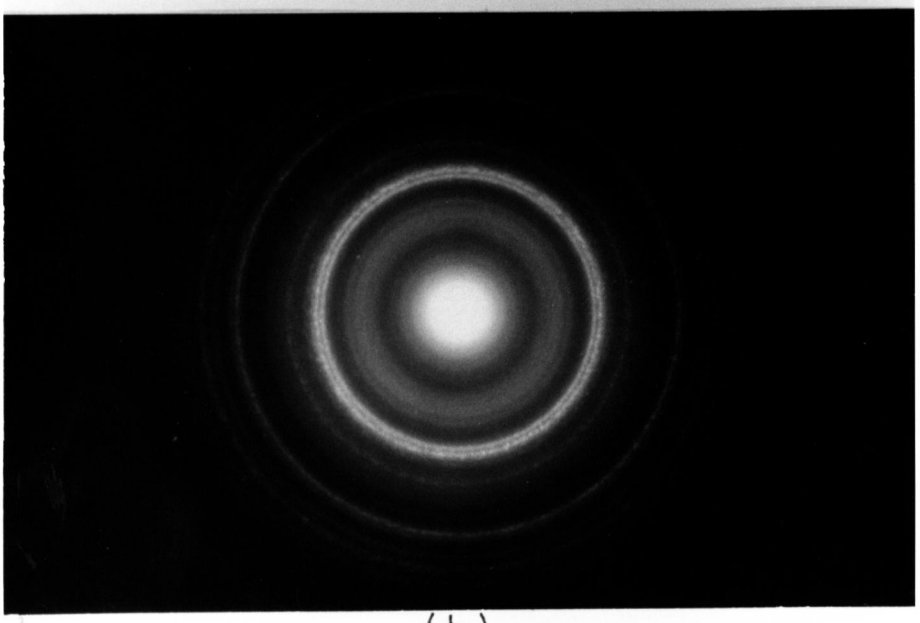

(b)

FIG. 38

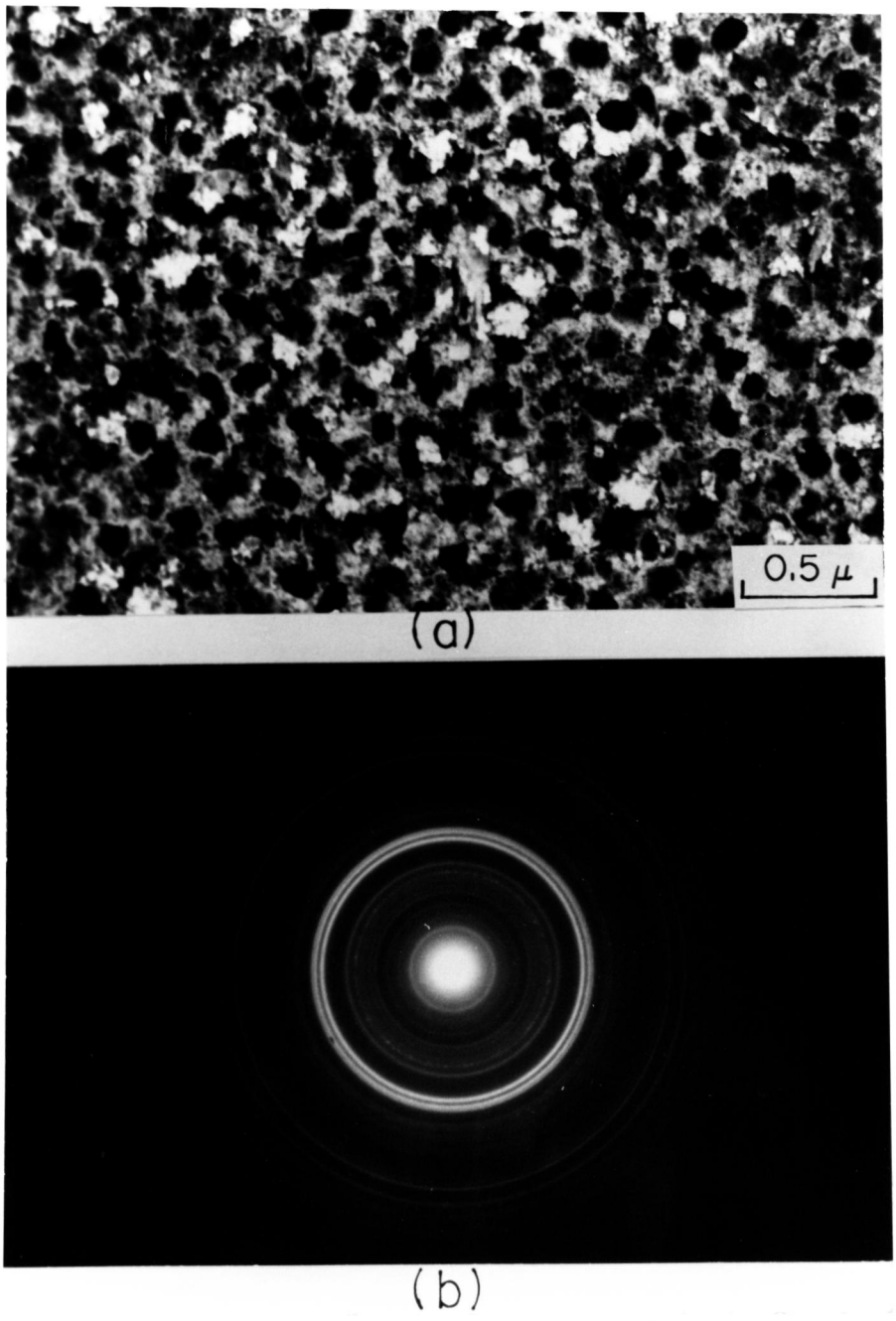

FIG. 39

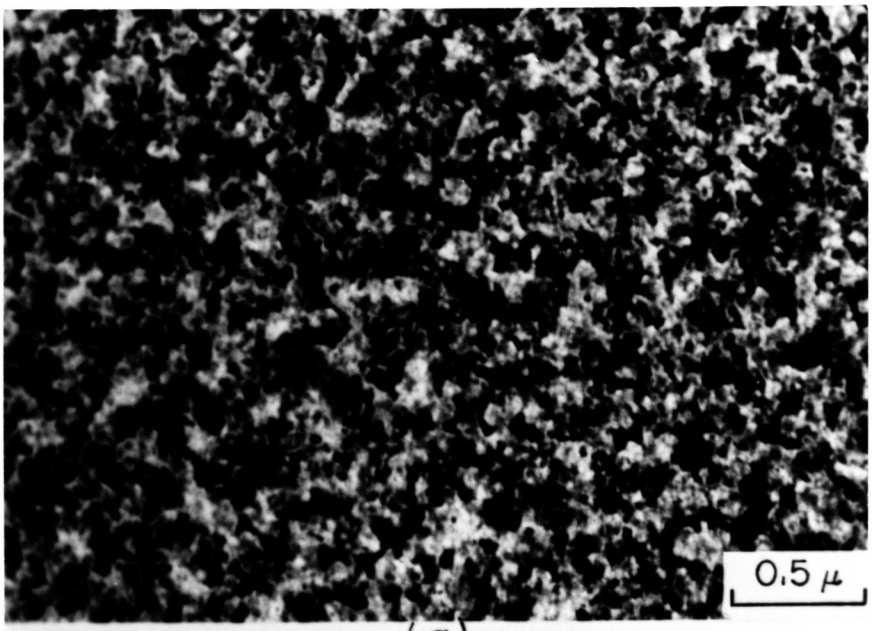

(a)

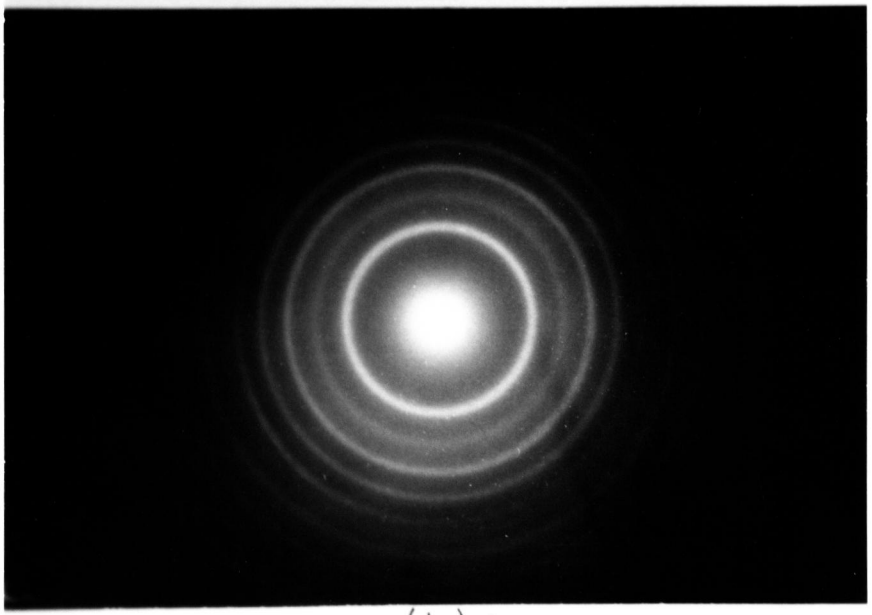

(b)

FIG. 40

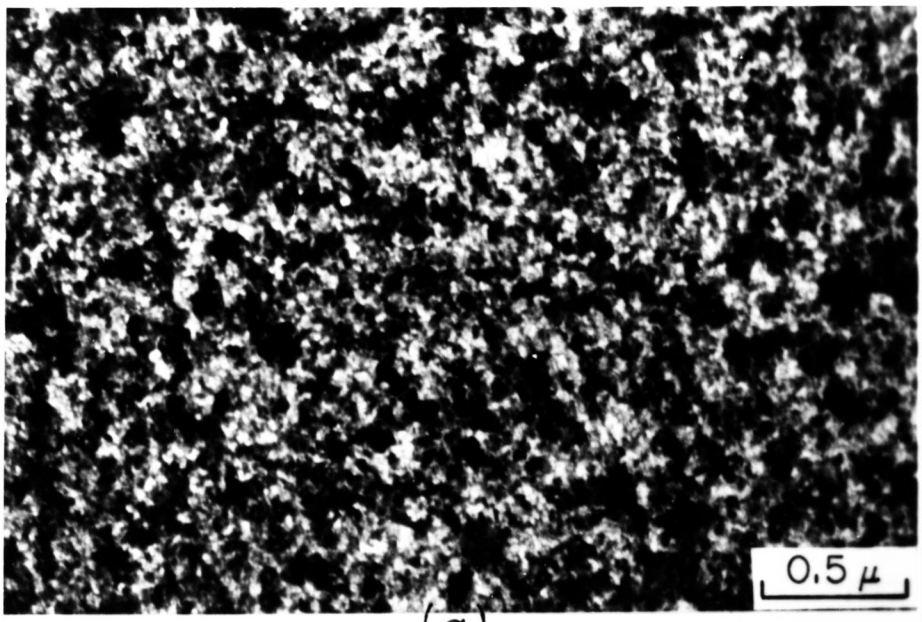

(a)

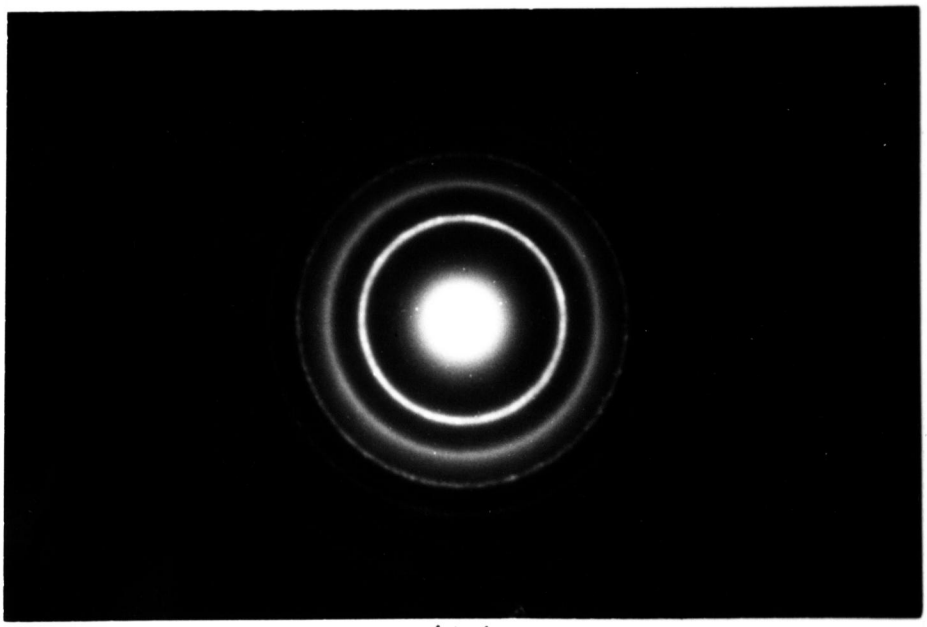

(b)

FIG. 4I

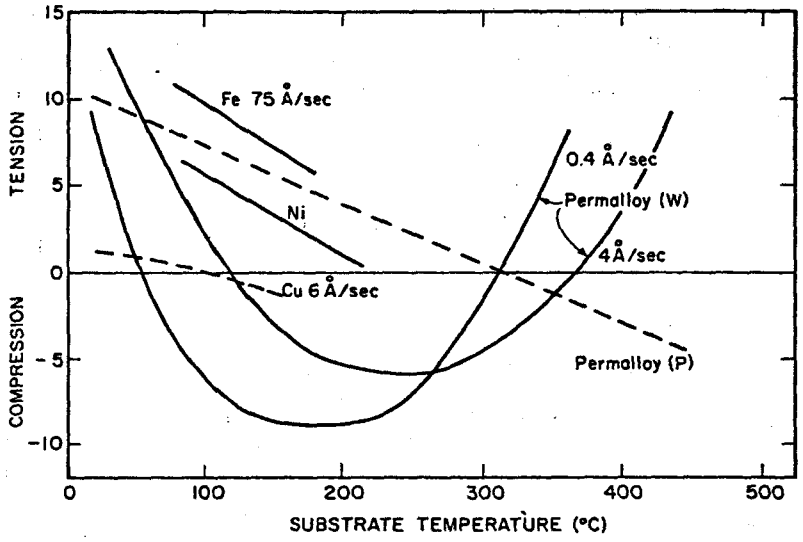
15
10
5
0
-5
-10
TENSION
COMPRESSION
Fe 75 Å/sec
Ni
Cu 6 Å/sec
0.4 Å/sec
Permalloy (W)
4 Å/sec
Permalloy (P)
0
100
200
300
400
500
SUBSTRATE TEMPERATURE (°C)

FIG. 42

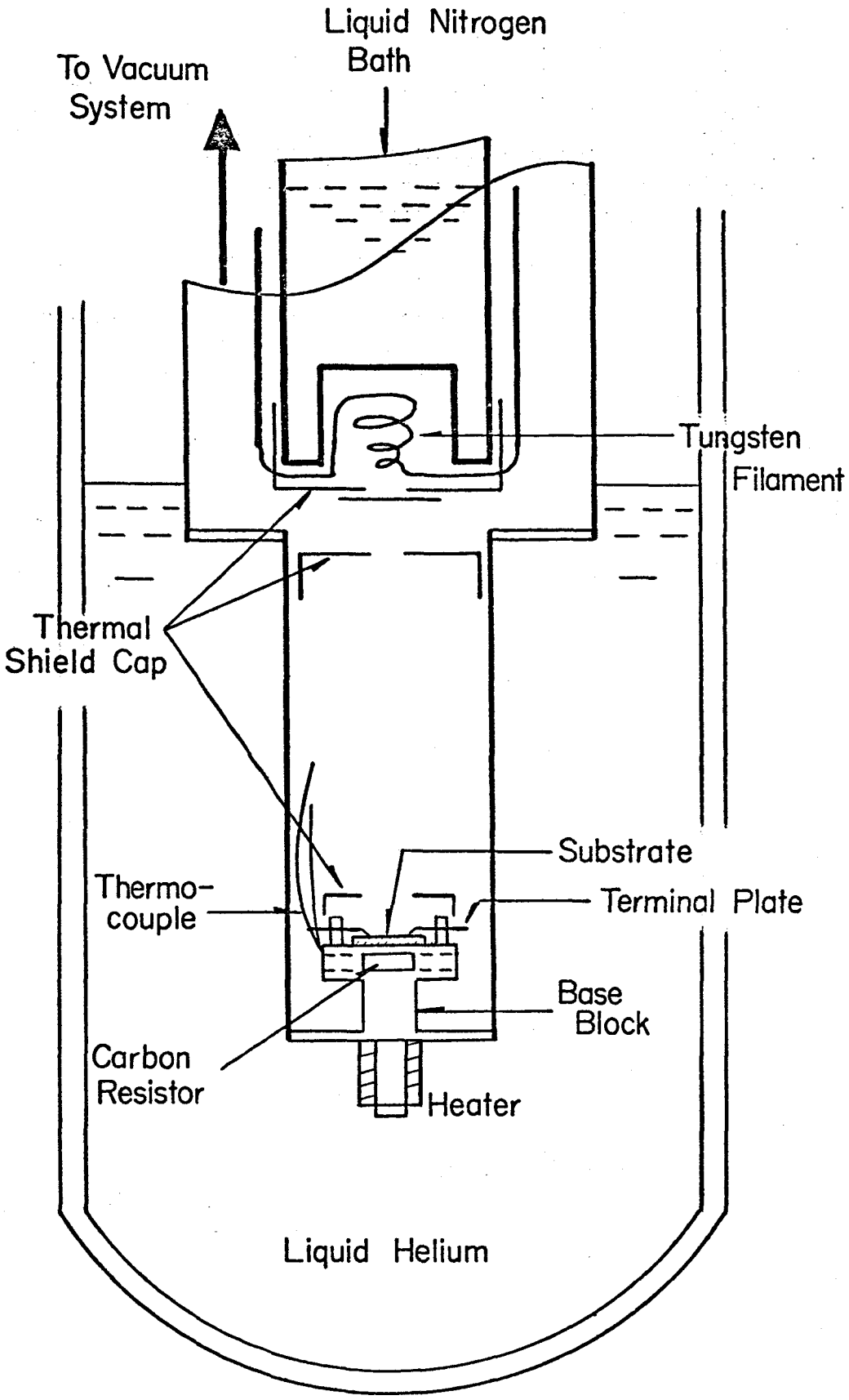
Liquid Nitrogen Bath
To Vacuum System
Tungsten Filament
Thermal Shield Cap
Substrate
Thermo-couple
Terminal Plate
Base Block
Carbon Resistor
Heater
Liquid Helium

FIG. 43

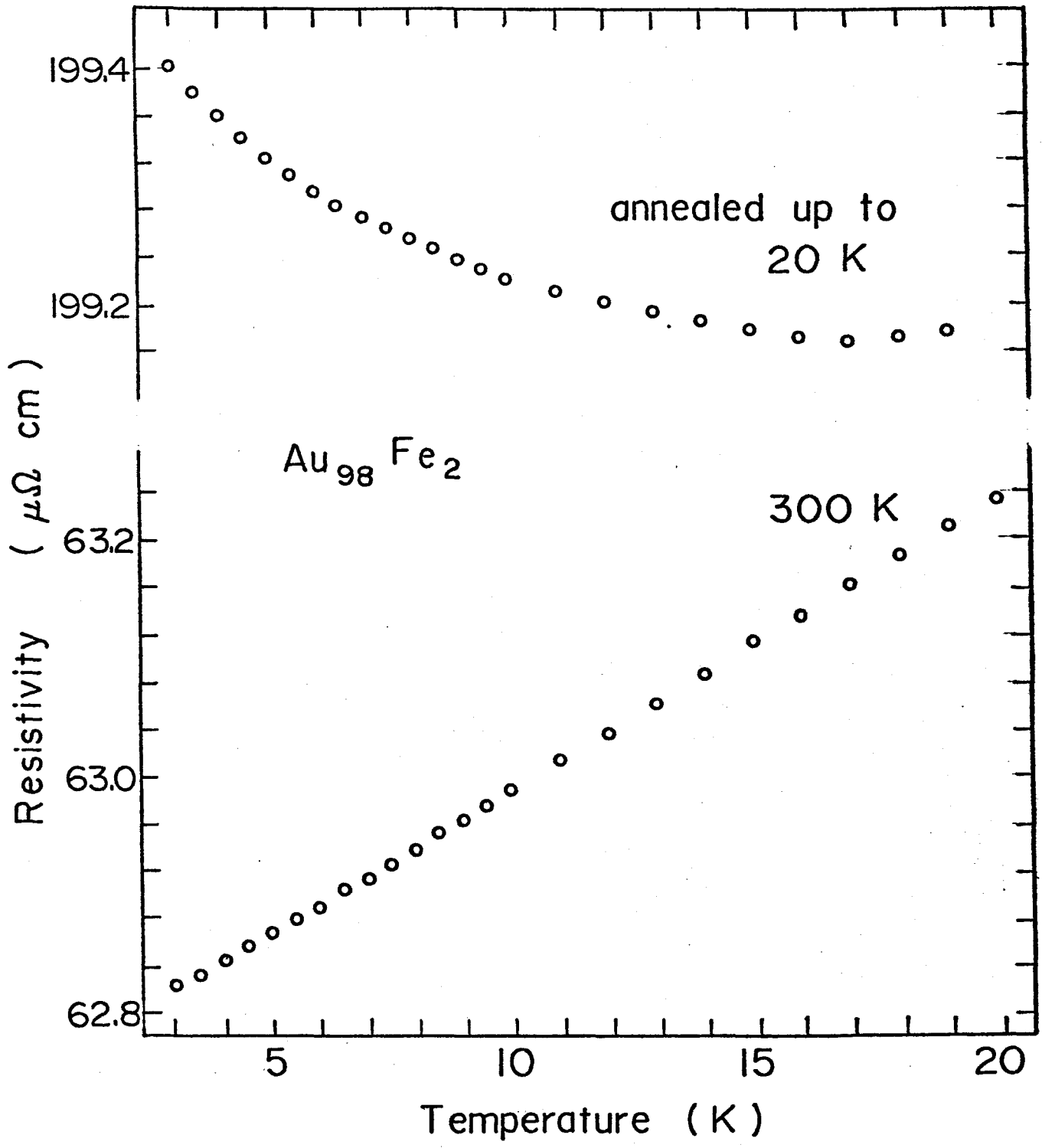
199.4
199.2
annealed up to
20 K
Au 98 Fe 2
300 K
63.2
63.0
62.8
Resistivity (μΩ cm)
5
10
15
20
Temperature (K)

FIG. 44

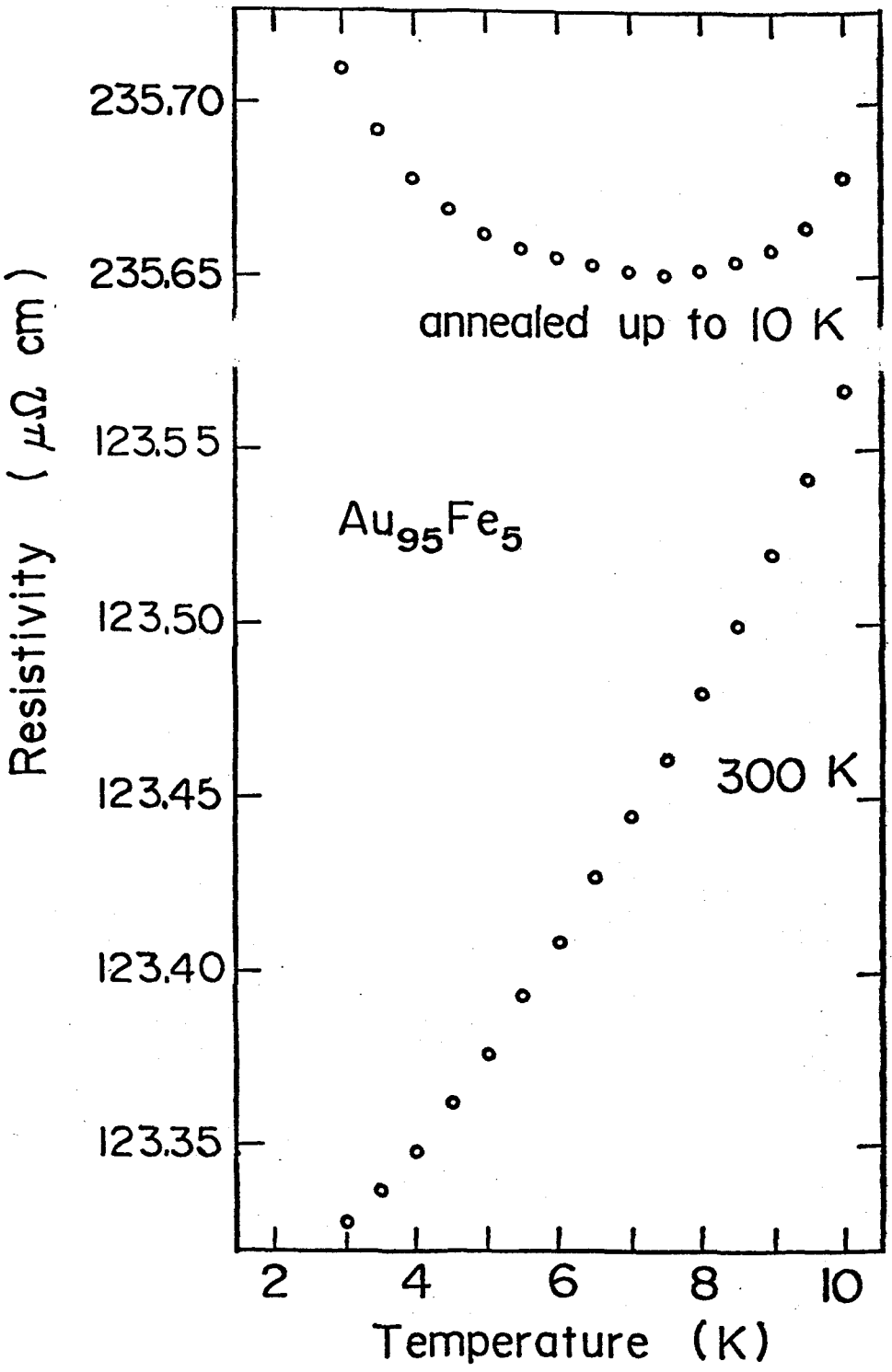
235.70
235.65
annealed up to 10 K
123.55
123.50
123.45
123.40
123.35
Au95Fe5
300 K
Resistivity (μΩ cm)
2
4
6
8
10
Temperature (K)

FIG. 45

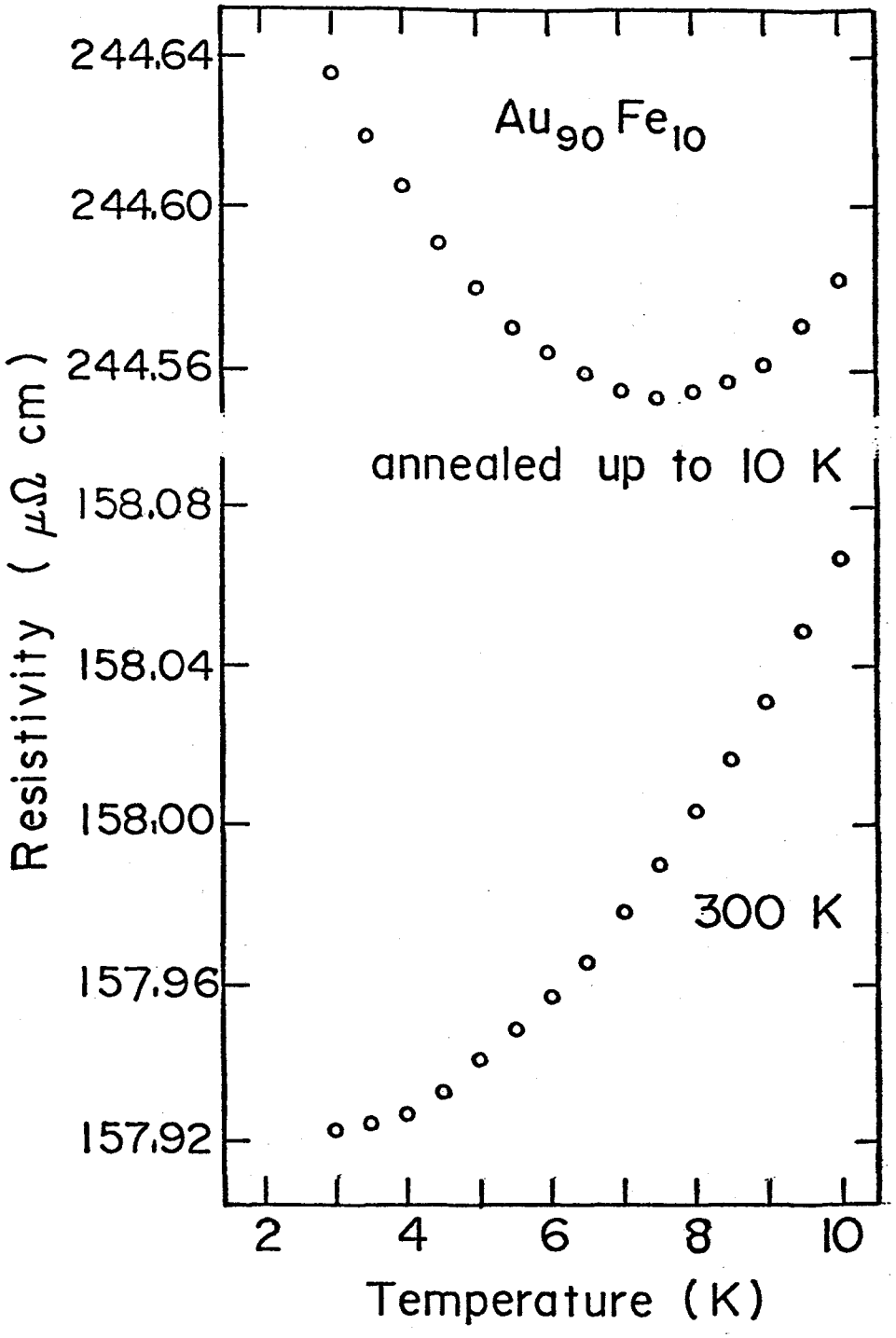
244.64
244.60
244.56
158.08
158.04
158.00
157.96
157.92
Resistivity (μΩ cm)
Au90 Fe10
annealed up to 10 K
300 K
2
4
6
8
10
Temperature (K)

FIG. 46

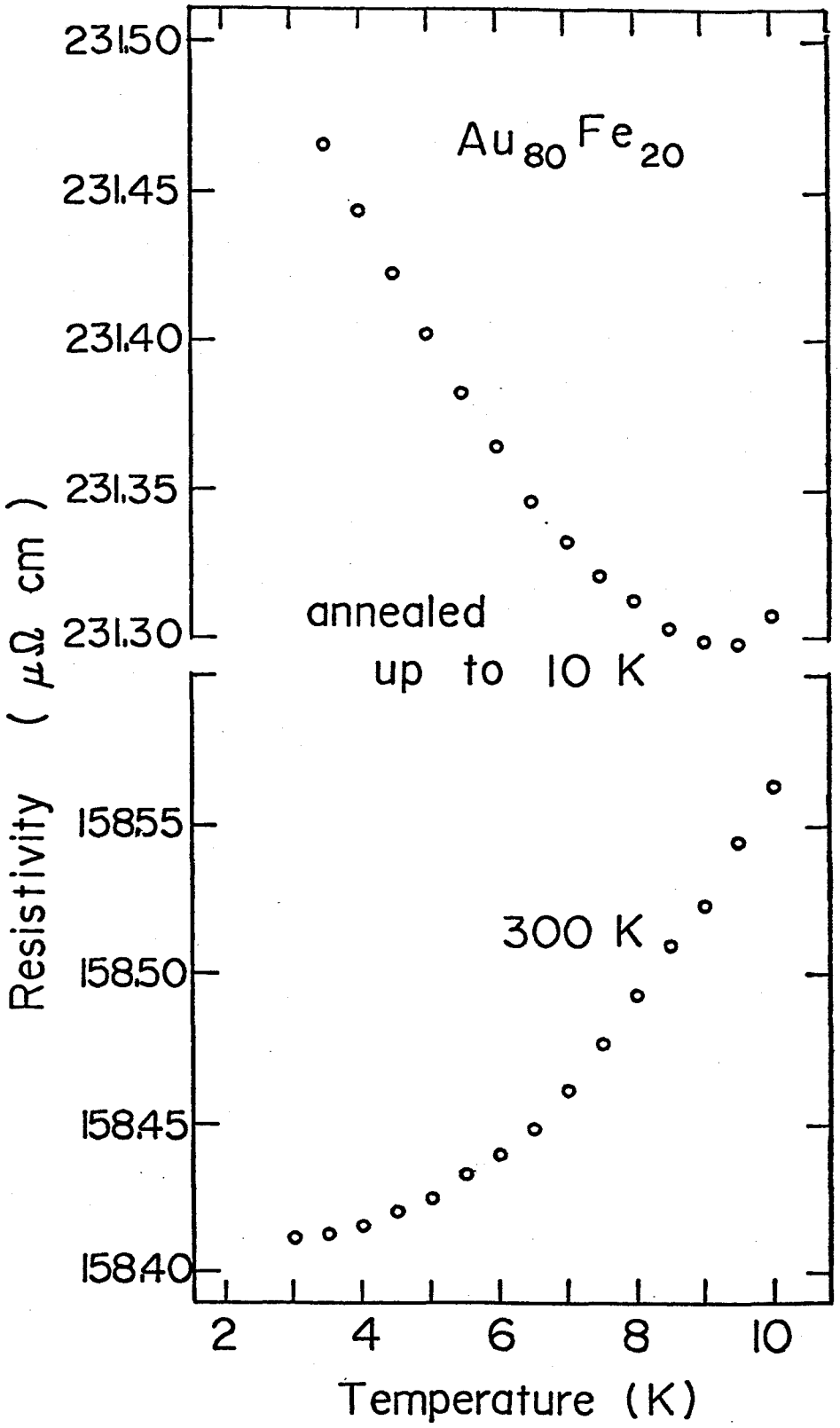
231.50
231.45
231.40
231.35
231.30
Au80Fe20
annealed
up to 10 K
Resistivity (μΩ cm)
158.55
158.50
158.45
158.40
300 K
2
4
6
8
10
Temperature (K)

FIG. 47

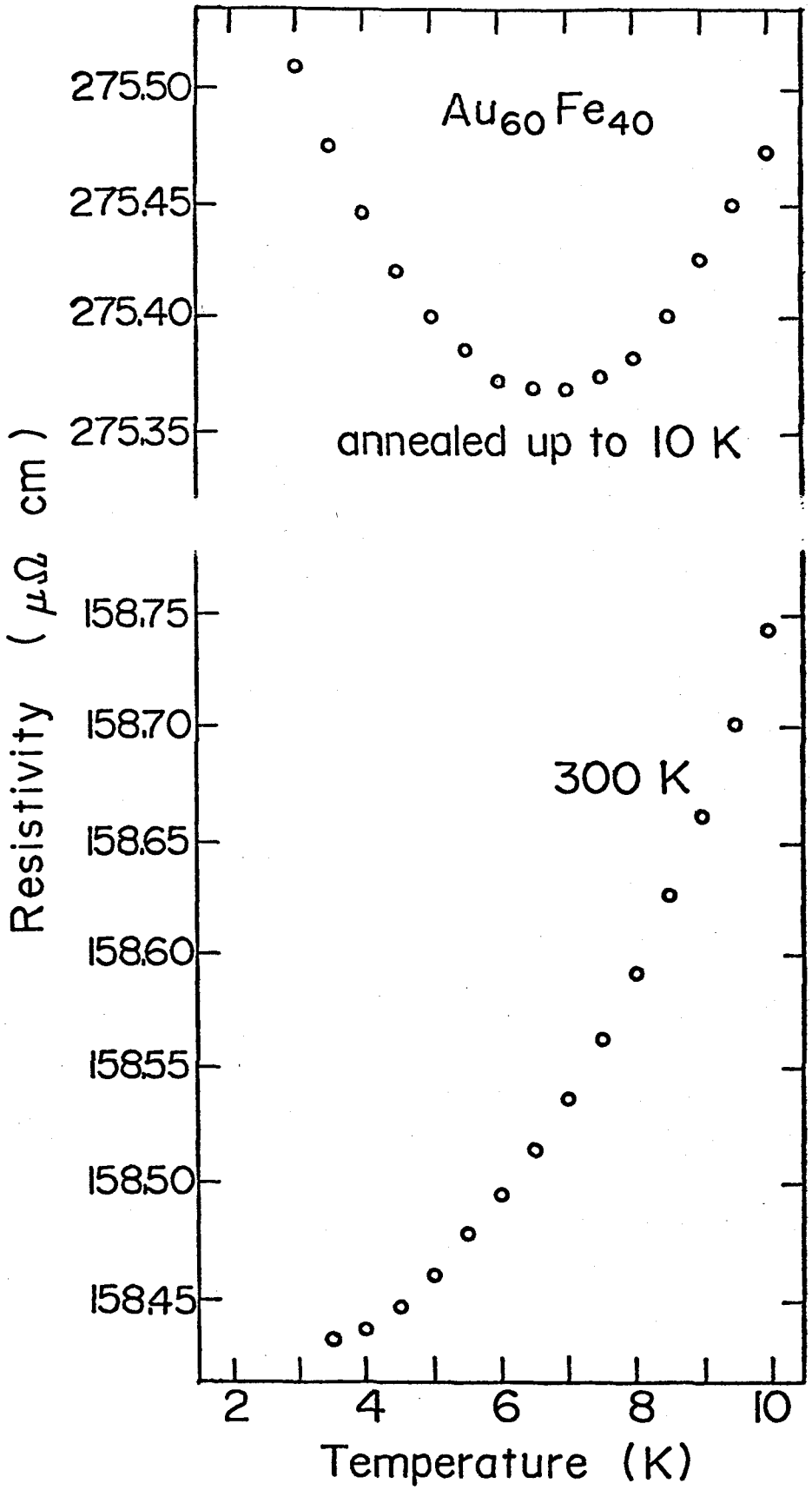
275.50
275.45
275.40
275.35
$Au_{60}Fe_{40}$
annealed up to 10 K
158.75
158.70
158.65
158.60
158.55
158.50
158.45
300 K
Resistivity (μΩ cm)
2
4
6
8
10
Temperature (K)

FIG. 48

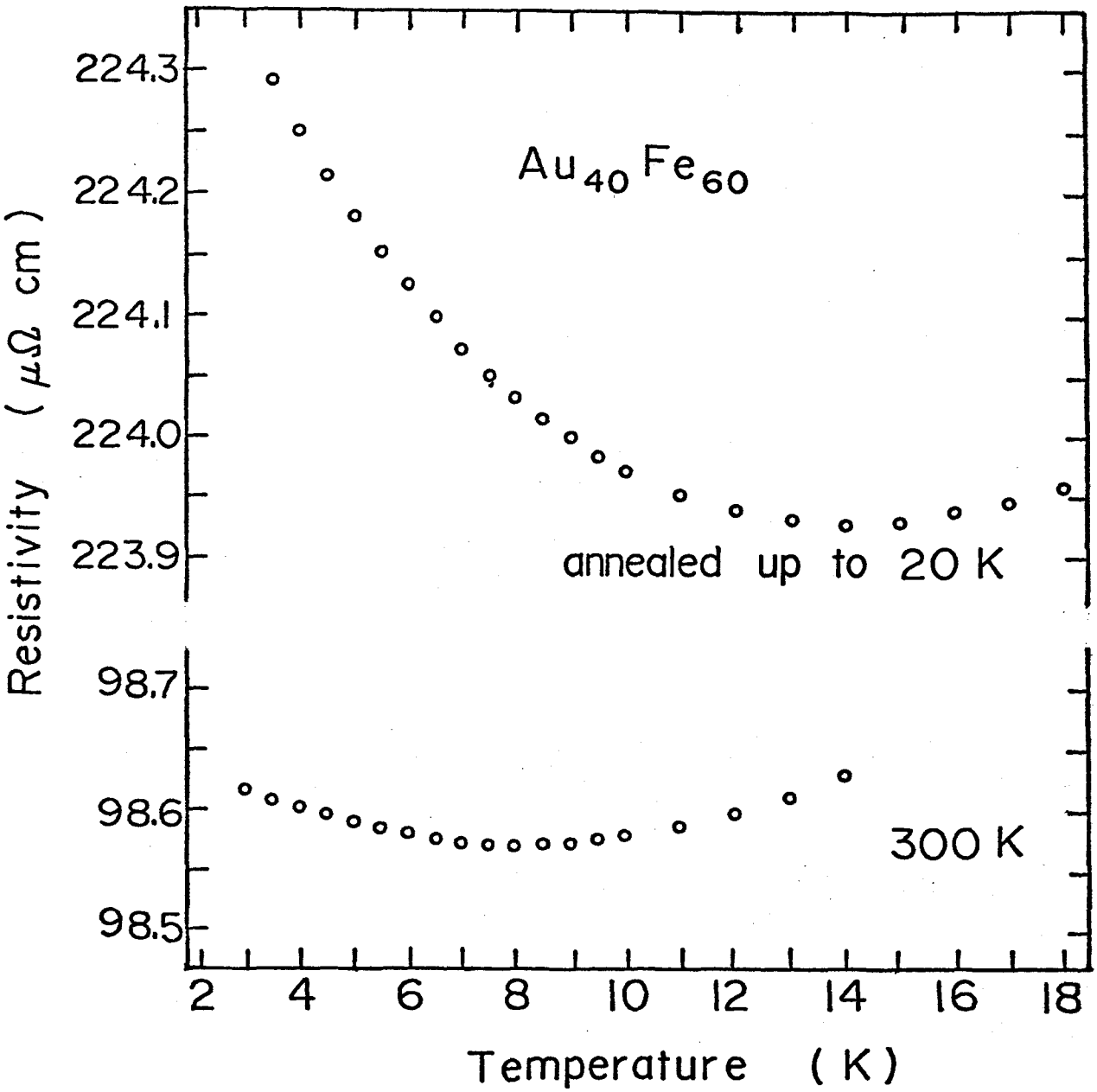
224.3
224.2
224.1
224.0
223.9
Au40 Fe60
annealed up to 20 K
98.7
98.6
98.5
300 K
2
4
6
8
10
12
14
16
18
Resistivity (μΩ cm)
Temperature (K)

FIG. 49

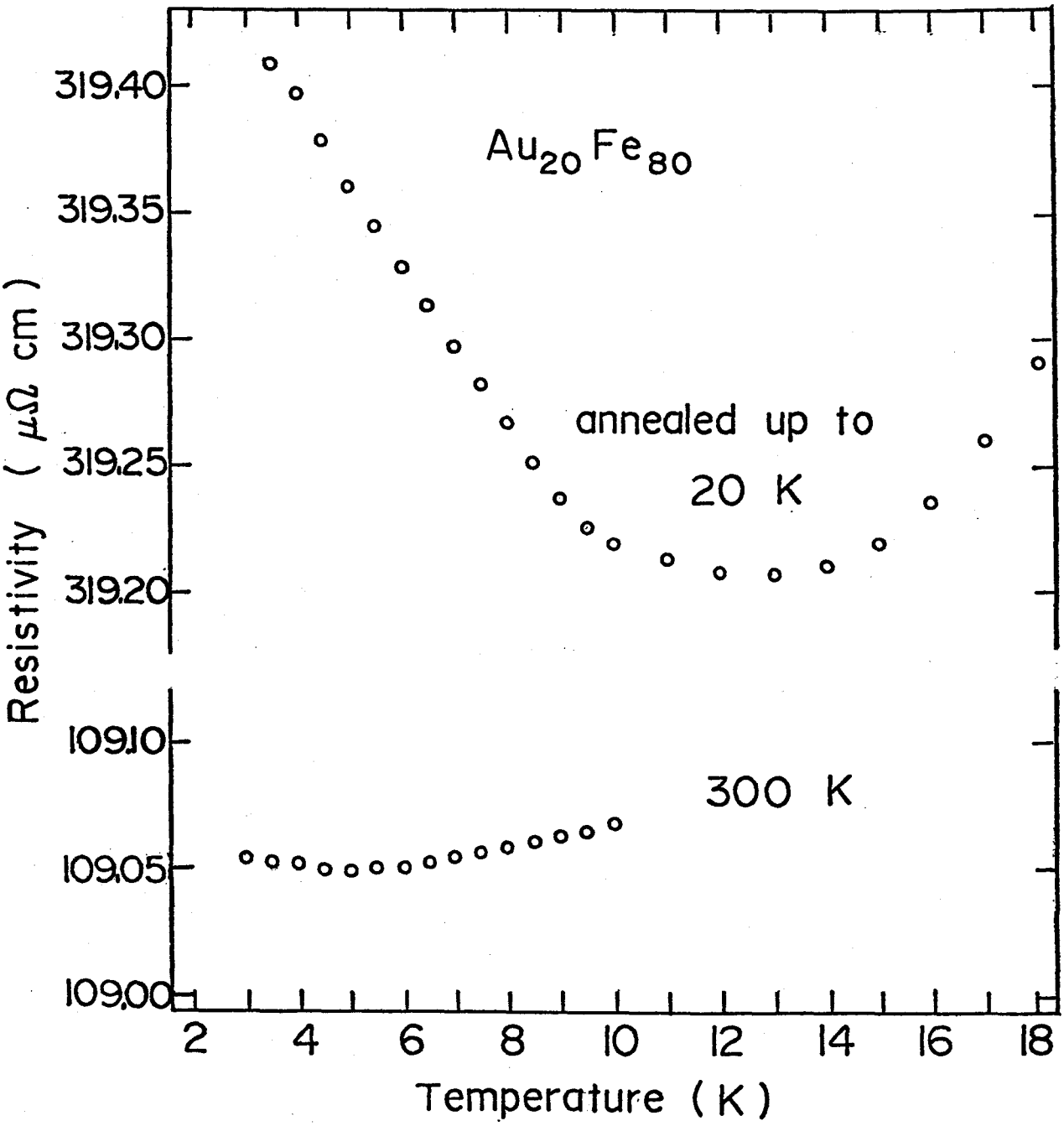
319.40
319.35
319.30
319.25
319.20
109.10
109.05
109.00
Resistivity (μΩ cm)
Au20 Fe80
annealed up to
20 K
300 K
2
4
6
8
10
12
14
16
18
Temperature (K)

FIG. 50

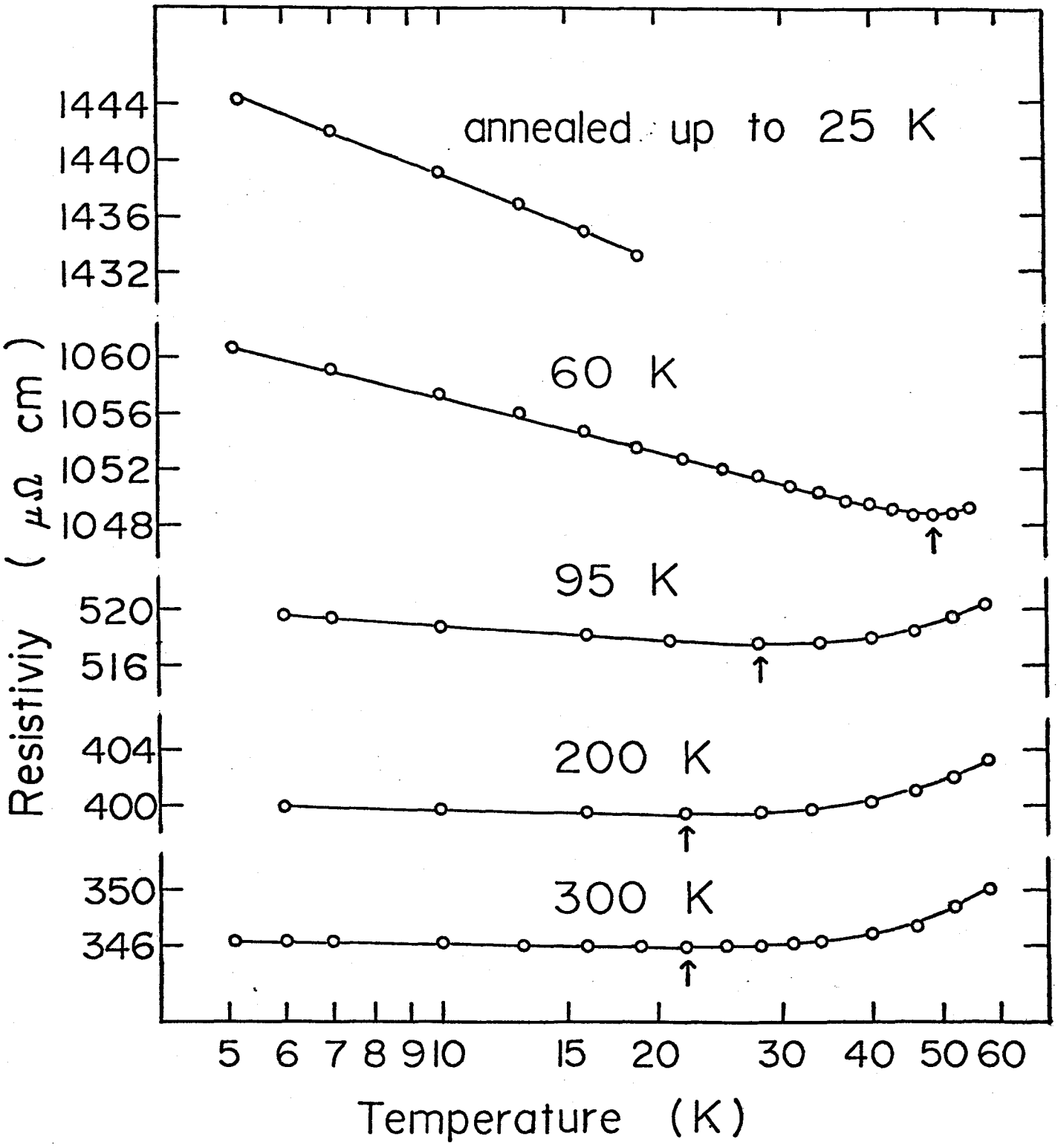
annealed up to 25 K
60 K
95 K
200 K
300 K
1444
1440
1436
1432
1060
1056
1052
1048
520
516
404
400
350
346
Resistiviy (μΩ cm)
5 6 7 8 9 10 15 20 30 40 50 60
Temperature (K)

FIG. 51

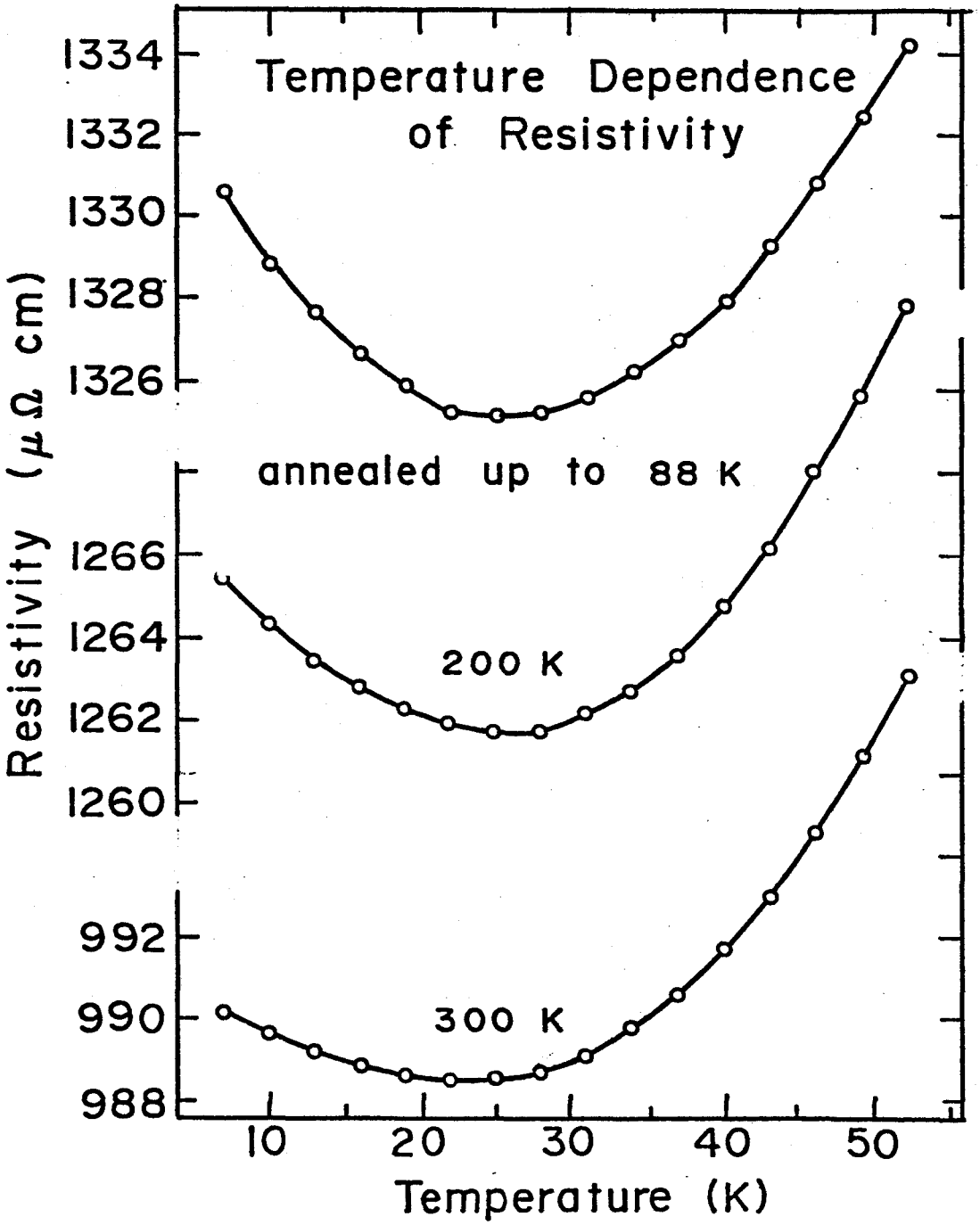
Temperature Dependence
of Resistivity
annealed up to 88 K
200 K
300 K
Resistivity (μΩ cm)
1334
1332
1330
1328
1326
1266
1264
1262
1260
992
990
988
10
20
30
40
50
Temperature (K)

FIG. 52

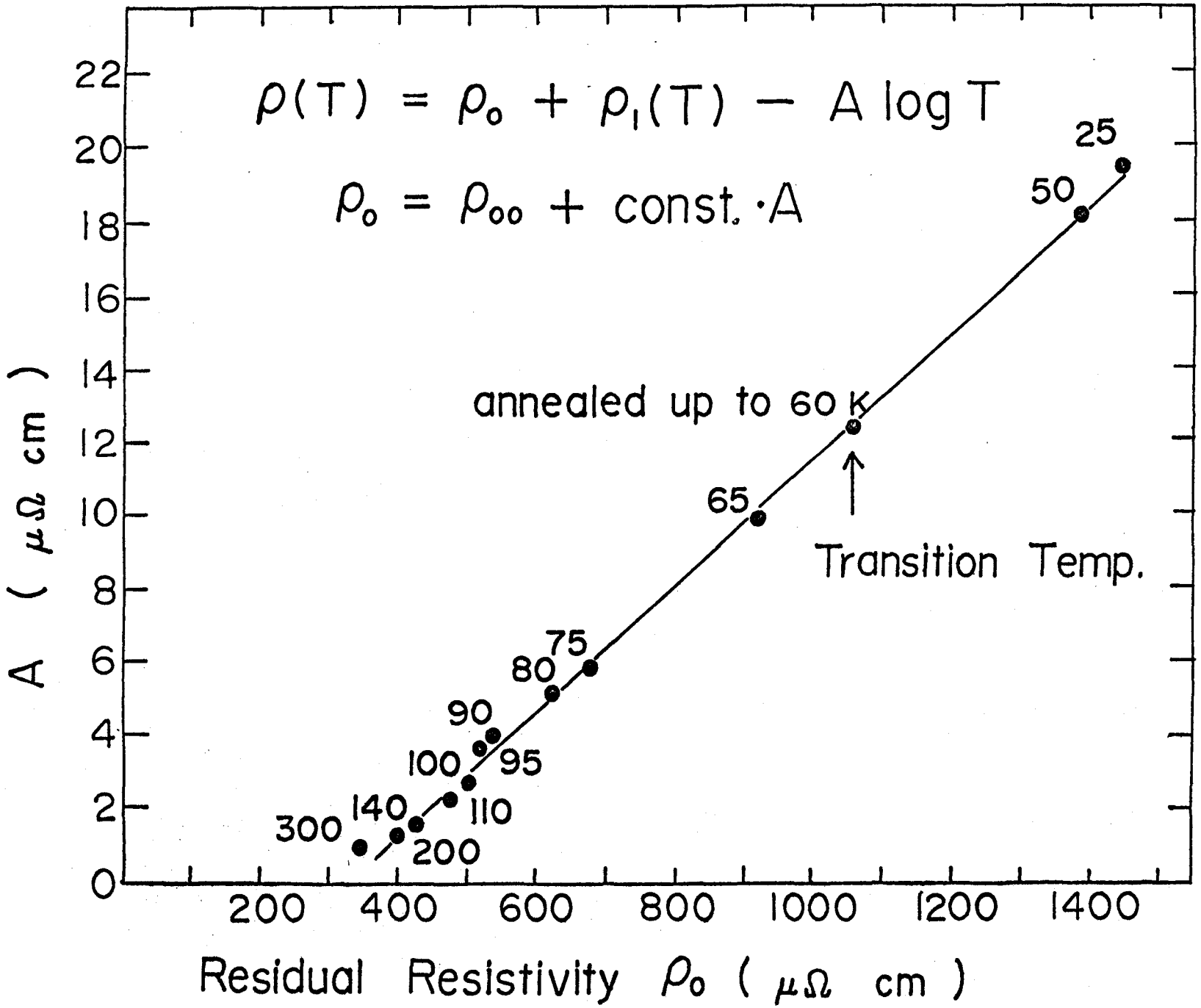
$\rho(T) = \rho_0 + \rho_1(T) - A \log T$
$\rho_0 = \rho_{00} + \text{const.} \cdot A$
A (μΩ cm)
Residual Resistivity ρ_0 (μΩ cm)
annealed up to 60 K
Transition Temp.
25
50
65
75
80
90
95
100
110
140
200
300
0
2
4
6
8
10
12
14
16
18
20
22
200
400
600
800
1000
1200
1400

FIG. 53